



NAVAL
POSTGRADUATE
SCHOOL

MONTEREY, CALIFORNIA

DISSERTATION

**UNSTRUCTURED HIGH-ORDER
GALERKIN-TEMPORAL-BOUNDARY METHODS FOR
THE KLEIN-GORDON EQUATION WITH
NON-REFLECTING BOUNDARY CONDITIONS**

by

Joseph Lindquist

June 2010

Dissertation Supervisors:

Francis X. Giraldo
Beny Neta

Approved for public release; distribution is unlimited

THIS PAGE INTENTIONALLY LEFT BLANK

REPORT DOCUMENTATION PAGE			Form Approved OMB No. 0704-0188	
Public reporting burden for this collection of information is estimated to average 1 hour per response, including the time for reviewing instruction, searching existing data sources, gathering and maintaining the data needed, and completing and reviewing the collection of information. Send comments regarding this burden estimate or any other aspect of this collection of information, including suggestions for reducing this burden, to Washington headquarters Services, Directorate for Information Operations and Reports, 1215 Jefferson Davis Highway, Suite 1204, Arlington, VA 22202-4302, and to the Office of Management and Budget, Paperwork Reduction Project (0704-0188) Washington DC 20503.				
1. AGENCY USE ONLY (Leave blank)		2. REPORT DATE June 2010	3. REPORT TYPE AND DATES COVERED Dissertation – Jan 09 - June 10	
4. TITLE AND SUBTITLE: Unstructured High-Order Galerkin-Temporal-Boundary Methods for the Klein-Gordon Equation with Non-Reflecting Boundary Conditions			5. FUNDING NUMBERS	
6. AUTHOR(S): Joseph M. Lindquist				
7. PERFORMING ORGANIZATION NAME(S) AND ADDRESS(ES) Naval Postgraduate School Monterey, CA 94942-5000			8. PERFORMING ORGANIZATION REPORT NUMBER	
9. SPONSORING/MONITORING AGENCY NAME(S) AND ADDRESS(ES)			10. SPONSORING/MONITORING AGENCY REPORT NUMBER	
11. SUPPLEMENTARY NOTES: The views expressed in this thesis are those of the author and do not reflect the official policy or position of the Department of Defense or the U.S. Government.				
12a. DISTRIBUTION / AVAILABILITY STATEMENT Approved for public release; distribution is unlimited			12b. DISTRIBUTION CODE A	
13. ABSTRACT (maximum 200 words) A reduced shallow water model under constant, non-zero advection in infinite domains is considered. High-Order Givoli-Neta (G-N) and Hagstrom-Hariharan (H-H) non-reflecting boundary conditions (NRBCs) are introduced to create a finite computational space and solved using a spectral element formulation with high-order time integration. Numerical examples are used to demonstrate the synergy of using high-order spatial, time and boundary discretizations. Several alternatives are also presented for solving open domain problems. These alternatives include adjustments to the G-N NRBC based on physical arguments as well as formulating the boundary condition for arbitrary domains using unstructured grids. The H-H polar NRBC is also formulated in an unstructured grid setting and extended to include dispersive effects. Results show that by balancing all numerical errors involved, high-order accuracy can be achieved for unbounded channel problems. Further, the adjustments to the G-N and H-H NRBCs to operate in an unstructured grid setting are shown to significantly reduce errors over first order non-reflecting boundary schemes when operating in an open domain configuration.				
14. SUBJECT TERMS Non-reflecting Boundary, Spectral Elements, Runge-Kutta, High-Order, Klein-Gordon, Shallow Water Equations			15. NUMBER OF PAGES 172	
			16. PRICE CODE	
17. SECURITY CLASSIFICATION OF REPORT Unclassified	18. SECURITY CLASSIFICATION OF THIS PAGE Unclassified	19. SECURITY CLASSIFICATION OF ABSTRACT Unclassified	20. LIMITATION OF ABSTRACT UU	

THIS PAGE INTENTIONALLY LEFT BLANK

Approved for public release; distribution is unlimited

**UNSTRUCTURED HIGH-ORDER GALERKIN-TEMPORAL-BOUNDARY
METHODS FOR THE KLEIN-GORDON EQUATION WITH NON-REFLECTING
BOUNDARY CONDITIONS**

Joseph M. Lindquist
Major, United States Army
B.S. Electrical Engineering, Milwaukee School of Engineering, Milwaukee, WI, 1995
M.S. Operations Analysis, Naval Postgraduate School, 2004

Submitted in partial fulfillment of the
requirements for the degree of

**DOCTOR OF PHILOSOPHY IN
APPLIED MATHEMATICS**

from the

**NAVAL POSTGRADUATE SCHOOL
June 2010**

Author:

Joseph Michael Lindquist

Approved By:

Beny Neta
Professor
Department of Appl. Math.
Dissertation Supervisor

Francis Giraldo
Professor
Department of Appl. Math.
Dissertation Supervisor

Clyde Scandrett
Professor
Department of Appl. Math.

Young Kwon
Professor
Department of Mech Eng.

Hong Zhou
Associate Professor
Department of Appl. Math.

Saša Gaberšek
Naval Research Laboratory

Approved By:

Carlos Borges, Professor and Chair, Department of Appl. Math.

Approved By:

Doug Moses, Vice Provost for Academic Affairs

THIS PAGE INTENTIONALLY LEFT BLANK

ABSTRACT

A reduced shallow water model under constant, non-zero advection in infinite domains is considered. High-Order Givoli-Neta (G-N) and Hagstrom-Hariharan (H-H) non-reflecting boundary conditions (NRBCs) are introduced to create a finite computational space and solved using a spectral element formulation with high-order time integration. Numerical examples are used to demonstrate the synergy of using high-order spatial, time and boundary discretizations. Several alternatives are also presented for solving open domain problems. These alternatives include adjustments to the G-N NRBC based on physical arguments as well as formulating the boundary condition for arbitrary domains using unstructured grids. The H-H polar NRBC is also formulated in an unstructured grid setting and extended to include dispersive effects. Results show that by balancing all numerical errors involved, high-order accuracy can be achieved for unbounded channel problems. Further, the adjustments to the G-N and H-H NRBCs to operate in an unstructured grid setting are shown to significantly reduce errors over first order non-reflecting boundary schemes when operating in an open domain configuration.

THIS PAGE INTENTIONALLY LEFT BLANK

TABLE OF CONTENTS

I.	INTRODUCTION	1
II.	EQUATIONS OF FLUID MOTION	5
A.	Conservation of Mass	5
B.	Importance of the Earth's Rotation	6
1.	Equations in a Rotating Frame	7
2.	3-Dimensional Rotating Earth Model	9
C.	Conservation of Momentum	11
1.	Gravity Effects	12
2.	Coriolis Effects	12
3.	Surface Force Effects	13
4.	Momentum Equations in a Rotating Frame	13
D.	Further Simplifications of the System	14
1.	Mathematical Simplifications	15
2.	Implication of Homogeneity	16
3.	Implication of Shallow Fluid	16
a.	<i>Primarily Horizontal Flow</i>	17
b.	<i>Continuity Equation Simplifications</i>	18
E.	Linearizing the Shallow Water Model	18
F.	Klein-Gordon Equivalent to the Shallow Water Model	19
G.	Recovering the Fluid Velocities	21
III.	HIGH ORDER NON-REFLECTING BOUNDARIES	23
A.	Higdon Scheme	24
1.	Accounting for Dispersion	25
2.	Reflection Caused by the Boundary	26
B.	Higdon Adjustments for Advection	28
C.	Givoli-Neta Auxiliary Variable Formulation	30
IV.	DISCRETIZATION VIA SPECTRAL ELEMENTS	35
A.	Interior Weak Integral Formulation	36
B.	Boundary Weak Integral Formulation	38
C.	Grid Generation and Choice of Basis Functions	39

D.	Galerkin Expansion	43
V.	SOLUTION OF THE DYNAMIC SYSTEM	49
A.	Runge-Kutta Methods	49
B.	Simple Example of Convergence	51
VI.	NUMERICAL EXPERIMENTS	55
A.	Analytic Benchmark Solution of Semi-Infinite Horizontal Channel	57
1.	Results	59
B.	Semi-Infinite Horizontal Channel	60
1.	Semi-Infinite Channel with Zero Advection Results	61
2.	Semi-Infinite Channel with Constant Advection Results . .	62
C.	Infinite Horizontal Channel	65
1.	Weak Form Adjustments	67
2.	Infinite Channel with Various Advection Velocities Results	67
D.	Open Domain Considerations	69
1.	Corner Compatibility Concerns	69
2.	Use of Sommerfeld Radiation Boundary Conditions for Auxiliary Variable Boundary Conditions	71
3.	Corner and Open Domain with Zero Advection Results . .	73
4.	Corner and Open Plane Domain with Constant Advection Results	76
E.	Effects of High-Order Time Integration	77
VII.	TOWARDS ARBITRARY DOMAINS	81
A.	Arbitrarily Shaped Boundaries	81
1.	Second Order (and Higher) Higdon Boundary Condition .	84
2.	G-N on the Unstructured Boundary	85
B.	Results for Adjusted G-N NRBCs on Arbitrary Domains	86
C.	Alternatives	89
1.	Hagstrom Hariharan Polar Boundary Conditions	90
2.	Results for the HH Formulation	93
3.	Adjustments to HH to Include Mild Dispersion	93
4.	Results for HH with Dispersion	98
VIII.	CONCLUSIONS AND AREAS FOR FUTURE RESEARCH	101
	APPENDIX A. DEPTH INTEGRATING THE CONTINUITY EQUATION . . .	103

APPENDIX B. LINEARIZING THE SHALLOW WATER EQUATIONS	105
APPENDIX C. ADJUSTING HIGDON'S CONDITION FOR ADVECTION . .	107
APPENDIX D. NORMAL TO TANGENTIAL DERIVATIVE TRANSFOR- MATION FOR EASTERN NRBC	111
APPENDIX E. METRIC TERMS DERIVATION	115
A. Derivation of Metric Terms	115
B. Consequences of Quadrilateral Grid Degeneration	116
APPENDIX F. NON-DIMENSIONALIZATION OF THE KGE	121
APPENDIX G. AUXILIARY VARIABLE FORMULATIONS FOR WESTERN, NORTHERN AND SOUTHERN BOUNDARIES	123
A. Formulation for the Western Boundary	123
B. Formulation for the Northern Boundary	125
C. Formulation for the Southern Boundary	127
APPENDIX H. OPEN PLANE DOMAIN ROTATION IN THE DIRECTION OF ADVECTION	129
APPENDIX I. ARBITRARILY SHAPED BOUNDARY FORMULATION . . .	133
A. Computing the Normal and Tangential Vector Components	137
B. Integration of Tangential Derivatives	139
1. Integration of First Order Tangential Derivatives	139
2. Integration of Second Order Tangential Derivatives	141
C. Relating the Boundary and Interior Formulations	142
D. Selection of C_j Terms	143
LIST OF REFERENCES	145
INITIAL DISTRIBUTION LIST	151

THIS PAGE INTENTIONALLY LEFT BLANK

LIST OF FIGURES

Figure 1.	Fixed (X, Y) and rotating (x, y) frameworks of reference.	7
Figure 2.	Local Cartesian framework on spherical earth.	10
Figure 3.	The shallow water model with irregular bottom topography.	15
Figure 4.	An infinite wave-guide truncated by artificial boundaries Γ_W and Γ_E .	23
Figure 5.	A semi-infinite channel truncated by artificial boundary Γ_E	26
Figure 6.	Normal Derivatives to Boundaries	37
Figure 7.	Arbitrary quadrilateral element formed by combining triangles.	40
Figure 8.	Sample mesh generated using Automesh-2D.	40
Figure 9.	Mapping from physical space to computational space	41
Figure 10.	L^2 error in solution of (V.2) using RK-2 – RK-10 time integration. . .	52
Figure 11.	L^2 error as a function of time-step refinement. Rates as defined by (V.3) should correspond to RK order.	53
Figure 12.	Canonical element using 8^{th} order basis functions showing distribu- tion of grid points.	57
Figure 13.	The semi-infinite channel domain under consideration. Domain is truncated by an artificial boundary \mathcal{B} at $x_E = 2$	58
Figure 14.	Semi-infinite channel comparing synthesized solution and the NRBC solution. 4^{th} order spectral elements using NRBC order $J = 4$ with zero advection at $t = 3$ are shown.	59
Figure 15.	Semi-infinite channel L^2_Ω error versus NRBC and spectral element order. Domain is discretized into 9,409 points for all spectral element orders with zero advection at $t = 3$	60
Figure 16.	Semi-infinite channel, 4^{th} order spectral elements ($J = 4$) using co- sine pulse initial condition and zero advection. Left Plot: Contour plot showing $h(x, y, 3)$ on extended and truncated domains. Right Plot: Corresponding L^2_Ω error versus NRBC and spectral element or- der. Domain is discretized into 9,409 points for all spectral element orders.	61
Figure 17.	Semi-infinite channel, 4^{th} order spectral elements ($J = 4$) using Gaussian initial condition with zero advection. Left Plot: Contour plot showing $h(x, y, 3)$ on extended and truncated domains. Right Plot: Corresponding L^2_Ω error versus NRBC and spectral element or- der. Domain is discretized into 9,409 points for all spectral element orders.	62

Figure 18.	Semi-infinite channel, 4^{th} order spectral elements ($J = 4$) using cosine pulse initial condition with advection velocities $U = 0.1$ and $V = 0$. Left Plot: Contour plot showing $h(x, y, 3)$ on extended and truncated domains. Right Plot: Corresponding L^2_Ω error versus NRBC and spectral element order. Domain is discretized into 9,409 points for all spectral element orders.	63
Figure 19.	Semi-infinite channel, 4^{th} order spectral elements ($J = 4$) using Gaussian initial condition with advection velocities $U = 0.1$ and $V = 0$. Left Plot: Contour plot showing $h(x, y, 3)$ on extended and truncated domains. Right Plot: Corresponding L^2_Ω error versus NRBC and spectral element order. Domain is discretized into 9,409 points for all spectral element orders.	64
Figure 20.	Semi-infinite channel, 4^{th} order spectral elements ($J = 4$) using Gaussian initial condition with advection velocities specified. Top Plots: Contour plots showing $h(x, y, 3)$ on extended and truncated domains. Bottom Plots: Corresponding L^2_Ω error versus NRBC and spectral element order. Domain is discretized into 9,409 points for all spectral element orders.	66
Figure 21.	The infinite channel domain under consideration. Domain is truncated by artificial boundaries at $x_W = -2$, and $x_E = 2$	67
Figure 22.	Infinite channel, 4^{th} order spectral elements ($J = 4$) using cosine pulse initial condition with advection velocities specified. Left Plots: Contour plots showing $h(x, y, 3)$ on extended and truncated domains. Right Plots: Corresponding L^2_Ω error versus NRBC and spectral element order. Domain is discretized into 9,409 points for all spectral element orders.	68
Figure 23.	Infinite channel, 4^{th} order spectral elements ($J = 4$) using Gaussian initial condition with advection velocities specified. Left Plots: Contour plots showing $h(x, y, 3)$ on extended and truncated domains. Right Plots: Corresponding L^2_Ω error versus NRBC and spectral element order. Domain is discretized into 9,409 points for all spectral element orders.	70
Figure 24.	Left Plot: A semi-infinite domain Ω truncated by artificial boundaries Γ_E and Γ_N . Right Plot: An infinite domain Ω truncated by artificial boundaries $\Gamma_S, \Gamma_E, \Gamma_N$ and Γ_W	71
Figure 25.	Time Evolution of quarter plane Gaussian (NRBC on Γ_N and Γ_E) using 4^{th} order spectral elements ($J = 4$) with zero advection.	73
Figure 26.	Time Evolution of open plane Gaussian (NRBC on all boundaries) using 4^{th} order spectral elements ($J = 4$) with zero advection.	75

Figure 27.	Time Evolution of open plane Gaussian (NRBC on all boundaries) using 4^{th} order spectral elements ($J = 4$) with advection velocities $U = 0.1$ and $V = 0.1$	77
Figure 28.	Error in the SE Solution of KGE using NRBCs of various order as a function of time integration order.	79
Figure 29.	A general domain Ω truncated by artificial boundary Γ	82
Figure 30.	Components of normal and tangential derivatives	83
Figure 31.	Open Domain, 4^{th} order spectral elements using Gaussian initial condition with zero advection. Top Plots: Contour plots of reference solution solved on extended domain. Full and truncated domains shown for comparison. Center Plots: Contour plots of various NRBC boundary configurations using $J = 1$. Bottom Plots: Contour plots of various NRBC boundary configurations using $J = 4$	88
Figure 32.	Open Domain, 4^{th} order spectral elements ($J = 4$) using oblique Gaussian initial condition shown for $t = 1, 2, 3$. Top Plots: Contour plots of reference solution solved on extended domain. Superimposed black circle indicates NRBC domain. Bottom Plots: Contour plots of various NRBC boundary configurations using $J = 4$	94
Figure 33.	Open Domain, 4^{th} order spectral elements ($J = 4$) using oblique Gaussian initial condition shown for $t = 1, 2, 3$ under dispersion $f^2 = 0.1$. Top Plots: Contour plots of reference solution solved on extended domain. Superimposed black circle indicates NRBC domain. Bottom Plots: Contour plots of various NRBC boundary configurations using $J = 4$	99
Figure 34.	Degenerate quadrilateral mapped to a canonical reference element. . .	117
Figure 35.	Generation of a new coordinate system in the direction of advection .	129
Figure 36.	Normal and tangential vectors along a canonical element boundary. . .	138

THIS PAGE INTENTIONALLY LEFT BLANK

LIST OF TABLES

Table 1.	Computational cost for RK methods used.	50
Table 2.	L^2_Ω Error as a function of NRBC Order for quarter plane using various spectral element orders. Gaussian initial condition and zero advection is used.	74
Table 3.	L^2_Ω Error as a function of NRBC Order for open plane using various spectral element orders. Gaussian initial condition and zero advection is used.	76
Table 4.	L^2_Ω Error as a function of NRBC Order for open plane using various spectral element orders . Gaussian initial condition with advection velocities $U = 0.1$ and $V = 0.1$ used.	78
Table 5.	L^2_Ω Error as a function of NRBC Order for open plane arbitrary domain formulation using various spectral element orders on square NRBC domain. Gaussian initial condition and zero advection is used.	89
Table 6.	L^2_Ω Error as a function of NRBC Order for open plane arbitrary domain formulation using various spectral element orders on rounded square NRBC domain. Gaussian initial condition and zero advection is used.	89
Table 7.	L^2_Ω Error as a function of NRBC Order for open plane arbitrary domain formulation using various spectral element orders on circular NRBC domain. Gaussian initial condition and zero advection is used.	90
Table 8.	L^2_Ω Error as a function of NRBC Order for Hagstrom Hariharan NRBC formulation using various spectral element orders on the circular NRBC domain. Oblique Gaussian initial condition is used.	95
Table 9.	L^2_Ω Error as a function of NRBC Order for Hagstrom Hariharan NRBC formulation using various spectral element orders on the circular NRBC domain. Oblique Gaussian initial condition is used with dispersion parameter set to $f^2 = 0.1$	100

THIS PAGE INTENTIONALLY LEFT BLANK

ACKNOWLEDGEMENTS

I would like to begin by thanking the Lord for creating me and giving me the challenges and blessings that this life offers.

I would also like to acknowledge my great research team. Thanks especially to Drs. Frank Giraldo and Beny Neta for the constant patience and prodding in the right direction. You allowed me to take detours along the way – many of which were interesting but did not progress the research. It is easy to feel small when in the presence of “Giants,” yet you always treated me as a member of the team. Thanks also to the members of the committee: Drs. Clyde Scandrett, Young Kwon, Hong Zhou and Saša Gaberšek. While I did not work with you daily, your comments and insights were invaluable in developing a stronger research product.

Thanks to Dr. Carlos Borges for your Thursday “Chairman stress relief seminars” in your office and great leadership in the best department on campus. I can’t say thanks enough to Dr. Jim Kelly, who was my “dumb question sounding board.” Jim so patiently tolerated my many concerns and provided timely advice on countless occasions. Numerous other faculty members here at NPS have also contributed to overcoming stumbling blocks along the way in this analysis, and to those folks, I say thank you.

A salute goes out also to my fellow students here in the math department who allowed me to get involved in on their research when my own progress was slow. Special thanks to Natalie Vanatta who was a superb study partner during our course work and in preparation for our comprehensive examinations.

Finally, I would like to thank my family. Diane, you always manage to keep me anchored in our faith, family and fun. Thanks also to Alex (Booga) and Jenna (Bean) who always make coming home the highlight of my day.

THIS PAGE INTENTIONALLY LEFT BLANK

I. INTRODUCTION

Simulation of wave propagation through large – perhaps unbounded – domains has been an active area of research for several decades. Such studies are important to many applications such as acoustics, electromagnetics, meteorology, solid geophysics and aerodynamics to name just a few. The combination of the complexity of the partial differential equation sets involved and the infinite possibilities of initial data mandates the numerical solution to such problems. Of course, to undertake the numerical solution on an infinite domain would be both foolhardy and impossible. Generally speaking, to overcome this computational challenge, it is quite common to truncate the infinite domain by imposing some type of boundary condition on a “sufficiently large” sub-domain that captures the area of interest.

When truncating the domain, the modeler must devise boundary conditions for the truncated domain. Of course, by imposing a boundary where one does not physically exist, the problem is changed – and unless chosen carefully, would certainly be expected to pollute the solution as the problem evolves and impinges on the boundary. Therefore, two main possibilities exist for the modeler:

- Choose a convenient, easily implementable boundary condition that does not necessarily reflect the physical problem and solve it on a large sub-domain. The idea behind this technique is that the boundary effects are negligible for a short time evolution of the problem in a small area of interest away from the boundaries.
- Choose a boundary condition that preserves the true *behavior* of the infinite solution at the boundary and solve the problem on a smaller sub-domain. The idea behind this technique is that the additional effort extended to impose a better boundary condition will be worth the effort and allow for solving the problem on a smaller domain.

For obvious reasons, the first possibility has only limited usefulness. To see why, suppose that we wanted to model the wave motion following a pebble dropped in the center of a

large, still pond. Now, suppose that we have a truncated domain to model this phenomena – say a bathtub. If the pebble is dropped in the bathtub, the waves generated by the pebble would propagate much like that in the pond – until, that is – the wave front reaches the hard walls of the bathtub. At this point, the bathtub model ceases to be a useful representation of the pond due to behavior caused by the non-physical boundary. If the modeler wishes to see what happens a short time later – a larger bathtub would be required. This same principle would apply for the numerical solution of this propagation problem – a poor choice of boundary condition mandates the use of a larger computational domain. This in turn, requires additional computational resources. For this reason, much effort has and continues to be exerted on finding suitable boundary conditions that apply on smaller domains.

This dissertation examines the use of high-order non-reflecting boundary conditions (NRBCs) to solve a class of infinite domain, wave propagation problems. In the last 35 years or so, much research has been done to develop NRBCs that, after discretization, lead to a scheme that is stable, accurate, efficient and easy to implement. Of course, it is difficult to find a single NRBC that is ideal in all respects and all cases; this is why the quest for better NRBCs and their associated discretization schemes continues.

Sequences of increasing-order NRBCs have been available for a long time (e.g., the Bayliss-Turkel conditions [1] constitute such a sequence), but they had been regarded as impractical beyond 2nd or 3rd order from the implementation point of view. Only since the mid 90s have practical high-order NRBCs been devised. The first *high-order* local NRBC was proposed by Collino [2], for two-dimensional time-dependent waves in rectangular domains. Its construction requires the solution of the one-dimensional wave equation on the boundary. Grote and Keller [3] developed a high-order converging NRBC for the three-dimensional time-dependent wave equation, based on spherical harmonic transformations. Sofronov [4, 5] proposed exact boundary conditions for the three- and two- dimensional wave equations in spherical and polar coordinates, respectively (it is proved that NRBCs demonstrated in [3] and [4] are reduced to each other).

Hagstrom and Hariharan [6] constructed high-order NRBCs for the two- and three-dimensional time-dependent wave equations based on the analytic series representation for the outgoing solutions of these equations. For time-dependent waves in a two-dimensional wave guide, Guddati and Tassoulas [7] devised a high-order NRBC by using rational approximations and recursive continued fractions. Givoli [8] has shown how to derive high-order NRBCs for a general class of wave problems, leading to a symmetric FE formulation. In [9], this methodology was applied to the particular case of time-harmonic waves, using optimally localized Dirichlet-to-Neumann (DtN) NRBCs (see also [10]).

Previous studies of this nature have encountered limits in the accuracy of such solutions. These accuracy limits can be caused by time and space discretization as well as from the boundary scheme used in the solution of the problem. We seek to employ *high-order* numerical methods in time and space to diminish the effects of discretization error in order to determine the true efficacy of a given non-reflecting boundary condition.

The rest of the dissertation is outlined as follows. Chapter II motivates and derives the equations for the problem under consideration. In Chapter III, we summarize the main boundary schemes currently in use and specifically show the Givoli-Neta (G-N) NRBC in detail. We then describe the high-order spectral element method used to discretize the problem in space (up to 16^{th} order polynomials) in Chapter IV. Chapter V discusses the Runge-Kutta time discretization demonstrated up to 10^{th} order. Chapter VI provides numerical examples in various configurations and conditions to demonstrate concepts. Chapter VII considers challenges associated with arbitrary boundary configurations and provides results for a low-order boundary treatment using unstructured grids. Chapter VIII examines the potential for exploiting other non-reflecting boundary conditions employed in an unstructured grid formulation and concludes with areas of future research.

THIS PAGE INTENTIONALLY LEFT BLANK

II. EQUATIONS OF FLUID MOTION

In order to scope the enormous problem of wave propagation and provide a good test bed of examples for simulation of the non-reflecting boundary conditions under examination, we will derive the shallow water equations. The set of equations under consideration have been used to predict Tsunamis and storm surges [11], as well as modeling atmospheric flows. The term “shallow water” is a bit deceiving, as the medium does not necessarily have to be water, nor does it have to be shallow. To elaborate – the equations under consideration are generated by very general physical principles, namely conservation of mass and momentum, that are then simplified using reasonable assumptions. In this derivation, we will abbreviate the approach taken by Cushman-Roisin [12], Pedlosky [13] and Batchelor [14] and further simplify the equations by reducing them to a scalar Klein-Gordon equation equivalent.

A. CONSERVATION OF MASS

One of the fundamental physical principles is that mass can neither be created nor destroyed. Consider a control volume – a fixed region in space where fluid is allowed to occupy and pass through. Within this control volume, mass is conserved. In other words, for the mass to change in a control volume, there must be mass passing through the boundary of the control volume. Suppose dm is an infinitesimal portion of the mass, dV and dA are infinitesimal portions of the control volume and its boundary, respectively, and ρ is the density of the fluid occupying the control volume. Then by this argument, the mass enclosed by the surface at any instant is $\int dm = \int \rho dV$. Further, the net rate that mass is flowing outwards across the boundary is $\int (\rho \mathbf{u}) \cdot \mathbf{n} dA$. Putting these two ideas together

we find that for mass to be conserved:

$$\underbrace{\frac{\partial}{\partial t} \int \rho \, dV}_{\text{Time rate of mass change in CV}} = - \underbrace{\int (\rho \mathbf{u}) \cdot \mathbf{n} \, dA}_{\text{Net rate of mass flux across boundary}}.$$

Here: $\mathbf{u} = (u, v, w)^T$ is the fluid velocity and \mathbf{n} is the outward pointing unit normal on the boundary.

Further, upon differentiation under the integral sign (remembering that the control volume is fixed in space) and transforming the surface integral using the divergence theorem:

$$\begin{aligned} \int \frac{\partial \rho}{\partial t} \, dV + \int \nabla \cdot (\rho \mathbf{u}) \, dV &= 0 \\ \int \left(\frac{\partial \rho}{\partial t} + \nabla \cdot \rho \mathbf{u} \right) \, dV &= 0 \end{aligned}$$

This relation is valid for all choices of the control volume, therefore, the integrand must also be identically zero. i.e.,

$$\frac{\partial \rho}{\partial t} + \nabla \cdot \rho \mathbf{u} = 0 \tag{II.1}$$

The differential equation (II.1) is commonly referred to as the continuity equation in fluid mechanics.

B. IMPORTANCE OF THE EARTH'S ROTATION

Modeling phenomena on a large scale, such as the currents of the ocean or winds in the atmosphere, may require special handling since the earth is not static. In fact, the earth rotates on its axis approximately once every 24 hours. This results in a mean rotation rate Ω of:

$$\Omega = \frac{2\pi}{\text{rotation period}}.$$

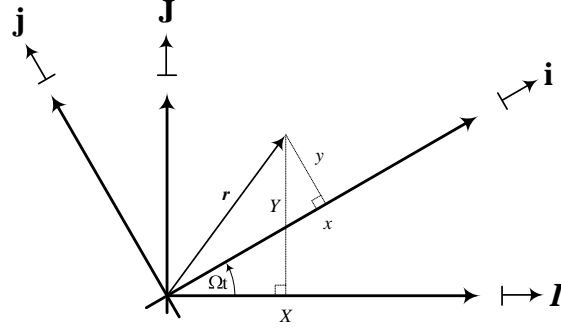


Figure 1: Fixed (X, Y) and rotating (x, y) frameworks of reference.

When the “exact”¹ rotation period of the earth is considered, this results in a mean angular velocity of $7.292 \times 10^{-5} \frac{\text{radians}}{\text{sec}}$ [15]. The trajectory of a fluid in motion is expected to be influenced by this rotation if the fluid traveling at the speed U covers a distance L in a time interval greater than the rotation period. This concept is captured by a non-dimensional parameter ε and is defined as:

$$\varepsilon = \frac{2\pi/\Omega}{L/U} = \frac{2\pi U}{\Omega L}$$

If ε is on the order of or less than unity ($\varepsilon \lesssim 1$), then we would expect that rotation is important. This number (neglecting the constant multiple 2π) is known as the *Rossby number* [12].

1. Equations in a Rotating Frame

Now, we examine this rotating frame of reference on the earth. From the human perspective on the surface of the earth, we appear to be on a 2-dimensional surface. Suppose that we have X – and Y – axes that are the fixed or *inertial* reference frame and x – and y – axes that form the same reference frame, but rotating at the angular rate of Ω . The unit vectors that follow this convention are defined by (\mathbf{I}, \mathbf{J}) and (\mathbf{i}, \mathbf{j}) as shown in Figure 1². It

¹The mean day is 23 hours, 56 minutes and 4.091 seconds, but variations caused by friction from the earth’s tides, as well as significant geophysical events on earth have been observed to cause fluctuations in this measure.

²Adapted from [12], Figure 2-1, p. 17.

follows that

$$\mathbf{i} = \mathbf{I} \cos \Omega t + \mathbf{J} \sin \Omega t \quad \mathbf{j} = -\mathbf{I} \sin \Omega t + \mathbf{J} \cos \Omega t$$

and the coordinates of the position vector $\mathbf{r} = X\mathbf{I} + Y\mathbf{J} = x\mathbf{i} + y\mathbf{j}$ are correspondingly

$$\begin{aligned} x &= X \cos \Omega t + Y \sin \Omega t \\ y &= -X \sin \Omega t + Y \cos \Omega t \end{aligned}$$

Differentiating once with respect to time gives the rate of change of the coordinates relative to the moving frame, $\mathbf{u} = \frac{d\mathbf{x}}{dt} = u\mathbf{i} + v\mathbf{j}$ (relative velocity). Differentiating again with respect to time gives the rate of change of the relative velocity in the moving frame, $\mathbf{a} = \frac{d\mathbf{u}}{dt} = \frac{d^2\mathbf{x}}{dt^2} = a\mathbf{i} + b\mathbf{j}$ (relative acceleration). When completed and simplified, the absolute acceleration in the inertial frame with respect to the relative acceleration is:

$$\begin{aligned} \mathbf{A} &= (a - 2\Omega v - \Omega^2 x) \mathbf{i} + (b + 2\Omega u - \Omega^2 y) \mathbf{j} \\ &= A\mathbf{i} + B\mathbf{j} \end{aligned} \tag{II.2}$$

These results could also be derived in a vector form as outlined in [13] by defining the vector rotation in a direction common to both the rotating and inertial frames of reference – $\boldsymbol{\Omega} = \Omega\mathbf{k}$, where \mathbf{k} is a unit vector orthogonal to the plane. In this case, we can write (II.2) as:

$$\mathbf{A} = \mathbf{a} + 2\boldsymbol{\Omega} \times \mathbf{u} + \boldsymbol{\Omega} \times (\boldsymbol{\Omega} \times \mathbf{x}) \tag{II.3}$$

where \mathbf{u} is extended to $\mathbf{u} = u\mathbf{i} + v\mathbf{j} + w\mathbf{k}$. It should be noted that there are three contributions to the acceleration in the rotating frame: relative acceleration (\mathbf{a}), one proportional to Ω and the velocity, and one proportional to Ω^2 and the position. The contribution proportional to Ω and the velocity is known as the Coriolis acceleration and the other, proportional to Ω^2 and the position is the centripetal acceleration.

For practical purposes, the centripetal acceleration terms are often neglected since $\Omega^2 \sim \mathcal{O}(10^{-9})$. Additionally, even though centripetal acceleration causes objects on the surface of the planet to feel an outward pull, these objects do not fly off into space. In fact, even objects at rest, $(u, v) = 0$ thus removing the Coriolis effect, for all intents and purposes, remain at rest as the gravitational pull of the earth keeps centripetal acceleration in check.

When we neglect the centripetal acceleration terms in (II.3), the absolute acceleration terms in the inertial frame simplify to

$$\begin{aligned}\mathbf{A} &= \mathbf{a} + 2\boldsymbol{\Omega} \times \mathbf{u} \\ &= (a - 2\Omega v)\mathbf{i} + (b + 2\Omega u)\mathbf{j} + c\mathbf{k}\end{aligned}\tag{II.4}$$

2. 3-Dimensional Rotating Earth Model

Now, we consolidate our results to apply to a 3-dimensional rotating earth model. Consider Figure 2³ where Ω is oriented along the axis of rotation and an object is located on the surface at a latitude ϕ . A local coordinate system is set up with the axis orientation $(x, y, z) \rightarrow (\text{east}, \text{north}, \text{radial})$ with standard convention of unit normal vectors. In this frame of reference, the earth's rotation vector is expressed as

$$\boldsymbol{\Omega} = \Omega \cos \phi \mathbf{j} + \Omega \sin \phi \mathbf{k}.\tag{II.5}$$

Using this to expand (II.4), we find that the acceleration in the inertial reference in terms of the rotating components has the following components:

$$\begin{aligned}\mathbf{i} : & \quad a + 2\Omega w \cos \phi - 2\Omega v \sin \phi \\ \mathbf{j} : & \quad b + 2\Omega u \sin \phi \\ \mathbf{k} : & \quad c - 2\Omega u \cos \phi.\end{aligned}\tag{II.6}$$

³Adapted from [12], Figure 2-8, p. 27.

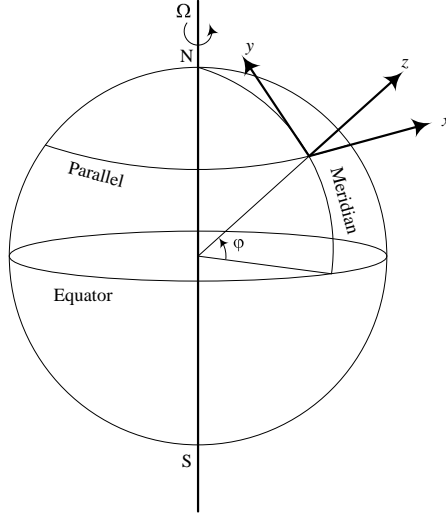


Figure 2: Local Cartesian framework on spherical earth.

Here, we notice the terms dependent on the latitude have common components, namely:

$$f = 2\Omega \sin \phi \quad (\text{II.7})$$

$$f_* = 2\Omega \cos \phi$$

The coefficient f is called the *Coriolis parameter* and the latter is the *reciprocal Coriolis parameter*. If we examine the scales of the components described in (II.6), we note that if we are describing geophysical fluid motion, the depth is much smaller than that of the surface it covers, and as such, the flows in this context tend to be parallel to the surface minimizing the effects of vertical flows. For our model, this implies that the effects of w are negligible compared to the effects of u and v . Additionally, any acceleration induced by the rotation in the vertical direction will be negligible compared to those along the surface.

This simplifies our acceleration in the inertial reference to:

$$\begin{aligned}\mathbf{i} : & \quad a - 2\Omega v \sin \phi \\ \mathbf{j} : & \quad b + 2\Omega u \sin \phi \\ \mathbf{k} : & \quad c.\end{aligned}$$

In vector form, this can be written as:

$$\mathbf{A} = \mathbf{a} + f (\mathbf{k} \times \mathbf{u}) \quad (\text{II.8})$$

Cushman-Rosin [12] provides two anecdotal justifications for this simplification. While the atmospheric layer that determines our weather is only about 10 km thick, cyclones and anticyclones spread over thousands of kilometers. The second in the context of oceanic currents notes that flows are generally confined to the upper hundred meters but spread over tens of kilometers.

C. CONSERVATION OF MOMENTUM

The linear momentum of an object of mass m moving with velocity \mathbf{u} is defined to be the product of the mass and velocity: $\mathbf{P} = m\mathbf{u}$, and in a closed system, must be conserved. Linear momentum is related to the forces acting using Newton's second law of motion – namely, that the time rate of change of the momentum of an object is equal to the resultant forces on the object. That is,

$$\mathbf{F} = \frac{\partial}{\partial t} \mathbf{P} \quad (\text{II.9})$$

This implies that if resultant forces are zero, the momentum of the particle must be constant. For this to happen, all of the forces (body and surface) acting on an object must sum to zero. In terms of the control volume framework discussed previously, this further implies that if

momentum is entering or leaving the control volume:

$$\frac{\partial}{\partial t} \mathbf{P} = \frac{\partial}{\partial t} m \mathbf{u}_* = \frac{\partial}{\partial t} \int \rho \mathbf{u}_* dV = \underbrace{\int \rho \mathbf{b} dV}_{\text{Body forces acting on } \Omega} - \underbrace{\int (\rho \mathbf{u}) \mathbf{u} \cdot \mathbf{n} dA}_{\text{Net momentum flux across bdry of } \Omega} + \underbrace{\int \mathbf{T} \mathbf{n} dA}_{\text{Forces acting on bdry of } \Omega}. \quad (\text{II.10})$$

Here, \mathbf{u}_* is the velocity in the inertial frame. Body forces are those acting on the fluid volume that are proportional to the mass. The body forces considered here are gravity and (indirectly) the Coriolis force described in II.B. Others could include electromagnetic and centrifugal forces pertinent in alternate applications.

1. Gravity Effects

Gravity acts on a control volume strictly towards the center of the earth, and in the local coordinate system is along $-\mathbf{k}$. This implies:

$$\rho \mathbf{b}_g = -\rho g \mathbf{k} \quad (\text{II.11})$$

Here, g is the gravitational constant which varies based on the distance from the center of the earth. At sea level, this value is approximately $9.798 \frac{m}{s^2}$, and in this context can be taken to be constant.

2. Coriolis Effects

Coriolis acts in a way to “adjust” the control volume’s acceleration when going from a rotating to an inertial frame. This term enters via the expression on the left hand side in the time change of momentum. Explicitly, this is

$$\begin{aligned} \frac{\partial}{\partial t} \int \rho \mathbf{u}_* dV &= \int \left(\frac{\partial \rho}{\partial t} \mathbf{u}_* + \rho \frac{\partial \mathbf{u}_*}{\partial t} \right) dV = \int \left(\frac{\partial \rho}{\partial t} \mathbf{u}_* + \rho \mathbf{A} \right) dV \\ &= \int \left[\frac{\partial \rho}{\partial t} \mathbf{u}_* + \rho \mathbf{a} + \rho f(\mathbf{k} \times \mathbf{u}) \right] dV \\ &= \frac{\partial}{\partial t} \int \rho \mathbf{u} dV + \int \rho f(\mathbf{k} \times \mathbf{u}) dV \end{aligned}$$

provided that ρ is constant in time.

3. Surface Force Effects

Surface forces are those exerted across the boundary by the surrounding matter. Typical surface forces include pressure and viscosity. Since we are examining the equations in the context of atmospheric and oceanic applications, the effects of viscosity are small in comparison to other forces, and as such, will not be considered here. VanJoolen [16] derives these terms in detail for the interested reader, but further concludes the contribution of viscosity can be neglected in this application. The total boundary force exerted by the surrounding matter at the surface of a control volume is

$$\int \mathbf{T} \mathbf{n} dA = - \int p \mathbf{n} dA$$

where p is the pressure exerted on the control volume by the surroundings. This surface integral may be transformed to an integral over the volume by the analogue of the divergence theorem for a scalar quantity [14, p. 15] giving

$$- \int p \mathbf{n} dA = - \int \nabla p dV.$$

Alternate derivations of this quantity can be found in [16] and [17], and provide further insights as from where this quantity is derived.

4. Momentum Equations in a Rotating Frame

We now apply the divergence theorem to transform the surface integral in (II.10) and collect results.

$$\frac{\partial}{\partial t} \int \rho \mathbf{u} dV + \int \nabla \cdot (\rho \mathbf{u} \mathbf{u}) dV - \int \rho g \mathbf{k} dV + \int \rho f (\mathbf{k} \times \mathbf{u}) dV + \int \nabla p dV = 0$$

Here, \mathbf{uu} is a tensor product of the velocity vector. Again, differentiating under the integral sign and consolidating terms yields:

$$\int \left[\frac{\partial}{\partial t} (\rho \mathbf{u}) + \nabla \cdot (\rho \mathbf{uu}) - \rho g \mathbf{k} + \rho f (\mathbf{k} \times \mathbf{u}) + \nabla p \right] dV = 0.$$

Since this relation is valid for all choices of the control volume, the integrand must identically be zero, i.e.,

$$\frac{\partial}{\partial t} (\rho \mathbf{u}) + \nabla \cdot (\rho \mathbf{uu}) + \nabla p = \rho g \mathbf{k} + \rho f (\mathbf{u} \times \mathbf{k}). \quad (\text{II.12})$$

Together with the continuity equation (II.1) we have our equations of fluid motion in a rotating frame.

D. FURTHER SIMPLIFICATIONS OF THE SYSTEM

Our equations of fluid motion have taken several physical principles into account, but we wish to simplify them more in order to get a tractable model that can serve as a launching point for more testing. In the case of this analysis, we wish to make the following assumptions about the physical problem in order to arrive at the shallow water equations:

The fluid is homogeneous: We assume that the fluid density is constant and uniform throughout the domain.

The fluid is inviscid: This implies that the only surface force acting on the fluid is pressure (neglects shear forces which would act to retard the motion of the fluid.)

The fluid is incompressible: Together with the assumption of homogeneity this decouples the dynamics from any thermodynamic considerations that might be used in another setting.

Centrifugal forces are balanced by gravity: This allows simplification of acceleration terms in the rotating frame of reference.

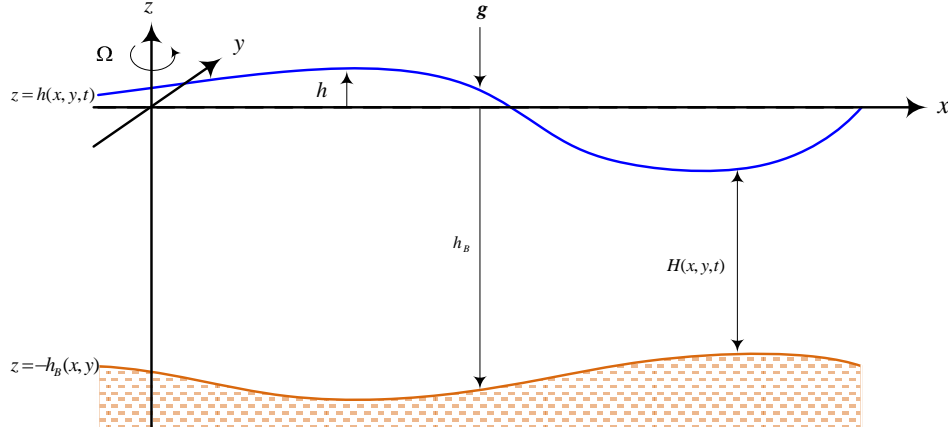


Figure 3: The shallow water model with irregular bottom topography.

The fluid is shallow: The depth terms in the applications considered are much smaller than the surface it covers, and therefore implies that flows are primarily along the surface.

We consider a sheet of fluid as shown in Figure 3 with properties as outlined above. Here, we define the irregular bottom height below a sensible reference value $z = 0$ as $h_B(x, y)$. This reference level could be considered the fluid height at rest. The height of the surface of the fluid above the same reference level is defined as $h(x, y, t)$. The depth of the fluid is therefore $H(x, y, t) = h(x, y, t) + h_B(x, y)$. To reiterate the shallow water assumption, we have a value for the height of the fluid $H(x, y, t)$ that is much smaller than the length and width of the fluid. Again, we consider a fluid that is in the presence of rotation Ω about the z -axis.

1. Mathematical Simplifications

As outlined in [17, Appendix A], the momentum equations (II.12) can be mathematically simplified using nothing but product rule expansions and the continuity equation

to yield:

$$\begin{aligned}
\frac{\partial u}{\partial t} + u \frac{\partial u}{\partial x} + v \frac{\partial u}{\partial y} + w \frac{\partial u}{\partial z} + \frac{1}{\rho} \frac{\partial p}{\partial x} &= f v \\
\frac{\partial v}{\partial t} + u \frac{\partial v}{\partial x} + v \frac{\partial v}{\partial y} + w \frac{\partial v}{\partial z} + \frac{1}{\rho} \frac{\partial p}{\partial y} &= -f u \\
\frac{\partial w}{\partial t} + u \frac{\partial w}{\partial x} + v \frac{\partial w}{\partial y} + w \frac{\partial w}{\partial z} + \frac{1}{\rho} \frac{\partial p}{\partial z} &= -g.
\end{aligned} \tag{II.13}$$

2. Implication of Homogeneity

Since the fluid is assumed to be homogeneous in nature (ρ is constant), the continuity equation (II.1) reduces to

$$\frac{\partial u}{\partial x} + \frac{\partial v}{\partial y} + \frac{\partial w}{\partial z} = \nabla \cdot \mathbf{u} = 0. \tag{II.14}$$

3. Implication of Shallow Fluid

This assumption allows significant simplification of our fluid motion model. Here, we assume that the surface scale of the problem at hand is much larger than that of any depth considerations. Pedlosky [13] outlines a scaling argument that shows how the relative importance of terms in the z –momentum equation allow all of the terms except for the pressure derivative and the gravity to be neglected. This collapses the z –momentum equation to

$$\frac{\partial p}{\partial z} = -\rho g.$$

We can then immediately depth integrate to yield

$$p = -\rho g z + A(x, y, t).$$

If the surface is under some constant ambient pressure $p(x, y, h) = p_0$, this implies that $A(x, y, t) = p_0 + \rho gh(x, y, t)$ thereby, giving us an expression for p

$$p(x, y, h) = \rho g (h(x, y, t) - z) + p_0.$$

We compute the pressure gradients in the x – and y – directions

$$\frac{\partial p}{\partial x} = \rho g \frac{\partial h(x, y, t)}{\partial x} \quad \frac{\partial p}{\partial y} = \rho g \frac{\partial h(x, y, t)}{\partial y}. \quad (\text{II.15})$$

Here, we note [13] that the pressure gradients are independent of z so that the horizontal accelerations must also be independent of z . For consistency, we therefore assume that the horizontal velocities will also be independent of z .

a. Primarily Horizontal Flow

We have already observed that since the flow in shallow waters is primarily along the surface, the z – momentum collapsed down significantly. We can use this argument to similarly simplify the x – and y – momentum equations. In this case, since w is significantly smaller than u or v , the terms $w \frac{\partial u}{\partial z}$ and $w \frac{\partial v}{\partial z}$ can also safely be neglected. Substituting these simplifications along with our pressure gradients (II.15) into (II.13) results in the x – and y – momentum equations:

$$\begin{aligned} \frac{\partial u}{\partial t} + u \frac{\partial u}{\partial x} + v \frac{\partial u}{\partial y} - f v &= -g \frac{\partial h(x, y, t)}{\partial x} \\ \frac{\partial v}{\partial t} + u \frac{\partial v}{\partial x} + v \frac{\partial v}{\partial y} - f u &= -g \frac{\partial h(x, y, t)}{\partial y}. \end{aligned} \quad (\text{II.16})$$

b. Continuity Equation Simplifications

We now depth integrate our continuity equation (II.14) from $z = -h_b(x, y)$ to $z = h(x, y, t)$. After dropping variable dependencies for clarity, this yields:

$$\begin{aligned} 0 &= \int_{-h_B}^h \nabla \cdot \mathbf{u} dz \\ &= \int_{-h_B}^h \left(\frac{\partial u}{\partial x} + \frac{\partial v}{\partial y} \right) dz + w|_{z=h} - w|_{z=-h_B}. \end{aligned} \quad (\text{II.17})$$

Considering reasonable boundary conditions for the last term as detailed in [12], we specify no normal flow on the rigid bottom ($-h_B$) and a corresponding kinematic condition at the fluid surface (h). These conditions are:

$$\begin{aligned} w(x, y, -h_B) &= -u \frac{\partial h_B}{\partial x} - v \frac{\partial h_B}{\partial y} \\ w(x, y, h, t) &= \frac{\partial h}{\partial t} + u \frac{\partial h}{\partial x} + v \frac{\partial h}{\partial y}. \end{aligned} \quad (\text{II.18})$$

Combining (II.17) and (II.18) yields (after simplification outlined in Appendix A)

$$\frac{\partial h}{\partial t} + \frac{\partial}{\partial x} (Hu) + \frac{\partial}{\partial y} (Hv) = 0. \quad (\text{II.19})$$

E. LINEARIZING THE SHALLOW WATER MODEL

The shallow water model in its current form is non-linear. We have three state variables, u , v , and h . Each of these are defined such that $u = u(x, y, t)$ and $v = v(x, y, t)$ are the unknown fluid velocities in the x and y directions, $h(x, y, t)$ is the unknown fluid elevation above the reference level, f is the Coriolis parameter, and g is the gravity acceleration. We now introduce the following shorthand for partial derivatives

$$\partial_a = \frac{\partial}{\partial a}, \quad \partial_{ab} = \frac{\partial^2}{\partial a \partial b}$$

We wish to find a linear version of these equations. Right now, we have

$$\begin{aligned}
\partial_t u + u \partial_x u + v \partial_y u - f v &= -g \partial_x h \\
\partial_t v + u \partial_x v + v \partial_y v + f u &= -g \partial_y h \\
\partial_t h + \partial_x (H u) + \partial_y (H v) &= 0.
\end{aligned} \tag{II.20}$$

Now, suppose that the bottom topography is flat such that h_B is constant and u and v can be described by a constant *mean* term and a small $O(\delta)$ deviation from that value, i.e.,

$$u = U + u^* \quad v = V + v^* \quad H = h_B + h$$

To be clear, U and V are the mean velocities and h_B is the mean water elevation. Using these substitutions and neglecting any $O(\delta^2)$ terms results in the linearized form of the shallow water equations (see Appendix B for details):

$$\begin{aligned}
\partial_t u^* + U \partial_x u^* + V \partial_y u^* - f(V + v^*) &= -g \partial_x h \\
\partial_t v^* + U \partial_x v^* + V \partial_y v^* + f(U + u^*) &= -g \partial_y h \\
\partial_t h + U \partial_x h + V \partial_y h + h_B (\partial_x u^* + \partial_y v^*) &= 0.
\end{aligned} \tag{II.21}$$

F. KLEIN-GORDON EQUIVALENT TO THE SHALLOW WATER MODEL

Using the linearized form of the shallow water equations, we can find a *Klein-Gordon* equation equivalent through a series of linear operations as outlined by Pedlosky [13]. We begin by defining the operator (linearized Lagrangian derivative)

$$\frac{D}{Dt} = \partial_t + U \partial_x + V \partial_y. \tag{II.22}$$

Substituting (II.22) into (II.21) we have the modified form

$$\frac{Du^*}{Dt} - f(V + v^*) = -g \partial_x h \quad (\text{II.23})$$

$$\frac{Dv^*}{Dt} + f(U + u^*) = -g \partial_y h \quad (\text{II.24})$$

$$\frac{Dh}{Dt} + h_B (\partial_x u^* + \partial_y v^*) = 0. \quad (\text{II.25})$$

Taking f as constant (along some latitude) and summing the partial derivative of (II.23) with respect to x and the partial derivative of (II.24) with respect to y , we have

$$\begin{aligned} & \partial_x \left(\frac{Du^*}{Dt} \right) - f \partial_x v^* = -g \partial_{xx} h \\ & + \quad \partial_y \left(\frac{Dv^*}{Dt} \right) + f \partial_y u^* = -g \partial_{yy} h \\ \hline & \frac{D}{Dt} (\partial_x u^* + \partial_y v^*) + f (\partial_y u^* - \partial_x v^*) = -g \nabla^2 h \end{aligned} \quad (\text{II.26})$$

Similarly, we find the difference of the partial derivative of (II.23) with respect to y and the partial derivative of (II.24) with respect to x to find

$$\begin{aligned} & \partial_y \left(\frac{Du^*}{Dt} \right) - f \partial_y v^* = -g \partial_{xy} h \\ & - \quad \partial_x \left(\frac{Dv^*}{Dt} \right) + f \partial_x u^* = -g \partial_{xy} h \\ \hline & \frac{D}{Dt} (\partial_y u^* - \partial_x v^*) - f (\partial_x u^* + \partial_y v^*) = 0 \end{aligned} \quad (\text{II.27})$$

We apply the operator $\frac{D}{Dt}$ to (II.26) and add $-f$ times (II.27)

$$\begin{aligned} & \frac{D^2}{Dt^2} (\partial_x u^* + \partial_y v^*) + f \frac{D}{Dt} (\partial_y u^* - \partial_x v^*) = -g \frac{D}{Dt} (\nabla^2 h) \\ & + \quad f^2 (\partial_x u^* + \partial_y v^*) - f \frac{D}{Dt} (\partial_y u^* - \partial_x v^*) = 0 \\ \hline & \frac{D^2}{Dt^2} (\partial_x u^* + \partial_y v^*) + f^2 (\partial_x u^* + \partial_y v^*) = -g \frac{D}{Dt} (\nabla^2 h). \end{aligned} \quad (\text{II.28})$$

From (II.25), we know that $-\frac{1}{h_B} \frac{Dh}{Dt} = \partial_x u^* + \partial_y v^*$, which can be used in (II.28)

$$\frac{D^2}{Dt^2} \left(-\frac{Dh}{Dt} \right) + f^2 \left(-\frac{Dh}{Dt} \right) = -gh_B \frac{D}{Dt} (\nabla^2 h)$$

which, after factoring $\frac{D}{Dt}$, becomes

$$\frac{D}{Dt} \left(\frac{D^2 h}{Dt^2} + f^2 h - gh_B \nabla^2 h \right) = 0.$$

We can rewrite this equation as

$$\frac{D^2 h}{Dt^2} + f^2 h - c_0^2 \nabla^2 h = S(x, y, t)$$

where $c_0^2 = gh_B$ and $\frac{D}{Dt} \left(S(x, y, t) \right) = \partial_t S + U \partial_x S + V \partial_y S = 0$. This source term we will assume to be zero, giving us the homogeneous form

$$\frac{D^2 h}{Dt^2} + f^2 h - c_0^2 \nabla^2 h = 0.$$

If we expand the operator $\frac{D}{Dt}$ twice, we get an expanded Klein-Gordon form

$$(\partial_t + U \partial_x + V \partial_y)^2 h - c_0^2 \nabla^2 h + f^2 h = 0 \quad (\text{II.29})$$

of the shallow water equations under constant advection U and V and dispersion evidenced by the f^2 term. This equation specifies the perturbation of the wave height h above a reference level h_B .

G. RECOVERING THE FLUID VELOCITIES

Suppose now that we have the solution for $h(x, y, t)$. In order to recover the fluid velocities $u(x, y, t)$ and $v(x, y, t)$, we consider the modified form of our shallow water model shown in (II.23)-(II.25). We first apply the operator $\frac{D}{Dt}$ to (II.23) and multiply (II.24)

by f to yield:

$$\frac{D^2 u^*}{Dt} - f \frac{Dv^*}{Dt} - f \frac{DV}{Dt} = -g \frac{D}{Dt} \left(\frac{\partial h}{\partial x} \right) \quad (\text{II.30})$$

$$f \frac{Dv^*}{Dt} + f^2 (U + u^*) = -gf \frac{\partial h}{\partial y} \quad (\text{II.31})$$

Adding (II.30) and (II.31) yields:

$$\left(\frac{D^2}{Dt} + f^2 \right) u^* + f^2 U = -g \left(\frac{D}{Dt} \left(\frac{\partial h}{\partial x} \right) + f \frac{\partial h}{\partial y} \right). \quad (\text{II.32})$$

The solution of this partial differential equation (no more difficult to solve than the equation for the perturbation of the wave height h) gives us the fluid velocity in the x direction.

A similar manipulation (subtracting f times (II.23) from $\frac{D}{Dt}$ operating on (II.24)) yields:

$$\left(\frac{D^2}{Dt} + f^2 \right) v^* + f^2 V = -g \left(\frac{D}{Dt} \left(\frac{\partial h}{\partial y} \right) - f \frac{\partial h}{\partial x} \right). \quad (\text{II.33})$$

The solution of this partial differential equation gives us the fluid velocity in the y direction.

III. HIGH ORDER NON-REFLECTING BOUNDARIES

The numerical solution of a wave propagation problem in a very large or unbounded domain provides a challenging computational difficulty – namely, solving the problem on a finite computational domain while maintaining the true *essence* of the solution. One of the modern techniques that has garnered a significant amount of attention in handling this challenge is the absorbing or non-reflecting boundary condition (NRBC) method. In using this method, the original infinite domain is truncated by an artificial boundary \mathcal{B} , resulting in a finite computational domain Ω and the residual domain D . Figure 4 illustrates the NRBC set-up using an infinite wave guide. Here, the artificial boundary \mathcal{B} extends from the southern (Γ_S) to the northern (Γ_N) boundaries of the wave-guide, thus creating the east (Γ_E) and west (Γ_W) boundaries of Ω at $x = x_E, x_W$ respectively. Appropriate boundary conditions are prescribed on the northern (Γ_N) and southern (Γ_S) boundaries. Outside of the area enclosed by these boundaries is the residual infinite domain D .

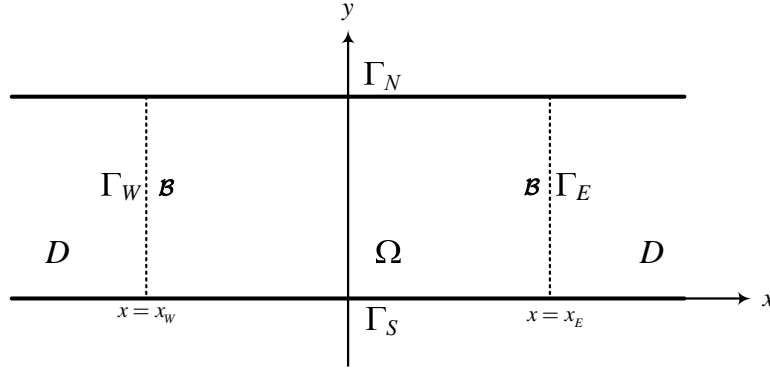


Figure 4: An infinite wave-guide truncated by artificial boundaries Γ_W and Γ_E

One would expect that the introduction of any boundary \mathcal{B} , where one does not physically exist, to pollute the solution through the reflection induced by such an artificial boundary. In the last two decades, significant efforts have been extended to find stable,

efficient, accurate and practical means of reducing this reflection through so-called NRBCs [18].

Several *high-order* NRBCs have been devised to reduce spurious reflections that would pollute the solution. Beginning in the late 1980s, the well-known Engquist-Majda [19] and Bayliss-Turkel conditions [1] gave way to Collino’s [2] low derivative, auxiliary variable formulation for the 2D scalar wave equation. This sparked a flurry of activity in an effort to find quality, high-order NRBCs that were easily implementable. The sheer volume of literature on the topic of boundary conditions for infinite problems suggests that there is no “perfect” boundary condition available for general purpose use. In reality, a modeler must make decisions on how to balance accuracy, efficiency and ease of implementation to yield reasonable solutions. Extensive reviews on the topic can be found in [18, 20, 21, 17]

A. HIGDON SCHEME

The starting point for the family of NRBCs discussed in this dissertation is the condition devised by Higdon in a series of papers [22, 23, 24, 25, 26, 27], that was demonstrated in a low-order finite difference setting. While in theory, Higdon’s NRBC is considered a high-order NRBC, the formulation requires evaluation of increasing high-order spatial and temporal derivatives as the order of the NRBC is increased. Higdon’s condition (and most NRBCs for that matter) seeks to annihilate waves impinging normal to a boundary. To see the idea behind this condition, consider a one-dimensional wave equation

$$\partial_{tt}h - c_0^2 \partial_{xx}h = 0$$

whose solution was obtained by d’Alembert in 1747 [28], as

$$h(x, t) = F(x - c_0t) + G(x + c_0t).$$

This solution implies that there are two components to the solution – one wave G of fixed shape moving to the left at velocity $-c_0$ and one wave F of fixed shape moving to the

right at velocity c_0 . Now, suppose that the right moving wave approaches a boundary. To perfectly absorb the wave impinging on the boundary, the boundary must satisfy $G = 0$ such that the boundary condition is $h(x, t) = F(x - c_0 t)$. Differentiating the boundary condition with respect to x and t results in:

$$\partial_x h = F'(x - c_0 t), \quad \partial_t h = -c_0 F'(x - c_0 t), \quad (\text{III.1})$$

which implies

$$\partial_t h + c_0 \partial_x h = 0. \quad (\text{III.2})$$

This is the Sommerfeld radiation condition for the eastern boundary. If we expand the discussion to two-dimensional problems, this condition implicitly assumes that by the time the wave front reaches the boundary, it is traveling primarily as a plane wave at speed c_0 .

1. Accounting for Dispersion

In a non-dispersive medium, waves can propagate without deformation. The challenge associated with dispersive waves such as the Klein-Gordon equivalent under consideration here, is that the wave speed depends on the frequency of the wave. Thus, if using the Sommerfeld radiation condition (III.2), only the waves traveling at phase speed c_0 will be absorbed – for all others, only a portion of the wave will be absorbed. Higdon considered a composition of J of these simple first order operators to yield his boundary condition:

$$H_J : \quad \left[\prod_{j=1}^J \left(\partial_n + \frac{1}{C_j} \partial_t \right) \right] h = 0 \quad \text{on } \Gamma \quad (\text{III.3})$$

where ∂_n is the normal derivative on the boundary. In the case of the wave guide shown in Figure 4, this derivative is ∂_x and $-\partial_x$ corresponding to the eastern and western boundaries respectively. The boundary condition contains parameters C_j that can be interpreted in terms of the phase velocities of waves absorbed exactly at the boundary. Except in contrived examples, there are infinitely many waves composing the solution, and in a dispersive

medium, a corresponding infinitely many phase velocities. A choice of the order J of the boundary condition seeks to annihilate the “most significant” J waves.

2. Reflection Caused by the Boundary

For purposes of illustration, consider a simplified version of (II.29) where U, V are both zero

$$\partial_{tt}h - c_0^2 \nabla^2 h + f^2 h = 0. \quad (\text{III.4})$$

Further, suppose that the domain is structured such that the NRBC is imposed only on the eastern boundary of a rectangular grid as shown in Figure 5. On the south and north

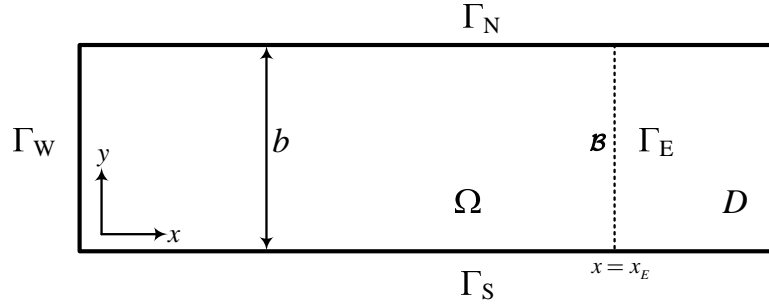


Figure 5: A semi-infinite channel truncated by artificial boundary Γ_E

boundaries (Γ_S and Γ_N), we have no normal flow, i.e.,:

$$\partial_y h = 0 \quad \text{on } \Gamma_N \text{ and } \Gamma_S \quad (\text{III.5})$$

and we impose $h = f(y, t)$ on Γ_W . As $x \rightarrow \infty$ the solution is known to be bounded and not to include any incoming waves. A solution to (III.4) has the form

$$h(x, y, t) = Y(y) \cos(kx - \omega t + \phi) \quad (\text{III.6})$$

such that $Y(y)$ satisfies (III.4). One such example $Y(y) = \cos \frac{n\pi y}{b}$ for $n = 0, 1, 2, \dots$ that satisfies these boundary conditions is given by Givoli and Neta [29]. Given this choice for

$Y(y)$, the dispersion relation is

$$\omega^2 = c_0^2 \left(k^2 + \frac{n^2 \pi^2}{b^2} \right) + f^2, \quad n = 0, 1, 2, \dots \quad (\text{III.7})$$

In this solution, k is the horizontal wavenumber, n is a parameter for controlling the shape of $Y(y)$, ω is the wave frequency and ϕ is the phase shift. The horizontal phase velocity [28] is therefore $C_k = \frac{\omega}{k}$ for a particular wave number. Suppose that one of the C_j 's in (III.3) equals C_k .

$$\begin{aligned} \partial_t h &= \omega Y(y) \sin(kx - \omega t + \phi) \\ \partial_x h &= -k Y(y) \sin(kx - \omega t + \phi) \\ \text{so that} \quad 0 &= \partial_t h + \frac{\omega}{k} \partial_x h \end{aligned}$$

thus, satisfying the Higdon boundary condition (III.3) exactly for that particular mode. If, however, none of the C_j 's were identically C_k , then a portion of the mode would be reflected and the boundary condition would not be exactly satisfied. To make the boundary condition true, it would have to be adjusted to incorporate the reflected modes. Higdon [27] sketches and Dea [17] details via a simple induction argument that proves the reflection coefficient R_J is

$$R_J = \prod_{j=1}^J \left| \frac{C_j - C_k}{C_j + C_k} \right|. \quad (\text{III.8})$$

We notice here that R_J is a product of factors that are each less than one. Therefore, simply increasing the order of the NRBC (J) reduces the amplitude of the reflected wave irrespective of the choice of C_j . van Joolen et al. [30, page 1045] notes, ‘‘Of course, a good choice for the C_j would lead to better accuracy with a lower order J , but even if the ‘wrong’ C_j 's are taken ... one is still guaranteed to reduce the spurious reflection as the order J increases.’’ We can use the dispersion relation together with the definition of the

horizontal phase velocity C_k to find that

$$\begin{aligned} C_k &= \frac{\sqrt{c_0^2 \left(k^2 + \frac{n^2 \pi^2}{b^2}\right) + f^2}}{k} \\ &= \sqrt{c_0^2 + \frac{c_0^2 \frac{n^2 \pi^2}{b^2} + f^2}{k^2}}, \end{aligned}$$

which shows that $C_k \geq c_0$ and therefore guides our selection of C_j to always be at least c_0 .

Based on the preceding discussion, we outline some of the inviting characteristics of the Higdon NRBC.

- The boundary condition is tractable, extending basic principles to arrive at the final condition.
- They are exact for all waves that propagate with speed C_j .
- Reflection is guaranteed to decrease by simply increasing the order of the NRBC.
- They have been applied to a wide variety of wave-type problems including those in dispersive media [17, 22, 23, 24, 25, 26, 27, 29, 31, 32].

The boundary condition, however, suffers from an implementation point of view. Due to the increasing order in the spatial and temporal derivatives required, even Higdon in his original papers considered practical implementation to be no more than $J = 3$.

B. HIGDON ADJUSTMENTS FOR ADVECTION

In the discussion of Higdon's boundary condition above, we considered the zero advection case. Eventually we wish to implement the Klein-Gordon equivalent which includes constant advection. Here, we discuss modifications to Higdon's scheme to accommodate non-zero, constant advection. This discussion will use physical arguments that will be reinforced by numerical considerations later in this dissertation. To begin, we consider a wave augmented by advection impinging on the NRBC of the semi-infinite channel shown

in Figure 5. Implicit in this derivation is that by the time the wave pulse arrives at the NRBC, it is traveling primarily as a plane wave (in the x -direction). The wave moves according to the equation under consideration,

$$(\partial_t + U\partial_x + V\partial_y)^2 h - c_0^2 \nabla^2 h + f^2 h = 0.$$

If, however, this wave is moving primarily in the x -direction, then any effects of y are negligible. Further, as in the derivation of the Sommerfeld radiation condition (III.2), we first consider a non-dispersive environment such that $f^2 = 0$ in this derivation to suggest an appropriate boundary condition. This simplifies our discussion to a wave that moves according to

$$(\partial_t + U\partial_x)^2 h - c_0^2 \partial_{xx} h = 0. \quad (\text{III.9})$$

As outlined in Appendix C, the solution takes the form

$$h(x, t) = F\left(x - (c_0 + U)t\right) + G\left(x + (c_0 - U)t\right) \quad (\text{III.10})$$

with the interpretation that the general solution is the sum of F , a wave of fixed shape moving to the right with velocity $c_0 + U$ and G , a wave of fixed shape moving to the left with velocity $c_0 - U$.

As described in III.A, if we consider the wave moving to the right approaching the eastern boundary, the boundary must satisfy $G = 0$ such that the boundary condition is $h(x, t) = F\left(x - (c_0 + U)t\right)$. Differentiating the boundary condition with respect to x and t results in:

$$\partial_x h = F'\left(x - (c_0 + U)t\right) \quad \partial_t h = -(c_0 + U)F'\left(x - (c_0 + U)t\right),$$

which implies

$$\partial_t h + (c_0 + U)\partial_x h = 0.$$

Following the discussion for the reflection coefficient, this suggests the “educated” choice of augmenting the Higdon parameter C_j with the added advection. This choice will be revisited later in this dissertation.

C. GIVOLI-NETA AUXILIARY VARIABLE FORMULATION

In [29], Givoli and Neta directly extended the Higdon scheme to high-order finite difference discretizations via an algorithm where the order of the NRBC was simply an input parameter. They later extended this formulation [33] to one that does not involve any high derivatives (hereafter referred to as the G-N formulation). The elimination of all high-order derivatives is enabled through the introduction of special auxiliary variables on \mathcal{B} . This construction demonstrated in [33] and [34] for finite differences was further extended in [35] for finite element schemes to solve the dispersive wave equation. Hagstrom and Warburton [36] also used the Higdon and auxiliary variable framework to develop a symmetric boundary formulation in a full-space configuration where special corner compatibility conditions were developed for the non-dispersive wave equation. Extensions and comparisons between the two methods were published by Givoli and Hagstrom et al. in [37] and [38].

We present a brief summary of the G-N auxiliary variable process as described in [35]. For the semi-infinite channel shown in Figure 5, this auxiliary formulation begins with the Higdon boundary condition given by:

$$H_J : \left[\prod_{j=1}^J \left(\partial_x + \frac{1}{C_j} \partial_t \right) \right] h = 0 \text{ on } \Gamma_E. \quad (\text{III.11})$$

Auxiliary functions $\phi_1, \dots, \phi_{J-1}$, which are defined on Γ_E as well as in the exterior domain D are now introduced. Eventually, we shall use these functions only on Γ_E , but the derivation requires that they be defined in D as well, or at least in a non-vanishing region

adjacent to Γ_E . The functions ϕ_j are defined via the relations

$$\left(\partial_x + \frac{1}{C_1}\partial_t\right)h = \phi_1, \quad (\text{III.12})$$

$$\left(\partial_x + \frac{1}{C_2}\partial_t\right)\phi_1 = \phi_2, \quad (\text{III.13})$$

\vdots

$$\left(\partial_x + \frac{1}{C_J}\partial_t\right)\phi_{J-1} = 0. \quad (\text{III.14})$$

By definition, these relations hold in D , and also on Γ_E . It is easy to see that (III.12 - III.14), when imposed as boundary conditions on Γ_E , are equivalent to the single boundary condition (III.11). If we also define

$$\phi_0 \equiv h \quad \phi_J \equiv 0, \quad (\text{III.15})$$

then we can write (III.12 - III.14) concisely as

$$\left(\partial_x + \frac{1}{C_j}\partial_t\right)\phi_{j-1} = \phi_j \quad j = 1, \dots, J. \quad (\text{III.16})$$

This set of conditions involves only first-order derivatives. However, due to the appearance of the x -derivative in (III.16), one cannot discretize the ϕ_j on the boundary Γ_E alone. Therefore we shall manipulate (III.16) in order to get rid of the x -derivative.

The function h satisfies the dispersive, advective wave equation (II.29) in D . Since the function ϕ_1 is obtained by applying the linear (constant coefficient) operator $\left(\partial_x + \frac{1}{C_1}\partial_t\right)$ to h , it can be shown that ϕ_1 should also satisfy the same equation in D^4 . Further, since ϕ_j is obtained by applying the same linear operator $j - 1$ times to ϕ_1 , the functions ϕ_j

⁴Here we must use the assumption that c_0 and f are constants. By applying the differential operator to (II.29), computing each of the ϕ_j derivatives present in (III.17) using the differential operator and simplifying, a simple induction argument shows that the ϕ_j 's must satisfy (III.17)

should satisfy an equation like (II.29), namely,

$$\begin{aligned} & \left(\partial_{tt} + (U^2 - c_0^2) \partial_{xx} + (V^2 - c_0^2) \partial_{yy} + \right. \\ & \left. 2U \partial_{xt} + 2V \partial_{yt} + 2UV \partial_{xy} + f^2 \right) \phi_j = 0 \end{aligned} \quad (\text{III.17})$$

Using the following identities:

$$\begin{aligned} \partial_{xx} \phi_j &= \left(\partial_x - \frac{1}{C_{j+1}} \partial_t \right) \left(\partial_x + \frac{1}{C_{j+1}} \partial_t \right) \phi_j + \frac{1}{C_{j+1}^2} \ddot{\phi}_j \\ \partial_{xt} \phi_j &= \partial_t (\partial_x \phi_j) \\ \partial_{xy} \phi_j &= \partial_y (\partial_x \phi_j) \end{aligned}$$

and combining with (III.16) allows us to write (III.17) as:

$$\begin{aligned} & \left(\frac{2U}{C_j} - 1 - \frac{U^2 - c_0^2}{C_j^2} \right) \ddot{\phi}_{j-1} + \left(\frac{2UV}{C_j} - 2V \right) \dot{\phi}'_{j-1} - (V^2 - c_0^2) \phi''_{j-1} + \\ & \left((U^2 - c_0^2) \left(\frac{1}{C_j} + \frac{1}{C_{j+1}} \right) - 2U \right) \dot{\phi}_j - 2UV \phi'_j - f^2 \phi_{j-1} = (U^2 - c_0^2) \phi_{j+1} \\ & \text{for } j = 1, \dots, J-1. \end{aligned} \quad (\text{III.18})$$

The details of this transformation are shown in Appendix D. In (III.18) and elsewhere, a prime indicates differentiation with respect to y along Γ_E , i.e., the tangential derivative along Γ_E . As desired, the new boundary condition (III.18) does not involve x -derivatives. In addition, there are no high- y or t derivatives beyond second order. It should be noted that van Joolen et al. [31] developed an equivalent formulation in using Lagrangian derivatives.

Rewriting (III.12), (III.18) and (III.15), the new formulation of the J^{th} -order NRBC on Γ_E can be summarized as follows:

$$\beta_0 \dot{h} + \partial_x h = \phi_1, \quad (\text{III.19})$$

$$\alpha_j \ddot{\phi}_{j-1} + \kappa_j \dot{\phi}'_{j-1} - \lambda_y \phi''_{j-1} + \beta_j \dot{\phi}_j - \gamma \phi'_j - f^2 \phi_{j-1} = \lambda_x \phi_{j+1} \quad (\text{III.20})$$

$$\phi_0 \equiv h \quad \phi_J \equiv 0 \quad (\text{III.21})$$

where

$$\begin{aligned} \beta_0 &= \frac{1}{C_1}, & \alpha_j &= \frac{2U}{C_j} - 1 - \frac{U^2 - c_0^2}{C_j^2}, & \kappa_j &= \frac{2UV}{C_j} - 2V, & \lambda_y &= V^2 - c_0^2, \\ \beta_j &= (U^2 - c_0^2) \left(\frac{1}{C_j} + \frac{1}{C_{j+1}} \right) - 2U, & \gamma &= 2UV, & \lambda_x &= U^2 - c_0^2 \end{aligned}$$

What remains is to link the boundary condition to the interior formulation. As will be shown in the next chapter, the means to link the two formulations will naturally follow from the spectral element framework.

THIS PAGE INTENTIONALLY LEFT BLANK

IV. DISCRETIZATION VIA SPECTRAL ELEMENTS

Once a suitable NRBC is devised, the problem must be solved numerically in Ω by the finite difference, or, as in the case of this analysis, the spectral element (SE) method. The SE method, originally introduced by Patera, "... combines the generality of the finite element method with the accuracy of spectral techniques ..." [39, p. 468]. The key to the spectral element (SE) method is the careful selection of the integration and interpolation points in order to yield accurate but efficient solutions.

As indicated in Chapter III, the Givoli-Neta auxiliary variable formulation has been previously demonstrated in both finite difference and finite element schemes to *arbitrarily high* NRBC order, however, accuracy gains realized by increasing the NRBC order slowed significantly after certain orders. The SE formulation used in this dissertation seeks to remedy this limitation by using a high-order treatment of space (SE) to show the benefits of using a high-order boundary (G-N) scheme. It should be noted that the only other spectral element, high-order boundary approach (to the author's knowledge) is [40] that is in press. That paper shows how a SE approach combined with high-order boundary treatment significantly improves the accuracy for the non-dispersive wave equation on a semi-infinite channel using the Hagstrom-Warburton formulation [36]. The key difference in our work is that we use high order space, boundary *and* time integration (discussed later in this dissertation) in both a dispersive and non-dispersive wave equation setting. We show the details of early results (absent of advection) in [41].

What follows in this chapter is a brief overview of the SE method as presented by Giraldo [42]. Additional treatment of this method can be found in Giraldo-Restelli [43] or Pozrikidis [44]. For this problem, we will discuss two formulations - one for the interior and one for implementing the boundary conditions.

A. INTERIOR WEAK INTEGRAL FORMULATION

Finite difference schemes seek to discretize differential operators based on Taylor series representations of the function near a point. Spectral element schemes seek to solve the equations in a weak integral form. It can be shown that if the governing equations satisfy the weak integral form, then they also satisfy the differential form provided the test functions used are sufficiently differentiable.

The weak form of the problem in Ω is now constructed for the semi-infinite channel described in III.A.2. Following a standard Galerkin approach, the solution is sought in the space of test functions,

$$\mathcal{V} = \{h|h \in H^1(\Omega) \text{ and } h = f(y, t) \text{ on } \Gamma_W\}. \quad (\text{IV.1})$$

Here, $H^1(\Omega)$ is the Sobolev space of functions whose first derivatives are also square-integrable in Ω . Now, Equation (II.29) is multiplied by the globally defined basis functions $\Psi_i(x, y) \in \mathcal{V}$ and integrated over Ω so the weak form is:

$$\begin{aligned} & \int_{\Omega} \Psi_i \ddot{h} \, d\Omega + \lambda_x \int_{\Omega} \Psi_i \frac{\partial^2 h}{\partial x^2} \, d\Omega + \lambda_y \int_{\Omega} \Psi_i \frac{\partial^2 h}{\partial y^2} \, d\Omega \\ & \quad + 2U \int_{\Omega} \Psi_i \frac{\partial \dot{h}}{\partial x} \, d\Omega + 2V \int_{\Omega} \Psi_i \frac{\partial \dot{h}}{\partial y} \, d\Omega \\ & + UV \int_{\Omega} \Psi_i \left(\frac{\partial^2 h}{\partial x \partial y} + \frac{\partial^2 h}{\partial y \partial x} \right) \, d\Omega + f^2 \int_{\Omega} \Psi_i h \, d\Omega = 0. \end{aligned} \quad (\text{IV.2})$$

Here, \dot{h} and \ddot{h} are the first second derivatives of h with respect to time. Further, $\frac{\partial \dot{h}}{\partial x}$ and $\frac{\partial \dot{h}}{\partial y}$ are the mixed second derivatives of h with respect to t, x and y .

In order to maintain a symmetric form of the problem, the mixed derivative has been split appropriately. To ensure the solution h is in the vector space H^1 requires some special handling of the second order derivatives, which is facilitated by the use of Green's theorem, i.e.,

$$\int_{\Omega} \Psi_i \frac{\partial^2 h}{\partial x^2} \, d\Omega = \int_{\Gamma} \Psi_i \frac{\partial h}{\partial x} n_x \, d\Gamma - \int_{\Omega} \frac{\partial \Psi_i}{\partial x} \frac{\partial h}{\partial x} \, d\Omega$$

where \vec{n} is the outward normal on Γ and n_x is the x -component of that outward normal.

Extending this idea for each second order derivative in (IV.2) gives the weak form:

$$\begin{aligned}
& \int_{\Omega} \Psi_i \ddot{h} \, d\Omega - \lambda_x \int_{\Omega} \frac{\partial \Psi_i}{\partial x} \frac{\partial h}{\partial x} \, d\Omega - \lambda_y \int_{\Omega} \frac{\partial \Psi_i}{\partial y} \frac{\partial h}{\partial y} \, d\Omega \\
& \quad - UV \int_{\Omega} \left(\frac{\partial \Psi_i}{\partial y} \frac{\partial h}{\partial x} + \frac{\partial \Psi_i}{\partial x} \frac{\partial h}{\partial y} \right) \, d\Omega \\
& + 2U \int_{\Omega} \Psi_i \frac{\partial \dot{h}}{\partial x} \, d\Omega + 2V \int_{\Omega} \Psi_i \frac{\partial \dot{h}}{\partial y} \, d\Omega + f^2 \int_{\Omega} \Psi_i h \, d\Omega \quad (\text{IV.3}) \\
& + \lambda_x \int_{\Gamma} \Psi_i \frac{\partial h}{\partial x} n_x \, d\Gamma + \lambda_y \int_{\Gamma} \Psi_i \frac{\partial h}{\partial y} n_y \, d\Gamma + UV \int_{\Gamma} \Psi_i \left(\frac{\partial h}{\partial x} n_y + \frac{\partial h}{\partial y} n_x \right) \, d\Gamma = 0.
\end{aligned}$$

Recall that for the semi-infinite channel described in Figure 5, the corresponding boundary conditions for Γ_N and Γ_S are $\partial_y h = 0$, displacement is specified on Γ_W and Γ_E is a non-reflecting boundary. Using these boundary conditions on the northern and southern borders along with the normal vectors specified by the structured, rectangular grid shown in Figure 6, the problem may be simplified to account for contributions on individual boundaries. Using this information along with (III.19) to eliminate the normal derivative term on Γ_E , we get:

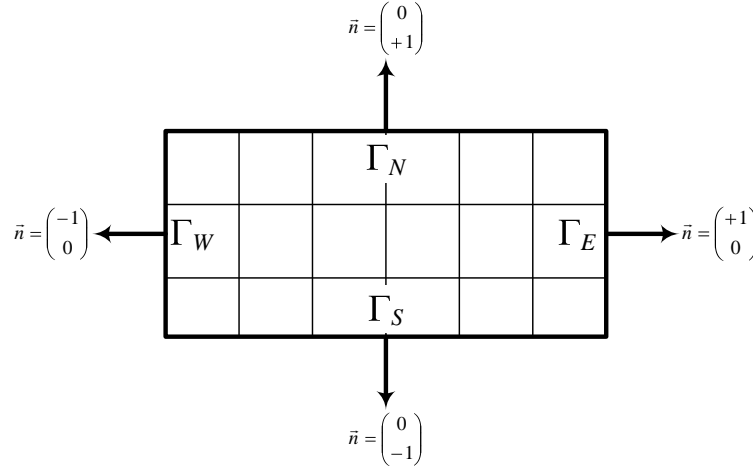


Figure 6: Normal Derivatives to Boundaries

$$\begin{aligned}
& \int_{\Omega} \Psi_i \ddot{h} \, d\Omega - \lambda_x \int_{\Omega} \frac{\partial \Psi_i}{\partial x} \frac{\partial h}{\partial x} \, d\Omega - \lambda_y \int_{\Omega} \frac{\partial \Psi_i}{\partial y} \frac{\partial h}{\partial y} \, d\Omega \\
& \quad - UV \int_{\Omega} \left(\frac{\partial \Psi_i}{\partial y} \frac{\partial h}{\partial x} + \frac{\partial \Psi_i}{\partial x} \frac{\partial h}{\partial y} \right) \, d\Omega \\
& + 2U \int_{\Omega} \Psi_i \frac{\partial \dot{h}}{\partial x} \, d\Omega + 2V \int_{\Omega} \Psi_i \frac{\partial \dot{h}}{\partial y} \, d\Omega + f^2 \int_{\Omega} \Psi_i h \, d\Omega \\
& \quad + \lambda_x \int_{\Gamma_E} \Psi_i \phi_1 \, d\Gamma_E - \beta_0 \lambda_x \int_{\Gamma_E} \Psi_i \dot{h} \, d\Gamma_E \\
& + UV \int_{\Gamma_N} \Psi_i \frac{\partial h}{\partial x} \, d\Gamma_N - UV \int_{\Gamma_S} \Psi_i \frac{\partial h}{\partial x} \, d\Gamma_S + UV \int_{\Gamma_E} \Psi_i \frac{\partial h}{\partial y} \, d\Gamma_E = 0.
\end{aligned} \tag{IV.4}$$

Note, that two of the boundary integrals (other than those on Γ_E) survive after simplification – namely on Γ_N and Γ_S . This occurs since the boundary condition (III.5) only specifies no flux (i.e., reflecting boundary conditions) on these boundaries. This is a common boundary condition for inviscid flow problems.⁵

B. BOUNDARY WEAK INTEGRAL FORMULATION

Since the term ϕ_1 appears in the interior formulation (IV.4), this is not a complete weak form of the problem in Ω . We turn our attention to computing a separate weak form for (III.20) to complete the problem statement. This solution is sought in the space of test functions,

$$\mathcal{V}_{\Gamma_E} = \{\phi_j | \phi_j \in H^1(\Gamma_E)\} \tag{IV.5}$$

where $H^1(\Gamma_E)$ is the Sobelov space of functions whose first derivatives are also square integrable on Γ_E .

As in the interior formulation, we multiply (III.20) by the globally defined, one-dimensional basis functions (on the boundary) $\zeta_i \in \mathcal{V}_{\Gamma_E}$ and integrate it over Γ_E . After

⁵It should be noted that in this analysis, the two-dimensional basis functions, Ψ_i , are constructed using tensor products of one-dimensional basis functions, ζ_i . This means that on the boundaries, these Ψ_i basis functions collapse to ζ_i on the boundary. Therefore, in practice the boundary integrals are constructed using ζ_i basis functions, requiring far less storage.

integration by parts and simplifying this yields:

$$\begin{aligned} \alpha_j \int_{\Gamma_E} \zeta_i \ddot{\phi}_{j-1} d\Gamma_E + \kappa_j \int_{\Gamma_E} \zeta_i \dot{\phi}'_{j-1} d\Gamma_E + \lambda_y \int_{\Gamma_E} \zeta'_i \phi'_{j-1} d\Gamma_E + \beta_j \int_{\Gamma_E} \zeta_i \dot{\phi}_j d\Gamma_E \\ - \gamma \int_{\Gamma_E} \zeta_i \phi'_j d\Gamma_E - f^2 \int_{\Gamma_E} \zeta_i \phi_{j-1} d\Gamma_E = \lambda_x \int_{\Gamma_E} \zeta_i \phi_{j+1} d\Gamma_E \end{aligned} \quad (\text{IV.6})$$

for $j = 1, \dots, J-1$. As in the interior formulation (IV.2), $\ddot{\phi}$ and $\dot{\phi}$ are the first and second derivatives of ϕ with respect to time and ϕ' is the tangential time derivative of ϕ . Recall from the auxiliary variable formulation (III.21) that $\phi_0 \equiv h$ and $\phi_J \equiv 0$.

The formal problem statement is then: Find $h \in \mathcal{V}$ and $\phi_j \in \mathcal{V}_{\Gamma_E}$ where $j = 1, \dots, J-1$, such that Equations (IV.4) and (IV.6) are satisfied $\forall \Psi_i \in \mathcal{V}$ and $\zeta_i \in \mathcal{V}_{\Gamma_E}$.

C. GRID GENERATION AND CHOICE OF BASIS FUNCTIONS

One of the key advantages of the spectral (finite) element formulation over differencing schemes is the ability to represent complex geometries by breaking up the domain into simple geometric shapes. Triangles and quadrilaterals are primarily used to represent these geometries in two-dimensions, while tetrahedra and hexahedra are primarily used to represent geometries in three-dimensions. The sheer volume of grid generation software available for generating triangles (tetrahedra) and the dearth of grid generation software for quadrilaterals (hexahedra) suggests that the former are the more common means of representing the geometry of a problem. However, there are some very nice properties of the latter that led to the choice of structured (and later unstructured) quadrilaterals to discretize the geometry in this analysis.

While triangular grids are typically easier to generate, quadrilateral elements can be formed directly, or more commonly, by combining two or four basic triangle elements as shown in Figure 7⁶. This idea can then be used to find an appropriate mesh for simple or complex geometries. For this analysis, unstructured quadrilaterals were generated using

⁶Adapted from [45], Figure 5.2, p. 141.

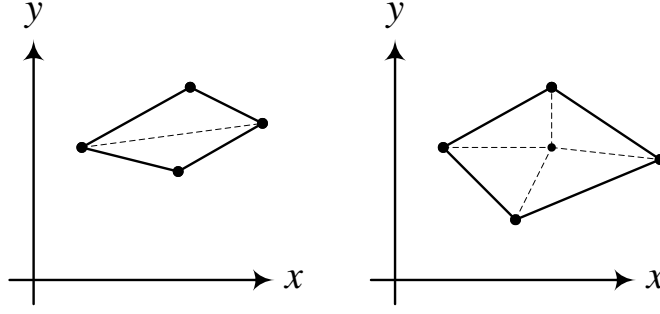


Figure 7: Arbitrary quadrilateral element formed by combining triangles.

Automesh-2D [46], an automatic mesh generator that provides high-quality results for the domains considered in this dissertation. A sample of the mesh that can be generated is shown in Figure 8⁷. Noteworthy in this mesh is that the complex geometry of each letter Ω has been broken up into approximately 200 non-overlapping quadrilateral elements Ω_e such that

$$\Omega = \bigcup_{e=1}^{Ne \approx 200} \Omega_e.$$

Further, each Ω_e is constructed such that all internal angles are all between 30° and 150° – a key criterion in providing a stable numerical solution.

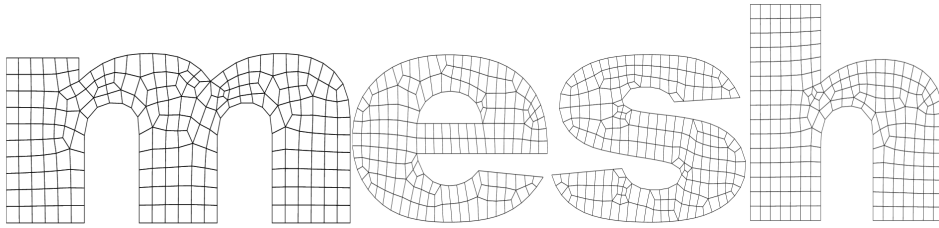


Figure 8: Sample mesh generated using Automesh-2D.

To see why this criterion is important, consider a mapping from the physical co-ordinate space to a canonical element space such that $x = x(\xi, \eta)$ and $y = y(\xi, \eta)$ where

⁷Geometry for the letters graciously provided by [46].

$(\xi, \eta) \in \Omega_c = [-1, 1]^2$. This nonsingular mapping is made to facilitate efficient and accurate computation of operations such as differentiation and integration [47]. One such element that illustrates this mapping can be seen in Figure 9. All derivatives are then mapped

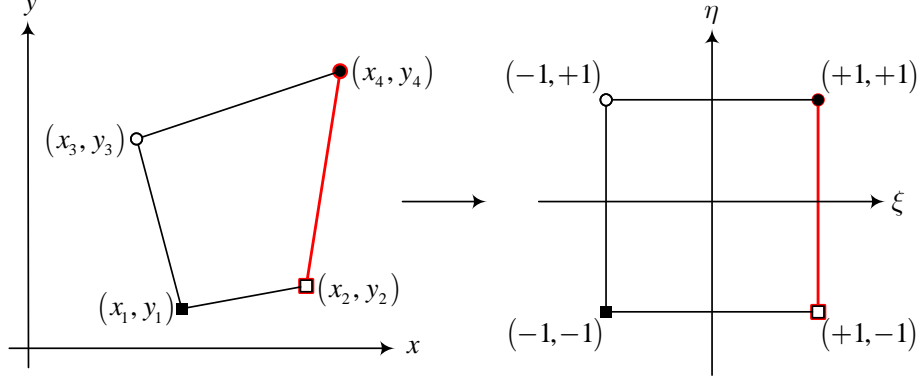


Figure 9: Mapping from physical space to computational space

to the canonical element space by virtue of the chain rule to yield the total derivative:

$$\begin{pmatrix} dx \\ dy \end{pmatrix} = \begin{pmatrix} \frac{\partial x}{\partial \xi} & \frac{\partial x}{\partial \eta} \\ \frac{\partial y}{\partial \xi} & \frac{\partial y}{\partial \eta} \end{pmatrix} \begin{pmatrix} d\xi \\ d\eta \end{pmatrix}.$$

From the total derivative, we can find key components required for the evaluation of the integrals induced by this canonical element mapping [42]. Such terms include the transformation Jacobian and its associated determinant:

$$J^e = \begin{pmatrix} \frac{\partial x}{\partial \xi} & \frac{\partial x}{\partial \eta} \\ \frac{\partial y}{\partial \xi} & \frac{\partial y}{\partial \eta} \end{pmatrix}, \quad |J^e| = \frac{\partial x}{\partial \xi} \frac{\partial y}{\partial \eta} - \frac{\partial y}{\partial \xi} \frac{\partial x}{\partial \eta}, \quad (\text{IV.7})$$

as well as mappings of metric terms:

$$\frac{\partial \xi}{\partial x} = \frac{1}{|J^e|} \frac{\partial y}{\partial \eta}, \quad \frac{\partial \xi}{\partial y} = -\frac{1}{|J^e|} \frac{\partial x}{\partial \eta}, \quad \frac{\partial \eta}{\partial x} = -\frac{1}{|J^e|} \frac{\partial y}{\partial \xi}, \quad \frac{\partial \eta}{\partial y} = \frac{1}{|J^e|} \frac{\partial x}{\partial \xi}. \quad (\text{IV.8})$$

If any of the nodes comprising the elements approach interior angles of 180° (degenerating the quadrilateral into a triangle), it can be shown that the transformation Jacobian at that

point tends to 0 causing each of the metric terms to tend toward infinity thus corrupting the solution. Derivation of the metric term mappings and consequences of degeneration of the quadrilateral are detailed in Appendix E.

Crucial to the construction of SE approximations is the representation of the solution variables in terms of smooth basis functions Ψ_i . While in theory these basis functions are defined throughout the entire domain Ω , they have compact support, and are in practice constructed locally. This implies that we can solve the global problem by simply summing up the contributions from the smaller elemental problems in a process known as *direct stiffness summation*. Ideally, these basis functions will not only support the grid chosen, but will also have properties that facilitate the numerical integration of the weak formulation [48].

For this analysis, the local element-wise solution h is represented by N^{th} order Lagrange polynomials in (ξ, η) such that

$$h_N(\xi, \eta) = \sum_{k=1}^{M_N} \psi_k(\xi, \eta) h(\xi_k, \eta_k)$$

where (ξ_k, η_k) are the $M_N = (N + 1)^2$ Legendre-Gauss-Lobatto (LGL) interpolation points and ψ_k are the associated multivariate Lagrange polynomial basis functions. The square structure of the canonical element simplifies matters in that we can express ψ_k by a tensor-product of the one-dimensional Lagrange polynomial basis functions as

$$\psi_k(\xi, \eta) = \nu_i(\xi) \nu_j(\eta)$$

where $i, j = 1, 2, \dots, N + 1$ and $k = 1, 2, \dots, M_N$. Further, ν_i and ν_j are the one-dimensional basis functions generated using the LGL points in ξ and η . To get from the one-dimensional local indices (i, j) to the two-dimensional local index k requires the mapping $k = i + (j - 1)(N + 1)$.

The choice of the LGL points for interpolant generation have the especially attractive property of allowing efficient quadrature. In particular, any polynomial of up to degree $2N - 1$ can be integrated *exactly* (to machine precision) by evaluating it at only $N + 1$ points. Additionally, if the interpolation points are also used as the sampling points in the Gaussian quadrature rule, it has the added benefit of yielding a diagonal mass matrix as the LGL-based basis functions Ψ satisfy a discrete orthogonality via the cardinality property of the Lagrange basis functions. The effect of these choices is to allow the appropriately weighted summation of the basis function expansion of h to evaluate all integrals. Therefore, to approximate a local elemental integral, we find

$$\begin{aligned} \int_{\Omega_e} h(x, y) d\Omega_e &= \int_{\Omega_c} h(\xi, \eta) |J^e| d\Omega_c \\ &\approx \sum_{i,j=1}^{N+1} \omega(\xi_i) \omega(\eta_j) h(\xi_i, \eta_j) |J^e(\xi_i, \eta_j)| \end{aligned}$$

where $\omega(\xi_i)$ and $\omega(\eta_j)$ are the quadrature weights associated with one-dimensional LGL quadrature and Ω_c is the canonical element region of integration. This process is described in greater detail in [42].

D. GALERKIN EXPANSION

We now turn our attention to the spatial discretization. First, we construct the N^{th} -order approximation of the variables h and ϕ_j using the same basis functions used in the weak form IV.4 and IV.6 as follows:

$$h_N = \sum_{k=1}^{N_p} \Psi_k h^k, \quad \phi_{jN} = \sum_{k=1}^{N_b} \zeta_k \phi_j^k, \quad j = 1, 2, \dots, J - 1.$$

Here, N_p and N_b are the number of points that Ω and Γ_E are discretized into, respectively. For a structured quadrilateral grid with N_e^x and N_e^y elements in the x and y directions, $N_p = (N_e^x N + 1)(N_e^y N + 1)$ and $N_b = N_e^y N + 1$. Next, we substitute this basis function

expansion directly into the weak formulations, resulting in the following interior

$$\begin{aligned} M\ddot{h} + (2UD_x + 2VD_y)\dot{h} + (-\lambda_x L_{xx} - \lambda_y L_{yy} + f^2 M - UV(L_{yx} + L_{xy}))h \\ + \lambda_x A_E \phi_1 - \beta_0 \lambda_x B_E \dot{h} + (UVC_N - UVC_S + UVC_E)h = 0 \end{aligned} \quad (\text{IV.9})$$

and boundary

$$\begin{aligned} \alpha_j M^b \ddot{\phi}_{j-1} + \zeta_j D^b \dot{\phi}_{j-1} + (\lambda_y L^b - f^2 M^b) \phi_{j-1} \\ + \beta_j M^b \dot{\phi}_j - \gamma D^b \phi_j - \lambda_x M^b \phi_{j+1} = 0, \quad j = 1, \dots, J-1 \end{aligned} \quad (\text{IV.10})$$

forms of the problem. Here, $M, D_x, D_y, L_{xx}, L_{yy}, L_{xy}$ and L_{yx} are interior formulation matrices of size $N_p \times N_p$. Further, B_E, C_N, C_S and C_E are interior formulation matrices integrated along the boundaries of size $N_p \times N_p$ while A_E is of size $N_p \times N_b$. Finally, M^b, D^b and L^b are auxiliary formulation matrices of size $N_b \times N_b$. These global matrices are obtained from analogous element arrays via assembly, given by:

$$\begin{aligned} M &= \bigwedge_{e=1}^{N_e} M^e, \quad B_E = \bigwedge_{e=1}^{N_e} B_E^e, & D_x &= \bigwedge_{e=1}^{N_e} D_x^e, \quad D_y = \bigwedge_{e=1}^{N_e} D_y^e \\ L_{xx} &= \bigwedge_{e=1}^{N_e} L_{xx}^e, \quad L_{yy} = \bigwedge_{e=1}^{N_e} L_{yy}^e, & L_{xy} &= \bigwedge_{e=1}^{N_e} L_{xy}^e, \quad L_{yx} = \bigwedge_{e=1}^{N_e} L_{yx}^e, \\ M^b &= \bigwedge_{b=1}^{N_b} m^b, \quad D^b = \bigwedge_{b=1}^{N_b} d^b, & L^b &= \bigwedge_{b=1}^{N_b} l^b, \quad C_N = \bigwedge_{e=1}^{N_e} C_N^e, \\ C_S &= \bigwedge_{e=1}^{N_e} C_S^e, \quad C_E = \bigwedge_{e=1}^{N_e} C_E^e, & A_E &= \bigwedge_{e=1}^{N_e} A_E^e \end{aligned}$$

where $\bigwedge_{e=1}^{N_e}$ is the direct stiffness summation operator required by all continuous Galerkin methods. The expressions for the element arrays are:

$$\begin{aligned}
M_{ij}^e &= \int_{\Omega_e} \psi_i \psi_j d\Omega_e & B_{E,ij}^e &= \int_{\Gamma_e} \psi_i \psi_j d\Gamma_e & D_{x,ij}^e &= \int_{\Omega_e} \psi_i \frac{\partial \psi_j}{\partial x} d\Omega_e \\
D_{y,ij}^e &= \int_{\Omega_e} \psi_i \frac{\partial \psi_j}{\partial y} d\Omega_e & L_{xx,ij}^e &= \int_{\Omega_e} \frac{\partial \psi_i}{\partial x} \frac{\partial \psi_j}{\partial x} d\Omega_e & L_{yy,ij}^e &= \int_{\Omega_e} \frac{\partial \psi_i}{\partial y} \frac{\partial \psi_j}{\partial y} d\Omega_e \\
L_{xy,ij}^e &= \int_{\Omega_e} \frac{\partial \psi_i}{\partial y} \frac{\partial \psi_j}{\partial x} d\Omega_e & L_{yx,ij}^e &= \int_{\Omega_e} \frac{\partial \psi_i}{\partial x} \frac{\partial \psi_j}{\partial y} d\Omega_e & m_{rs}^b &= \int_{\Gamma_e} \nu_r \nu_s d\Gamma_e \\
d_{rs}^b &= \int_{\Gamma_e} \nu_r \nu'_s d\Gamma_e & l_{rs}^b &= \int_{\Gamma_e} \nu'_r \nu'_s d\Gamma_e & C_{N,ij}^e &= \int_{\Gamma_e^N} \psi_i \frac{\partial \psi_j}{\partial x} d\Gamma_e^N \\
C_{S,ij}^e &= \int_{\Gamma_e^S} \psi_i \frac{\partial \psi_j}{\partial x} d\Gamma_e^S & C_{E,ij}^e &= \int_{\Gamma_e^E} \psi_i \frac{\partial \psi_j}{\partial y} d\Gamma_e^E & A_{E,ir}^e &= \int_{\Gamma_e^E} \psi_i \nu_r d\Gamma_e^E
\end{aligned}$$

where Ω_e and Γ_e denote, the part of Ω and Γ associated with element e . Also, ψ_i and ν_i are the locally defined basis functions from which the global basis functions (Ψ_i and ζ_i) are formed. For quadrilateral elements with polynomial order N as used in this analysis, ψ_i will be discretized into $(N+1)^2$ points, and ν_i into $(N+1)$ points, thus, $i, j = 1, 2, \dots, (N+1)^2$ and $r, s = 1, 2, \dots, N+1$.

Now, let:

$$\begin{aligned}
\mathbb{A} &= M^{-1} (\beta_0 \lambda_x B_E - 2U D_x - 2V D_y) \\
\mathbb{B} &= M^{-1} (\lambda_x L_x + \lambda_y L_y - f^2 M + UV (L_{xy} + L_{yx} - C_N + C_S - C_E)) \\
\mathbb{C} &= -\lambda_x M^{-1} A_E^b
\end{aligned} \tag{IV.11}$$

and substitute equations (IV.11) into (IV.9) to get the matrix form of the interior problem:

$$\ddot{h} = \mathbb{A} \dot{h} + \mathbb{B} h + \mathbb{C} \phi_1 \tag{IV.12}$$

If we examine the boundary auxiliary variable formulation (III.20), we see that the selection of appropriate C_j values for the auxiliary variables has not yet been fully addressed. As discussed in III.A.2, *any* choice of C_j is guaranteed to reduce spurious reflection as the order of the NRBC (J) increases, however based on the discussion in III.B, the Higdon parameter should somehow be augmented with the advection.

Armed with this, we choose convenient values for our C_j 's that cause the second order in time (α_j) terms to vanish. In the case of the semi-infinite channel, on the eastern boundary this value is: $C_j = c_0 + U$. A physical argument for this choice is that since the predominant speed of the wave, absent the advection terms, is c_0 , the C_j terms “correct” the boundary formulation to account for the advection. This selection for the C_j 's then makes:

$$\alpha_1 = \alpha_2 = \dots = \alpha_{J-1} = 0,$$

$$\kappa_1 = \kappa_2 = \dots = \kappa_{J-1} = \kappa,$$

$$\beta_1 = \beta_2 = \dots = \beta_{J-1} = \beta$$

Now, let:

$$\mathbb{D} = f^2 M^b - \lambda_y L^b \tag{IV.13}$$

and substitute (IV.13) into (IV.10) to get the following form of the problem:

$$\begin{aligned} \beta M^b \dot{\phi}_1 &= \mathbb{D} h_{\Gamma_E} - \kappa D^b \dot{u}_\Gamma + \gamma D^b \phi_1 + \lambda_x M^b \phi_2 \\ \kappa D^b \dot{\phi}_1 + \beta M^b \dot{\phi}_2 &= \mathbb{D} \phi_1 + \gamma D^b \phi_2 + \lambda_x M^b \phi_3 \\ \kappa D^b \dot{\phi}_2 + \beta M^b \dot{\phi}_3 &= \mathbb{D} \phi_2 + \gamma D^b \phi_3 + \lambda_x M^b \phi_4 \\ &\vdots \\ \kappa D^b \dot{\phi}_{J-2} + \beta M^b \dot{\phi}_{J-1} &= \mathbb{D} \phi_{J-2} + \gamma D^b \phi_{J-1} \end{aligned}$$

where h_{Γ_E} is the value of h on Γ_E . If we now collect the terms on the left and right, we get the matrix form of the problem:

$$\mathbb{E}\dot{\Phi} = \mathbb{F}\Phi + \bar{h} \quad (\text{IV.14})$$

where:

$$\mathbb{E} = \begin{pmatrix} \beta M^b & 0 & \dots & 0 \\ \kappa D^b & \beta M^b & \dots & 0 \\ \vdots & \vdots & \ddots & \vdots \\ 0 & 0 & \kappa D^b & \beta M^b \end{pmatrix}, \quad \mathbb{F} = \begin{pmatrix} \gamma D^b & \lambda_x M^b & 0 & \dots & 0 \\ \mathbb{D} & \gamma D^b & \lambda_x M^b & \dots & 0 \\ \vdots & \ddots & \ddots & \ddots & \vdots \\ 0 & 0 & \mathbb{D} & \gamma D^b & \lambda_x M^b \\ 0 & 0 & 0 & \mathbb{D} & \gamma D^b \end{pmatrix}$$

$$\Phi = \begin{pmatrix} \phi_1 \\ \phi_2 \\ \vdots \\ \phi_{J-1} \end{pmatrix}, \quad \dot{\Phi} = \begin{pmatrix} \dot{\phi}_1 \\ \dot{\phi}_2 \\ \vdots \\ \dot{\phi}_{J-1} \end{pmatrix} \quad \text{and} \quad \bar{h} = \begin{pmatrix} \mathbb{D}h_{\Gamma_E} - \kappa D^b \dot{h}_{\Gamma_E} \\ 0 \\ \vdots \\ 0 \end{pmatrix}.$$

THIS PAGE INTENTIONALLY LEFT BLANK

V. SOLUTION OF THE DYNAMIC SYSTEM

The equations described by (IV.12) and (IV.14) constitute a coupled system of ODEs that must be solved for $h(x, y, t)$. Our approach uses standard k^{th} order explicit Runge-Kutta (RK) methods to integrate the system in time. Recall that RK is used to solve first order ODEs, and as such, the second order systems described must be converted into a larger system of first order ODEs. Using the substitution $v = \dot{h}$, $\dot{v} = \ddot{h}$ yields the first order systems:

$$\begin{bmatrix} I & 0 \\ 0 & I \end{bmatrix} \begin{bmatrix} \dot{h} \\ \dot{v} \end{bmatrix} = \begin{bmatrix} 0 & I \\ \mathbb{B} & \mathbb{A} \end{bmatrix} \begin{bmatrix} h \\ v \end{bmatrix} + \begin{bmatrix} 0 \\ \mathbb{C}\phi_1 \end{bmatrix} \quad (\text{V.1})$$

$$\mathbb{E}\dot{\Phi} = \mathbb{F}\Phi + \bar{h}.$$

This system was solved using a two-stage approach at each time step. First, the auxiliary system was solved to find the component ϕ_1 required for the main system. Then the main system was solved to find h at the next time step. This process was continued until the final time t_f was reached.

A. RUNGE-KUTTA METHODS

RK methods are convenient in this analysis in that the machinery to decrease the truncation error is the same for 2^{nd} , 3^{rd} or even k^{th} order schemes. While there are other schemes that require fewer function evaluations and, in fact, are more efficient than the explicit RK schemes used in this dissertation, we desired a method that could change the order of the time integration method simply as a parameter while using the same basic formulation. RK methods use a standard formulation that is outlined as follows.

To obtain an approximation to the solution of the initial value problem

$$y' = f(t, y(t)), \quad y(t_0) = y_0$$

a successive approximation y_{n+1} to y_n is given by

$$y_{n+1} = y_n + \Delta t \sum_{i=1}^s b_i k_i$$

where $k_i = f\left(t_n + c_i \Delta t, y_n + \Delta t \sum_{j=1}^s a_{ij} k_j\right) \quad i = 1, 2, \dots, s.$

Here, the coefficients a_{ij} , b_i and c_i are given by the Butcher tableau for the given RK scheme. The classical explicit RK-4 scheme is given by

$$\begin{array}{c|cccc} c_1 & a_{11} & a_{12} & a_{13} & a_{14} \\ c_2 & a_{21} & a_{22} & a_{23} & a_{24} \\ c_3 & a_{31} & a_{32} & a_{33} & a_{34} \\ c_4 & a_{41} & a_{42} & a_{43} & a_{44} \\ \hline & b_1 & b_2 & b_3 & b_4 \end{array} \Rightarrow \begin{array}{c|cccc} 0 & 0 & 0 & 0 & 0 \\ \frac{1}{2} & \frac{1}{2} & 0 & 0 & 0 \\ \frac{1}{2} & 0 & \frac{1}{2} & 0 & 0 \\ 1 & 0 & 0 & 1 & 0 \\ \hline \frac{1}{6} & \frac{1}{3} & \frac{1}{3} & \frac{1}{6} \end{array}.$$

For this analysis, all coefficients were computed using MapleTM using routines coded by Stone [49]. These routines allow for high precision computation of the coefficients required for each high-order tableau. Of course, the computational complexity increases for increased RK order. To be specific, the required number of function evaluations (stages) and non-zero parameters required for the k^{th} order RK method are given in Table 1

Table 1: Computational cost for RK methods used.

RK Order	2	3	4	5	6	7	8	9	10
Stages	2	3	4	6	7	9	11	16	18
Parameters	3	8	10	22	33	45	59	102	113

B. SIMPLE EXAMPLE OF CONVERGENCE

To see the effect of high-order time integration, consider the simple initial value problem

$$\frac{dy}{dt} = f(t, y) = (2 - t) y, \quad y(0) = e^{-2} \quad (\text{V.2})$$

whose solution is

$$y(t) = e^{-0.5(t-2)^2}.$$

Now, we integrate (V.2) in time using our RK schemes (RK-2 - RK-10) from $t = 0$ to $t = 5$ and quantify the errors observed over time between the exact and RK solution using the normalized L^2 error defined as follows:

$$\|error\|_{L^2} = \left(\frac{\sum_{n=1}^N \left(y_n - y(n\Delta t + t_0) \right)^2}{\sum_{n=1}^N y(n\Delta t + t_0)^2} \right)^{\frac{1}{2}}$$

where y_n and $y(n\Delta t + t_0)$ are the numerical and reference solutions at a given time.

Using a time-step $\Delta t = 0.05$, we see exponential convergence (to near machine precision) of the error as indicated in Figure 10. It should be noted that in this example, even if an extremely fine time step is chosen, the computed error using lower order RK methods cannot achieve machine precision.

Take for instance the RK-4 method that has a truncation error of $O(\Delta t^4)$. A step size of $\Delta t = 10^{-4}$ should result in an error $O(10^{-16})$, yet experimentally, the error is $O(10^{-12})$. This apparent discrepancy can be explained by the *round-off* error due to the finite-precision arithmetic (double) used in the computation. This error increases with the total number of integration steps used. This implies that to integrate (V.2) from $t = 0$ to $t = 5$, we must evaluate $f(t, y)$ a total of 200,000 times for RK-4 at a time-step of $\Delta t = 10^{-4}$. If we compare this with a time-step of $\Delta t = 0.025$ using RK-10, this should result in an error $O(10^{-16})$. To integrate (V.2) using RK-10 for the same period of time,

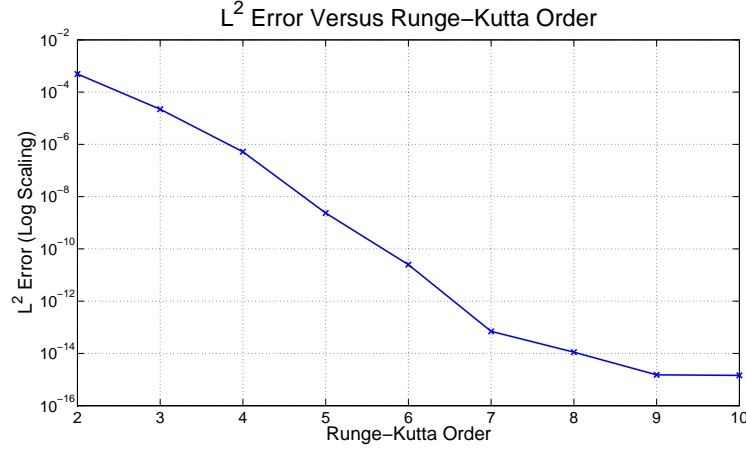


Figure 10: L^2 error in solution of (V.2) using RK-2 – RK-10 time integration.

we must evaluate $f(t, y)$ only 3,600 times. Experimentally, RK-10 achieves this $O(10^{-16})$ error convergence, thus highlighting the importance of *round-off* error in the convergence of the time integration scheme.

To check the convergence of these RK methods for *reasonable* time-step values $\Delta t \in [0.001, 1]$, consider the rate of convergence adapted from [50] and defined as follows:

$$rate = \frac{\log(error_{\Delta t_{n+1}}) - \log(error_{\Delta t_n})}{\log(\Delta t_{n+1}) - \log(\Delta t_n)}. \quad (V.3)$$

This rate is a measure of how rapidly a given time integration method converges as a function of the time-step refinement. Figure 11 shows the normalized L^2 error as a function of the time-step refinement. For each RK order, the rate of convergence is averaged over all Δt refinement levels. This average rate is annotated for each RK order and shows, as expected, that the maximum rate of convergence is the RK order. From this figure, we see that this theoretical rate of convergence is nearly reached in every case. It should be noted that once errors reach $O(10^{-15})$, round off errors prevent further improvements using a given RK method, and as already discussed, these errors actually prevent theoretical improvements of lower order (RK-2 and RK-4) methods.

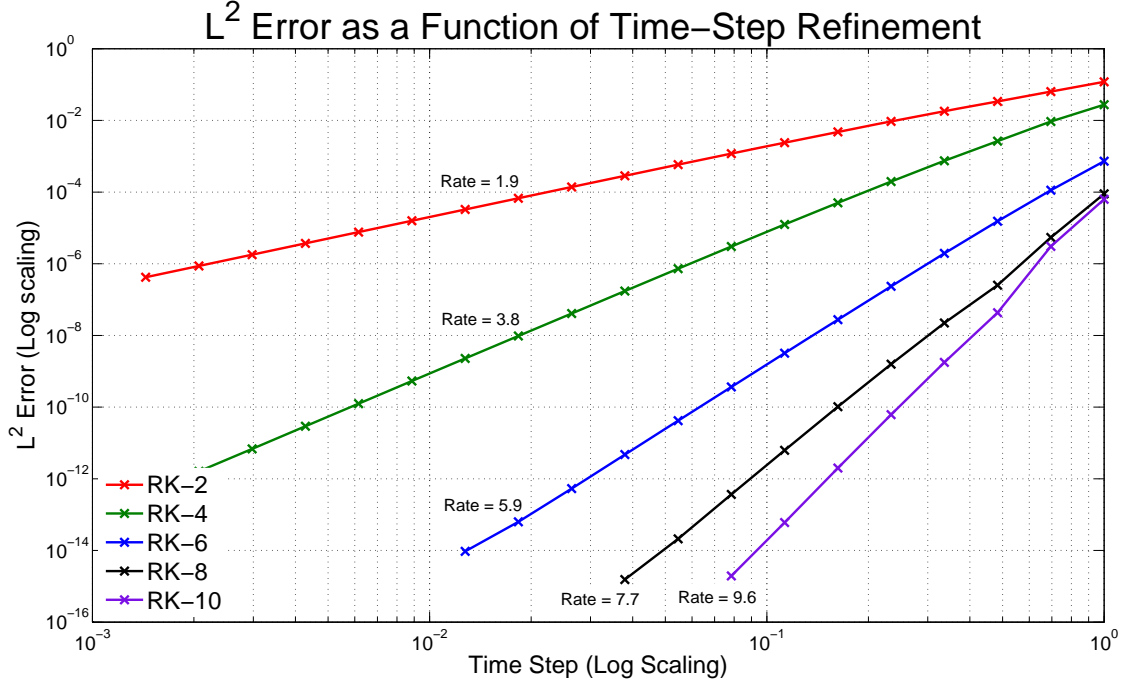


Figure 11: L^2 error as a function of time-step refinement. Rates as defined by (V.3) should correspond to RK order.

Of course, one might wonder why such high precision when integrating in time would ever be required. For most engineering applications, where the model parameters themselves are approximated, this argument is a strong one. Perhaps a lower order time integrator would result in errors that are on the same order as the model parameters and any computational effort incurred in using a high-order time integrator would be wasted. However, since this work centers on the use of high-order spectral elements along with high-order boundary conditions; high-order time-integrators were also explored to examine all of the limiting factors of high-order accuracy.

We propose that in order to see the full improvements of high-order boundary conditions requires a balance of truncation errors (and *round-off* errors) between all of the components of the numerical model; this includes the boundary conditions, the spatial discretization method, and the time-integrators. Practically speaking, we believe that the mathematical formulation should be the strong point of any model evaluation, specifically,

the order of the method should be chosen to match (or exceed) other errors inherent in the model. Experiments in this dissertation were conducted using boundary conditions up to order 20, SE polynomials up to order 16, and time-integrators up to order 10.

VI. NUMERICAL EXPERIMENTS

Several numerical experiments were performed to solve the Klein-Gordon equivalent (II.29) with and without dispersion and advection. Additionally, we consider five primary configurations: semi-infinite channel, infinite channel, quarter plane, open plane, and open unstructured plane. Each of these configurations will be described in detail later in this chapter.

In order to simplify the numerical simulation of the problem at hand, the KGE (II.29) is converted to a non-dimensional form as described in [51]. Using typical mesoscales in the ocean, the length scales were chosen $O(100 \text{ km})$, vertical depth scales $O(100 \text{ m})$ and the dispersion parameter f for Coriolis $O(10^{-4} \text{ s}^{-1})$. Majda [51, page 61] describes typical advective velocities as roughly $\frac{3}{100}$ that of the medium wave speed c_0 . Here, we choose to challenge the boundary further by choosing faster advective velocities at $\frac{1}{10}$ that of the medium wave speed. The derivation details of the non-dimensional formulation are given in Appendix F.

For experiments that follow, the reference wave speed is $c_0 = 1$, which allows the initial wave to propagate through the region of interest in a *reasonable* time for all experiments. Given the scale choices above yields a dispersion parameter f^2 of 0.1, however, to ensure that dispersion is *felt*, we choose $f^2 = 0.5$ corresponding to more than doubling of the angular velocity of the earth. Further, U and V are set to 0.0 or 0.1 under a two-dimensional Gaussian initial condition to test the formulation in a semi-infinite and infinite channel setting.

The experiments begin with an analytic benchmark where a solution is synthesized to the KGE and compared to results obtained using the NRBCs. The chapter continues with more general experiments, which do not have analytic solutions. In channel experiments, two different initial conditions were tested. The first is a two-dimensional cosine pulse where b is the height of the channel (in all cases we used $b = 4$). This pulse is chosen with compact support such that the waves are generated only in a narrow region of the domain

and is zero elsewhere. Additionally, the initial condition (by design) satisfies the no-flux boundary conditions on the northern and southern boundaries. The initial condition is given by

$$h(x, y, 0) = e^{-10x^2} \cos\left(\frac{4\pi y}{b}\right), \quad \dot{h}(x, y, 0) = 0. \quad (\text{VI.1})$$

The other initial condition used in the channel and remaining experiments is a two-dimensional Gaussian centered at $x = 0, y = 0$, given by

$$h(x, y, 0) = e^{-10(x^2+y^2)}, \quad \dot{h}(x, y, 0) = 0. \quad (\text{VI.2})$$

In order to see the effect of the NRBC, we compare our solutions to the one computed on a larger domain (for all experiments except the analytic benchmark). We consider this reference solution “exact” when using equal order basis functions on a *fine* mesh, defined in greater detail in each of the subsequent experiments. Time integration was performed using various order Runge-Kutta schemes using a time-step chosen to ensure a Courant number of 0.25, where the Courant number is conservatively defined:

$$\text{Courant number} = \frac{c_0 \Delta t}{\sqrt{(\Delta x)^2 + (\Delta y)^2}} \quad (\text{VI.3})$$

Here, Δx and Δy are chosen as the minimum distance between any two points in the x or y directions respectively. This choice is made since the interpolation points are not uniformly distributed when using spectral elements. Consider a canonical element using 8^{th} order basis functions with points chosen using the LGL interpolation points described in Chapter IV. As shown in Figure 12, these points are distributed in such a way to facilitate interpolation and integration and are *not* uniformly distributed.

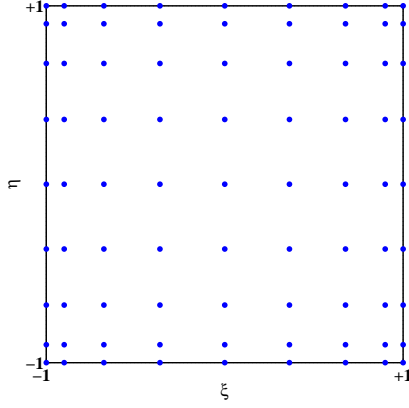


Figure 12: Canonical element using 8^{th} order basis functions showing distribution of grid points.

In order to quantify the errors observed between the reference and NRBC solutions, we use the normalized L^2_Ω error defined as follows:

$$||error||_{L^2_\Omega} = \left(\frac{\sum_{k=1}^{N_p} (h_k^N - h_k^R)^2}{\sum_{k=1}^{N_p} (h_k^R)^2} \right)^{\frac{1}{2}} \quad (\text{VI.4})$$

where N_p is number of points in Ω and h_k^N and h_k^R are the numerical and reference solutions at point k . What follows is a series of experiments that were designed to demonstrate the efficacy of the G-N NRBCs.

A. ANALYTIC BENCHMARK SOLUTION OF SEMI-INFINITE HORIZONTAL CHANNEL

Recall the semi-infinite channel formulation discussed in Chapter IV that we now implement. Specifically, Γ_W is introduced at $x_W = -2$ and no-flux boundary conditions are specified on Γ_N and Γ_S such that $\partial_y h = 0$. Finally, the G-N NRBC \mathcal{B} is introduced at

$x_E = 2$ and advection in the x and y directions are set to zero. This specific situation is shown in Figure 13.

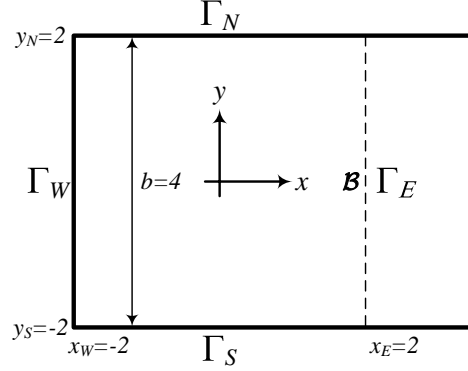


Figure 13: The semi-infinite channel domain under consideration. Domain is truncated by an artificial boundary \mathcal{B} at $x_E = 2$.

A priori, we synthesize a solution that satisfies the KGE with zero advection. Kuchеров and Givoli [40] use a similar benchmark in a non-dispersive environment for a single wave mode. The solution used here is a linear combination of two waves and has the form

$$h_{bm}(x, y, t) = \sum_{m=1}^2 \cos\left(\frac{n_m \pi y}{b}\right) \cos(k_m x - \omega_m t + \phi_m) \quad (\text{VI.5})$$

where the parameters are the same as defined in (III.6). Given choices for k, b, c_0, n, f and ϕ , we can determine ω to satisfy the KGE. Here, we choose $k = \{\frac{\pi}{2}, \frac{\pi}{4}\}$, $b = 4$, $c_0^2 = 1$, $n = \{2, 4\}$, $f^2 = 0.5$ and $\phi = \{0, \pi\}$. These choices ensure that the no-flux boundary conditions on Γ_N and Γ_S are upheld and the gradients on either side of the NRBC are matched at $t = 0$. For the NRBC solution, we specify the values for h_{Γ_W} based on the analytic solution. These parameter choices result in horizontal phase velocities C_k of 1.48 and 4.22 for each of the waves.

The NRBC parameters are selected simply as $C_j = c_0$, $\forall j$ as described in Chapter IV.D. Recall that this choice eliminates the second order time integration terms in the boundary formulation. In theory, if the C_j parameters were chosen to match the horizon-

tal phase velocities, $J = 2$ would be highest order NRBC required. In general problems, however, these phase velocities are not normally known a priori. We therefore keep our formulation general, relying on the fact that simply increasing the NRBC order is guaranteed to reduce the reflection caused by the boundary.

1. Results

In Figure 14, we show the reference solution on the top panel and the solution on the $J = 4$ NRBC truncated domain on the bottom panel at $t = 3$. The NRBC solution uses 4th order spectral elements on a 24×24 element grid, discretizing the domain into 9,409 points. Qualitatively speaking, the results show very little reflection when compared to the synthesized solution.

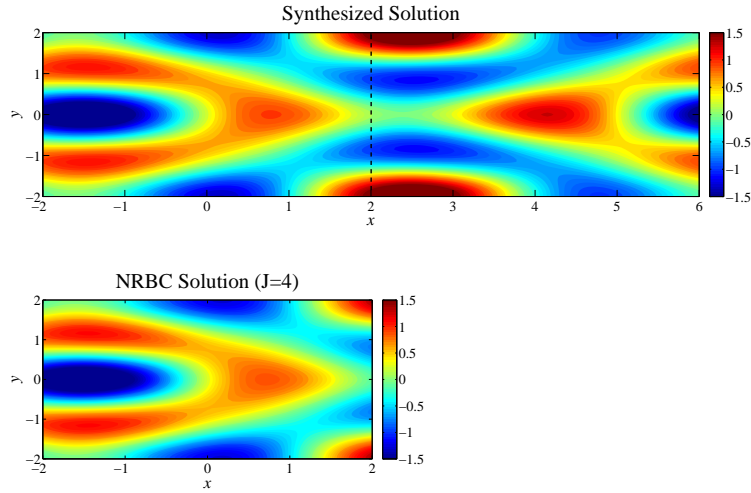


Figure 14: Semi-infinite channel comparing synthesized solution and the NRBC solution. 4th order spectral elements using NRBC order $J = 4$ with zero advection at $t = 3$ are shown.

Quantitative results can be observed in Figure 15 showing the error on Ω as a function of spectral and NRBC order ($J = 1, \dots, 10, 15, 20$). The number of elements is adjusted for each spectral order to maintain an equal number of points (9,409) that the domain is discretized into. It is clear that increasing the NRBC order yields significant gains in accuracy, but by $J = 5$, the spatial discretization error dominates NRBC error in the low

order element (order 1 and 2) cases. However, by increasing the polynomial order of the elements, this spatial discretization error decreases and allows the true accuracy of the NRBC to be realized.

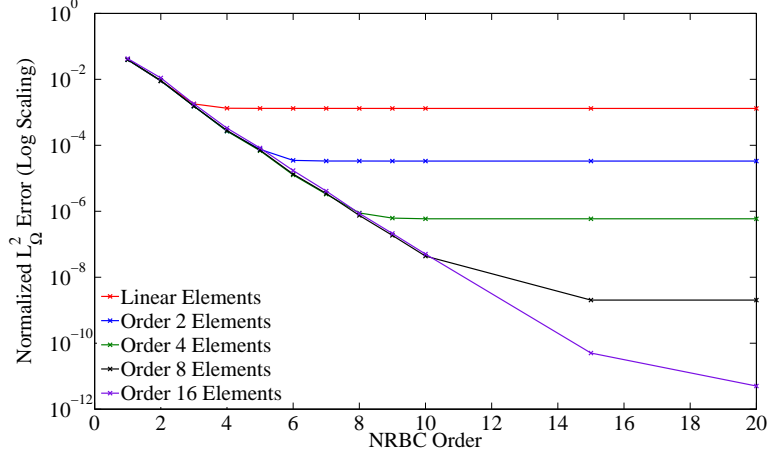


Figure 15: Semi-infinite channel L^2_Ω error versus NRBC and spectral element order. Domain is discretized into 9,409 points for all spectral element orders with zero advection at $t = 3$.

B. SEMI-INFINITE HORIZONTAL CHANNEL

For most problems, where initial data is generated from physical measurements, it would be impossible to generate an analytic solution with which to compare the NRBC solution. In this experiment, we use the initial data as described in (VI.1) and (VI.2) to generate the waves in the solution. To see the effect of the boundary condition, we compare our solution to one computed on a larger domain, i.e., $-2 < x < 10$ where a homogeneous Dirichlet boundary condition $h(10, y, t) = 0$ is prescribed for Γ_E , replacing the NRBC. For this experiment, the discretization is chosen to maintain a mesh of 28,033 grid points for each spectral order. Time integration is performed with RK-8 to ensure the time discretization is not a limiting factor in computing the reference solution. We then solve the extended domain solution for $t = 3$, ensuring that the disturbance has time to propagate through the artificial boundary, yet has not had time to reach the eastern boundary.

1. Semi-Infinite Channel with Zero Advection Results

In Figure 16(a), we plot the reference solution on the top panel and the solution of the truncated domain using the $J = 4$ G-N NRBC on the bottom panel. The solution on the truncated domain uses 4^{th} order spectral elements on a 24×24 element grid, discretizing the domain into 9,409 grid points. Qualitatively speaking, the results show very little reflection using the combination of high-order elements and NRBC. Quantitative results can

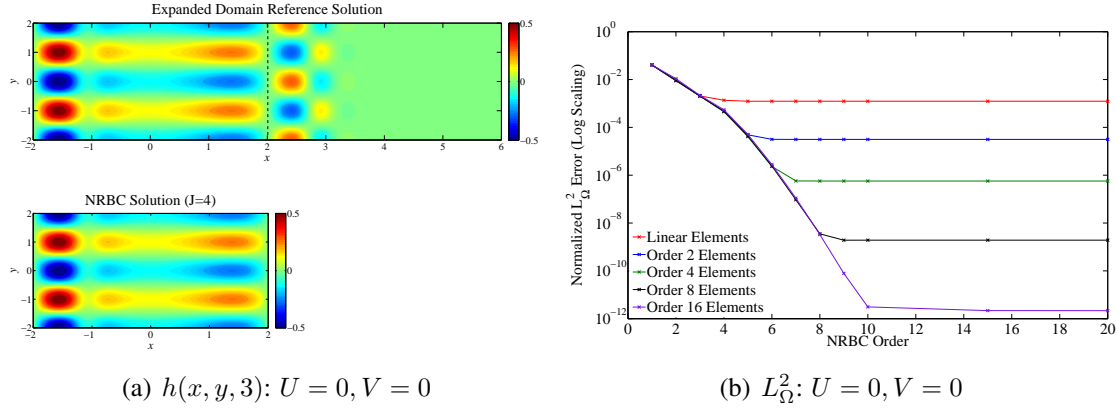


Figure 16: Semi-infinite channel, 4^{th} order spectral elements ($J = 4$) using cosine pulse initial condition and zero advection. **Left Plot:** Contour plot showing $h(x, y, 3)$ on extended and truncated domains. **Right Plot:** Corresponding L^2_{Ω} error versus NRBC and spectral element order. Domain is discretized into 9,409 points for all spectral element orders.

be observed in Figure 16(b) showing the error on Ω as a function of SE and NRBC order ($J = 1, \dots, 10, 15, 20$). The number of elements is adjusted for each polynomial order to maintain an equal number of points (9,409) that the domain is discretized into.

It is clear that increasing the NRBC order yields significant gains in accuracy, but by $J = 5$, the spatial discretization error dominates NRBC error in the low order element (order 1 and 2) cases. However, by increasing the spectral order of the elements, this spatial discretization error decreases and allows the true accuracy of the NRBC to be realized. Similar qualitative and quantitative results are found using the Gaussian initial data and are shown in Figure 17.

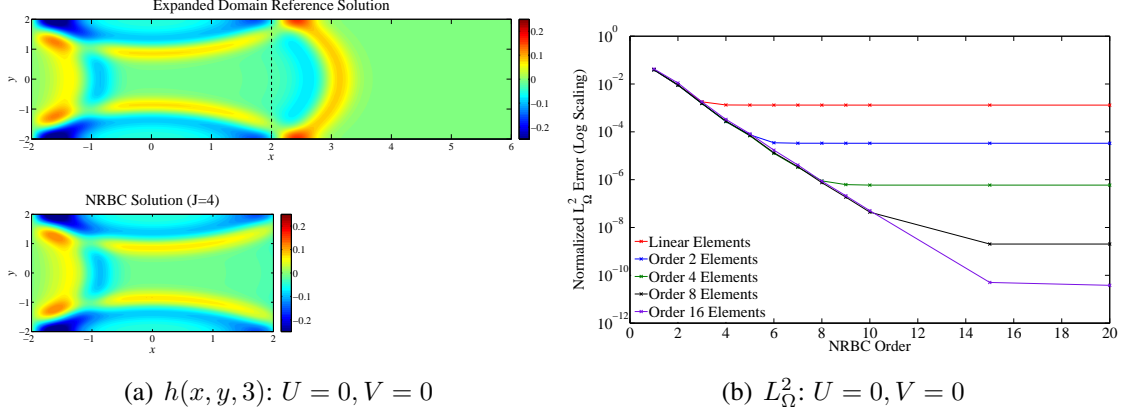


Figure 17: Semi-infinite channel, 4^{th} order spectral elements ($J = 4$) using Gaussian initial condition with zero advection. **Left Plot:** Contour plot showing $h(x, y, 3)$ on extended and truncated domains. **Right Plot:** Corresponding L^2_{Ω} error versus NRBC and spectral element order. Domain is discretized into 9,409 points for all spectral element orders.

2. Semi-Infinite Channel with Constant Advection Results

In this section, we continue the analysis on the semi-infinite channel, this time adding constant advection in various directions. In this setting, we again must consider the selection of the Higdon parameters C_j . For the semi-infinite channel, we make our educated choice described in Chapters III.B and IV.D of augmenting the parameter value with the added advection. In the case of the eastern boundary NRBC, this yields a choice of $C_j = c_0 + U$ which has the simplifying feature of making the boundary condition only first order in time.

In Figure 18(a), we replicate the comparison plot between the reference solution and the truncated domain solution. Here, we use $J = 4$ G-N NRBC and 4^{th} order spectral elements on the same 24×24 element grid, this time with constant advection $U = 0.1$ and $V = 0$. Qualitatively speaking, the results show very little reflection using the combination of high-order elements and NRBC. Further, if comparing this solution with the zero advection case, one notes the expansion of the wave in the direction of advection and compression where the wave is traveling against the direction of advection. These results match intuition and is the same behavior that van Joolen noted in [16, p. 108].

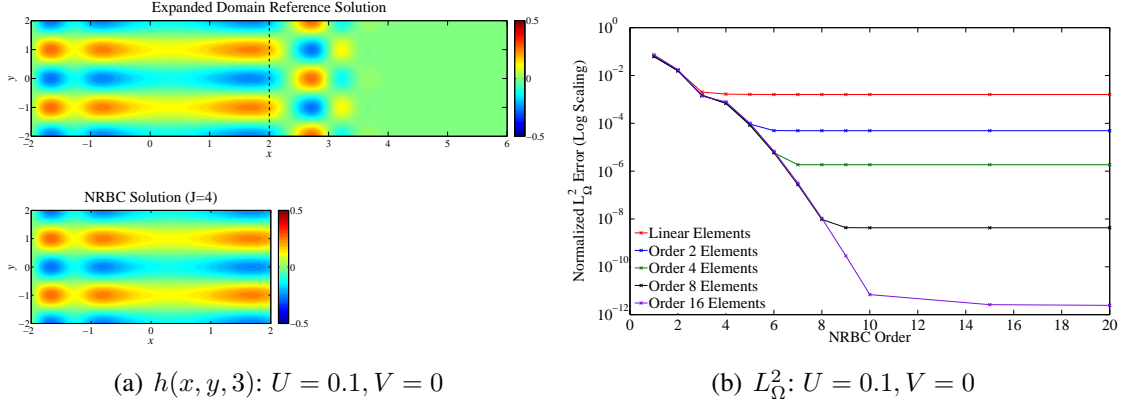


Figure 18: Semi-infinite channel, 4^{th} order spectral elements ($J = 4$) using cosine pulse initial condition with advection velocities $U = 0.1$ and $V = 0$. **Left Plot:** Contour plot showing $h(x, y, 3)$ on extended and truncated domains. **Right Plot:** Corresponding L^2_{Ω} error versus NRBC and spectral element order. Domain is discretized into 9,409 points for all spectral element orders.

Quantitative results can be observed in Figure 18(b) showing the error on Ω as a function of SE and NRBC order ($J = 1, \dots, 10, 15, 20$). The number of elements is again adjusted for each polynomial order to maintain an equal number of points (9,409) that the domain is discretized into. It is again clear that increasing the NRBC order yields significant gains in accuracy, but the spatial discretization error dominates NRBC error in the low order element (order 1 and 2) cases.

Error is monotonically decreasing for each SE order, however, an interesting “dip” occurs for $J = 3$. Anomalies such as this can occur when choosing the C_j ’s in a general manner as we have undertaken in this example. While the reflection coefficient guarantees that the reflection caused by the boundary will decrease as J increases, it says nothing about how much it will decrease. This depends heavily on the choice of the C_j ’s; in this example, it is believed that our general C_j choice for $J = 3$ happened to annihilate a significant wave mode or modes, resulting in better performance of the boundary condition. Similar qualitative and quantitative results are found using the Gaussian initial data and are shown in Figure 19.

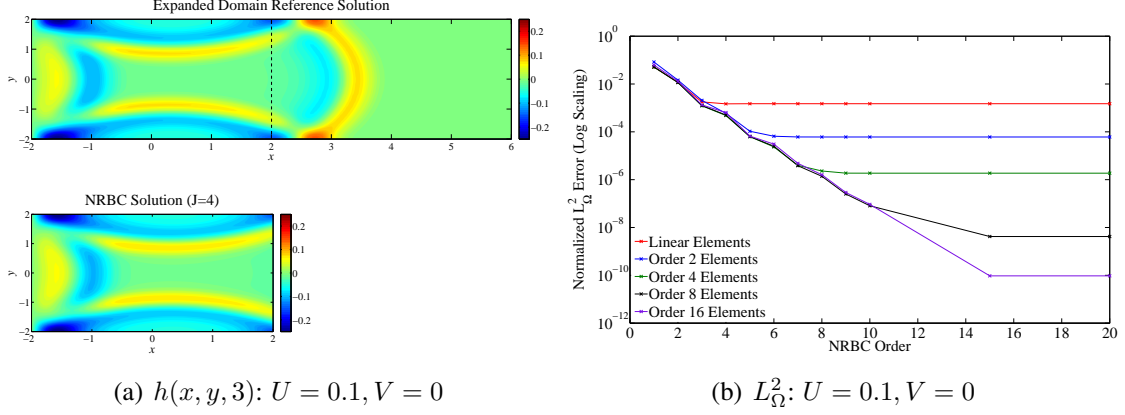


Figure 19: Semi-infinite channel, 4^{th} order spectral elements ($J = 4$) using Gaussian initial condition with advection velocities $U = 0.1$ and $V = 0$. **Left Plot:** Contour plot showing $h(x, y, 3)$ on extended and truncated domains. **Right Plot:** Corresponding L^2_Ω error versus NRBC and spectral element order. Domain is discretized into 9,409 points for all spectral element orders.

As discussed in Chapter III, the Higdon NRBC implicitly assumes that any wave impinging on the NRBC is traveling primarily as a plane wave normal to the boundary. The previous example, where the advection velocity was in the same direction as the channel does not significantly challenge this assumption. In other words, to really test the value of the boundary condition, one must try advection velocities with some tangential component to the boundary. For these experiments, we consider only the Gaussian initial condition⁸.

Figures 20(c) and 20(d) show the same L^2_Ω plots for advection velocities in other directions, one being the contrived case where the advection is perfectly tangential to the NRBC. These L^2_Ω plots correspond with the contour plots directly above that show the comparative solutions. Examining these results, it is clear that the boundary condition – even when put to a test with a wave pulse containing a significant tangential component to the boundary – performs well. It is noted that the order of the error suffers more under diagonal advection when compared to its individual axial counterparts. This may be due to

⁸Since the cosine pulse initial condition was constructed to ensure that the boundary condition on Γ_N and Γ_S were automatically satisfied, any tangential advection would cause this condition to break down. For this reason, we choose to illustrate general results using only the Gaussian initial condition.

the additional terms activated in the interior and boundary formulations (IV.9) and (IV.10) when U and V are simultaneously nonzero.

It should be further noted that as advection velocities are taken larger, the associated errors grow as well. In fact, experimentation shows that the formulation actually becomes unstable for high-order NRBCs as the velocities approach the reference wave speed c_0 . This is the same behavior noted by van Joolen in [31] when examined in a finite difference setting. This behavior does not seem to manifest itself, however, unless the advection velocities are taken much larger than would be expected in a geophysical setting. Further, this behavior seems to be exacerbated in all diagonal advection cases when using high-order ($N = 16$) basis functions. To counter this high-order instability, we implement high-frequency wave filtering as described by Giraldo et al. in [47, 50] when using $N = 16$ basis functions. As in [47], we apply the filter every 10 time-steps at 20% strength.

C. INFINITE HORIZONTAL CHANNEL

For the next set of experiments, the domain is an infinite channel with the NRBCs located at $x = \pm 2$. The set-up is similar to that of the semi-infinite channel in that no-flux boundary conditions are specified on Γ_N and Γ_S . Further, Γ_E is exactly the same NRBC defined previously. This time, however, we prescribe another NRBC \mathcal{B} on Γ_W . This specific situation is shown in Figure 21.

The adjustments required for the western NRBC follow from the original derivation of the Higdon boundary condition as given in Chapter III.A. Now, instead of considering the right moving component of the wave approaching Γ_E , we consider the left moving component of the wave approaching Γ_W . To perfectly absorb the wave impinging on the boundary, we insist that $F = 0$ in (III.10) such that the boundary satisfies the one-way advection equation $h(x, t) = G(x + (c_0 - U)t)$. The corresponding Higdon boundary condition is then given by:

$$H_J : \left[\prod_{j=1}^J \left(\partial_x - \frac{1}{C_j} \partial_t \right) \right] h = 0 \text{ on } \Gamma_W. \quad (\text{VI.6})$$

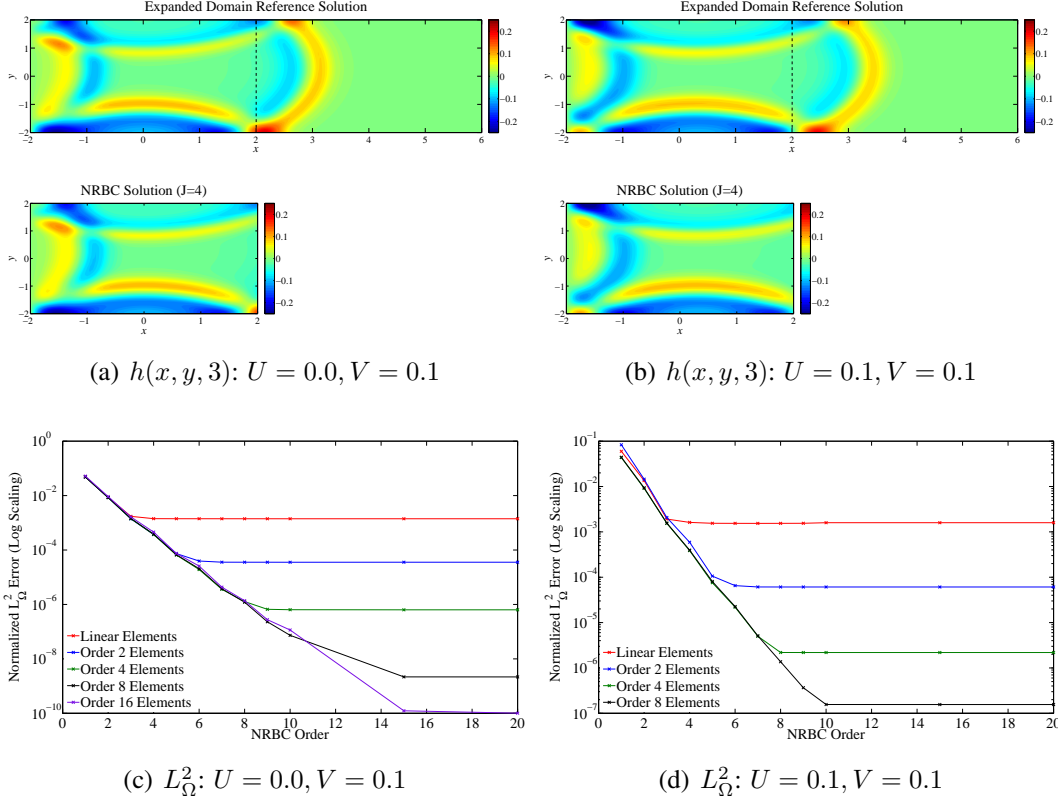


Figure 20: Semi-infinite channel, 4^{th} order spectral elements ($J = 4$) using Gaussian initial condition with advection velocities specified. **Top Plots:** Contour plots showing $h(x, y, 3)$ on extended and truncated domains. **Bottom Plots:** Corresponding L^2_Ω error versus NRBC and spectral element order. Domain is discretized into 9,409 points for all spectral element orders.

In the experiments that follow, we use the initial data as described in (VI.1) and (VI.2) to generate the waves in the solution. To see the effect of the boundary condition, we compare our solution to one computed on a larger domain, i.e., $-6 < x < 6$ where homogeneous Dirichlet boundary conditions $h(-6, y, t) = 0$ and $h(6, y, t) = 0$ are prescribed for Γ_W and Γ_E , replacing the NRBCs. The discretization is again chosen to maintain a mesh of 28,033 grid points for each SE order. Time integration is performed with RK-8 to ensure the time discretization is not a limiting factor in computing the reference solution. We then solve the extended domain solution for $t = 3$, ensuring that the

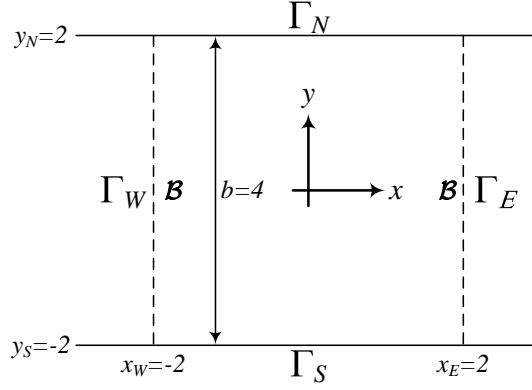


Figure 21: The infinite channel domain under consideration. Domain is truncated by artificial boundaries at $x_W = -2$, and $x_E = 2$.

disturbance has time to propagate through the artificial boundaries, yet has not had time to reach the Dirichlet boundaries.

1. Weak Form Adjustments

Using a similar strategy for introducing a set of auxiliary variables for the western NRBC, applying them to the KGE equivalent, then converting any normal derivatives on the boundary to time and tangential boundaries, results in another, very similar formulation that is directly incorporated into the weak form (IV.3). The details of this formulation can be viewed in Appendix G. The selection of parameters C_j follows the “convenient” choice as developed for the eastern boundary, namely, to remove the second order in time auxiliary variable term by augmenting the reference wave speed with advection. This choice is $C_j = c_0 - U$ for the western boundary. Similar experiments to those run in the semi-infinite channel were conducted using various advective velocities.

2. Infinite Channel with Various Advection Velocities Results

Qualitative and quantitative results using the cosine pulse initial condition are shown in Figure 22. In Figure 22(a), we plot the reference solution on the top panel and the solution of the truncated domain using the $J = 4$ G-N NRBC on the bottom panel. Quantitative

results can be observed in Figure 22(b) showing the error on Ω as a function of SE and NRBC order. In Figure 22(c), we replicate the comparison plot between the reference solution and the truncated domain solution, this time with left to right advection. Quantitative results can be observed in Figure 18(b) showing the error on Ω as a function of SE and NRBC order. In both cases, the number of elements is again adjusted for each polynomial order to maintain an equal number of points (9,409) that the domain is discretized into.

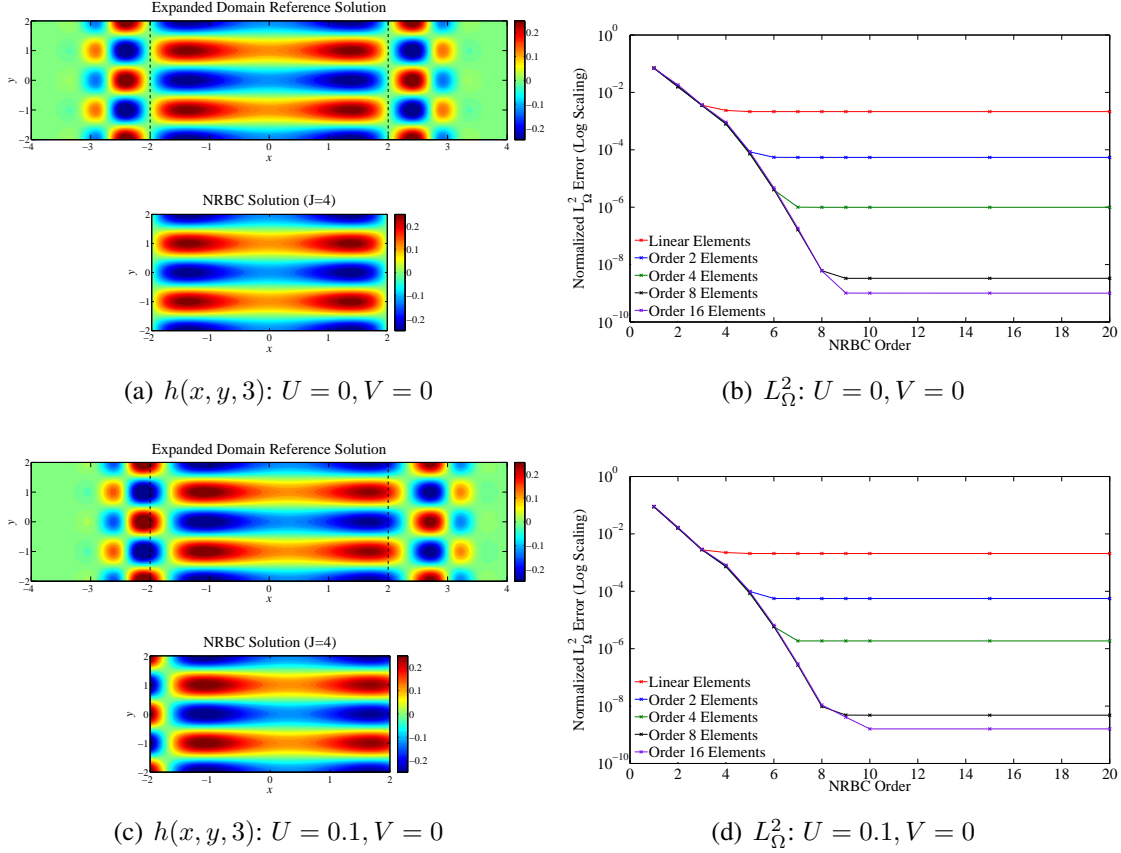


Figure 22: Infinite channel, 4^{th} order spectral elements ($J = 4$) using cosine pulse initial condition with advection velocities specified. **Left Plots:** Contour plots showing $h(x, y, 3)$ on extended and truncated domains. **Right Plots:** Corresponding L^2_Ω error versus NRBC and spectral element order. Domain is discretized into 9,409 points for all spectral element orders.

Similar qualitative and quantitative results are found using the Gaussian initial data and are shown in Figure 23. It is noted that the order of the error again suffers more under diagonal advection when compared to its individual axial counterparts.

D. OPEN DOMAIN CONSIDERATIONS

In the construction of the G-N NRBCs presented thus far, we have assumed that all boundaries are aligned with the axial coordinates. Further, no two NRBCs have ever been placed adjacent to each other. In this section, we examine the consequences of placing NRBCs adjacent to each other in two configurations, namely the quarter plane and the open plane. This set-up is similar to the channel configurations described thus far in that the infinite domain is truncated via artificial boundaries \mathcal{B} thus dividing the domain into a finite computational domain Ω and a residual domain D . The only thing that changes is the configuration of the artificial boundaries.

Specifically, the quarter plane is described as a domain that is bounded by physical boundaries Γ_W and Γ_S . NRBCs are introduced at $x = x_E$ and $y = y_N$. The physical boundaries are homogeneous Dirichlet conditions $h = 0$ on Γ_W and Γ_S . This set-up is illustrated in Figure 24(a). The open plane is described as a domain that is unbounded on all sides. To compute a solution on such a domain, NRBCs are introduced at $x = x_W, x_E$ and $y = y_S, y_N$. This setup is illustrated in Figure 24(b). Artificial boundaries for Γ_S and Γ_N are developed as outlined in Appendix G.

1. Corner Compatibility Concerns

To begin this discussion, consider the quarter plane. A source of concern is the method of handling the intersection point of Γ_E and Γ_N . After all, the auxiliary variable form described in (III.20) and (G.9) are PDEs themselves and therefore require appropriate boundary conditions to be well-posed. In the channel, the no-flux conditions specified by the problem statement were applied to the auxiliary variables to make the problem well-posed. In the quarter plane, we have the homogeneous Dirichlet conditions for the western boundary of Γ_N and the south boundary of Γ_E , but there are no such boundary conditions

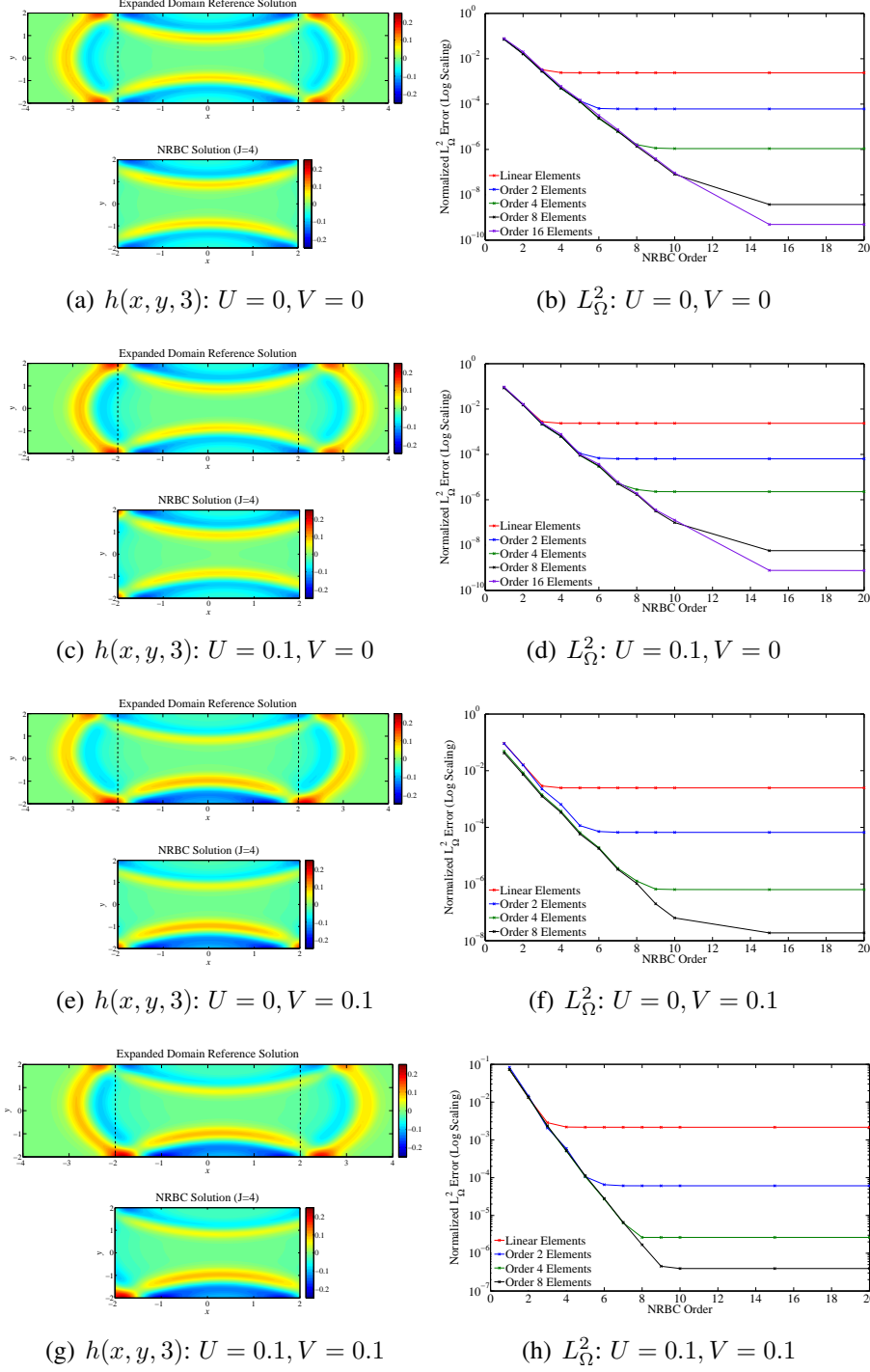


Figure 23: Infinite channel, 4th order spectral elements ($J = 4$) using Gaussian initial condition with advection velocities specified. **Left Plots:** Contour plots showing $h(x, y, 3)$ on extended and truncated domains. **Right Plots:** Corresponding L^2_{Ω} error versus NRBC and spectral element order. Domain is discretized into 9,409 points for all spectral element orders.

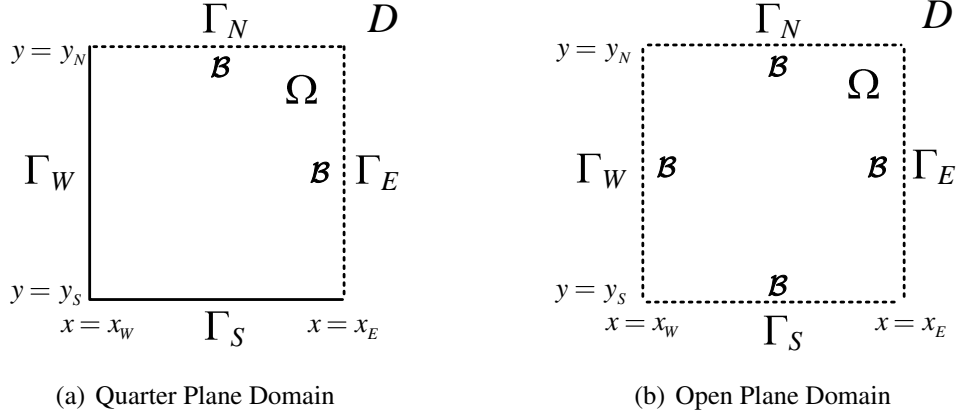


Figure 24: **Left Plot:** A semi-infinite domain Ω truncated by artificial boundaries Γ_E and Γ_N . **Right Plot:** An infinite domain Ω truncated by artificial boundaries $\Gamma_S, \Gamma_E, \Gamma_N$ and Γ_W .

that can be applied to the east of Γ_N and north of Γ_E . The question therefore arises, what *are* the appropriate boundary conditions for the auxiliary variables at these points? This problem is compounded in the open domain as there are no explicitly defined boundary conditions for *any* of the boundaries of the auxiliary variables.

2. Use of Sommerfeld Radiation Boundary Conditions for Auxiliary Variable Boundary Conditions

For this analysis, we suggest that the desired *behavior* of the boundary data on the auxiliary variables at these corners should minimize auxiliary variable reflection back into the computational (boundary) domain. In other words, the auxiliary variables should themselves be non-reflecting. Ultimately, we would like these boundary conditions to be easily implementable while still maintaining the true essence of the auxiliary variables. To implement this *behavior*, we consider a simple order $J = 1$ G-N NRBC (Sommerfeld condition) for the intersection points of two NRBCs, i.e.,

$$\phi'_j(x_E, y_N) = -\frac{1}{c_{0,y}} \dot{\phi}_j(x_E, y_N) \quad \text{for } \Gamma_E \quad (\text{VI.7})$$

$$\phi'_j(x_E, y_N) = -\frac{1}{c_{0,x}} \dot{\phi}_j(x_E, y_N) \quad \text{for } \Gamma_N \quad (\text{VI.8})$$

Here, $c_{0,y}$ and $c_{0,x}$ are the y and x components of the radial wave velocity and prime indicates the tangential derivative along the particular boundary, i.e., $\phi'_j = \frac{\partial \phi_j}{\partial y}$ along Γ_E and $\phi'_j = \frac{\partial \phi_j}{\partial x}$ along Γ_N . We now recall the auxiliary form of the boundary condition for the ϕ_j terms on Γ_E

$$\begin{aligned} \alpha_j \int_{\Gamma_E} \zeta_i \ddot{\phi}_{j-1} d\Gamma_E + \kappa_j \int_{\Gamma_E} \zeta_i \dot{\phi}'_{j-1} d\Gamma_E - \lambda_y \int_{\Gamma_E} \zeta_i \phi''_{j-1} d\Gamma_E + \beta_j \int_{\Gamma_E} \zeta_i \dot{\phi}_j d\Gamma_E \\ - \gamma \int_{\Gamma_E} \zeta_i \phi'_j d\Gamma_E - f^2 \int_{\Gamma_E} \zeta_i \phi_{j-1} d\Gamma_E = \lambda_x \int_{\Gamma_E} \zeta_i \phi_{j+1} d\Gamma_E. \end{aligned}$$

To ensure that the auxiliary form lies in $H^1(\Gamma_E)$, we integrate the second order in space term by parts to yield

$$\begin{aligned} \alpha_j \int_{\Gamma_E} \zeta_i \ddot{\phi}_{j-1} d\Gamma_E + \kappa_j \int_{\Gamma_E} \zeta_i \dot{\phi}'_{j-1} d\Gamma_E + \lambda_y \int_{\Gamma_E} \zeta'_i \phi'_{j-1} d\Gamma_E - \lambda_y \zeta_i \phi'_j \Big|_{y_S}^{y_N} + \beta_j \int_{\Gamma_E} \zeta_i \dot{\phi}_j d\Gamma_E \\ - \gamma \int_{\Gamma_E} \zeta_i \phi'_j d\Gamma_E - f^2 \int_{\Gamma_E} \zeta_i \phi_{j-1} d\Gamma_E = \lambda_x \int_{\Gamma_E} \zeta_i \phi_{j+1} d\Gamma_E \end{aligned}$$

We now see that the boundary term contains ϕ'_j evaluated at the northern boundary. To implement the non-reflecting behavior, we make the substitution (VI.7) into the boundary term. The complete weak boundary form (for Γ_E) then takes the form

$$\begin{aligned} \alpha_j \int_{\Gamma_E} \zeta_i \ddot{\phi}_{j-1} d\Gamma_E + \kappa_j \int_{\Gamma_E} \zeta_i \dot{\phi}'_{j-1} d\Gamma_E + \lambda_y \int_{\Gamma_E} \zeta'_i \phi'_{j-1} d\Gamma_E + \lambda_y \frac{1}{c_{0,y}} \zeta_i \dot{\phi}_{j-1} + \beta_j \int_{\Gamma_E} \zeta_i \dot{\phi}_j d\Gamma_E \\ - \gamma \int_{\Gamma_E} \zeta_i \phi'_j d\Gamma_E - f^2 \int_{\Gamma_E} \zeta_i \phi_{j-1} d\Gamma_E = \lambda_x \int_{\Gamma_E} \zeta_i \phi_{j+1} d\Gamma_E \end{aligned}$$

for $j = 1, \dots, J-1; \forall \zeta_i, \phi_j \in \mathcal{V}_{\Gamma_E}$ and $\phi_j = 0$ at y_s . A similar construct is readily computed for Γ_N .

The only thing left to do is consider the problem of “double counting” the contribution at the corner. In other words, there are two values for the auxiliary variables at the corner; the one resulting from the evaluation of Γ_E and the one from Γ_N . Which auxiliary variable contribution at the corner should be used, that of Γ_E or that of Γ_N ? For this analysis, we adopt the “node-splitting” approach described by Pozrikidis [44, p. 215],

which amounts to averaging the corner auxiliary variable values. Of course, this formulation is inherently low order in the boundary treatment of the auxiliary variables. As such, we would not expect to see spectral convergence as shown in previous examples, however, there should be improvement over the $J = 1$ Sommerfeld condition.

3. Corner and Open Domain with Zero Advection Results

Figure 25 shows a series of contour plots showing how the initial disturbance propagates through the domain for $0 \leq t \leq 4.5$ with zero advection. In this example, we run the simulation using 4^{th} order basis functions on a 24×24 - element grid (9,409 global points), using NRBC order $J = 4$. The simulation is run just long enough for the primary wave to exit the computational domain. Qualitatively speaking, the results appear to behave as desired – allowing the wave to propagate through the NRBC unimpeded.

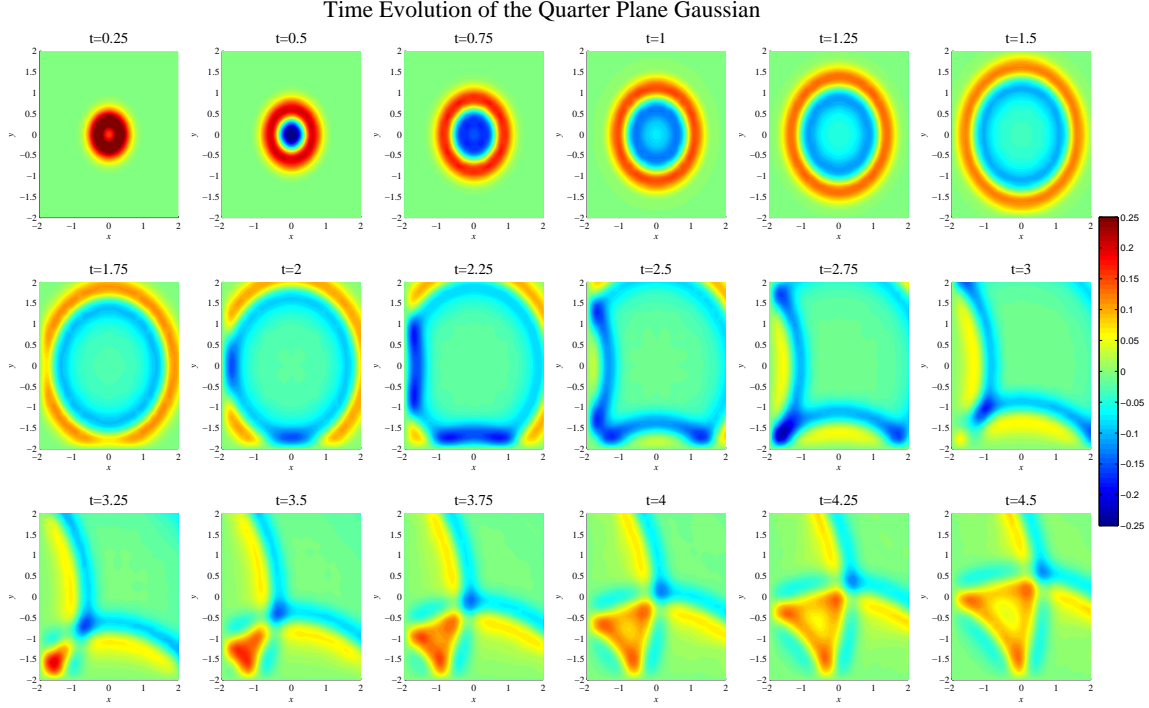


Figure 25: Time Evolution of quarter plane Gaussian (NRBC on Γ_N and Γ_E) using 4^{th} order spectral elements ($J = 4$) with zero advection.

Quantitatively, the results confirm that errors are not exponentially decaying as a function of NRBC order. As the order of the NRBC is increased, the crude approximation of the corner boundary condition on the auxiliary variables shows its weakness. In fact, experimentation shows that the boundary condition error quickly overtakes spatial and time discretization errors. Taking the Gaussian initial condition with $t_f = 3.0$ for various basis function orders and boundary condition orders yields the L^2_Ω errors (using an extended domain solution as the reference) as shown in Table 2.

Table 2: L^2_Ω Error as a function of NRBC Order for quarter plane using various spectral element orders. Gaussian initial condition and zero advection is used.

NRBC Order	L^2_Ω Error Linear Elements	L^2_Ω Error Order 2 Elements	L^2_Ω Error Order 4 Elements
$J = 1$	0.11002	0.10519	0.10470
$J = 2$	0.07204	0.04173	0.05126
$J = 3$	0.04067	0.03377	0.03277
$J = 4$	0.03948	0.02919	0.03274
$J = 5$	0.03647	0.02579	0.02941
$J = 10$	0.03446	0.02517	0.02539
$J = 20$	0.03446	0.02513	0.02526

Similar experiments were performed for the open plane. G-N boundary conditions are implemented along all four boundaries and the order 1 Sommerfeld boundary condition is applied to each auxiliary variable boundary as described in the previous section. Figure 26 shows a series of contour plots showing how the initial disturbance propagates through the domain for $0 \leq t \leq 4.5$ with zero advection. In this example, we run the simulation using 4th order basis functions on a 24×24 - element grid (9,409 Global Points), using NRBC order $J = 4$. Again, qualitatively speaking, the results appear to behave as desired – allowing the wave to propagate through the NRBC unimpeded.

Again, taking the Gaussian initial condition with $t_f = 3.0$ for various basis function and boundary condition orders yields the L^2_Ω errors (using an extended domain solution as the reference) as shown in Table 3. Two main observations can be drawn from these results. First, the major source of error appears to be with the boundary treatment. While there are

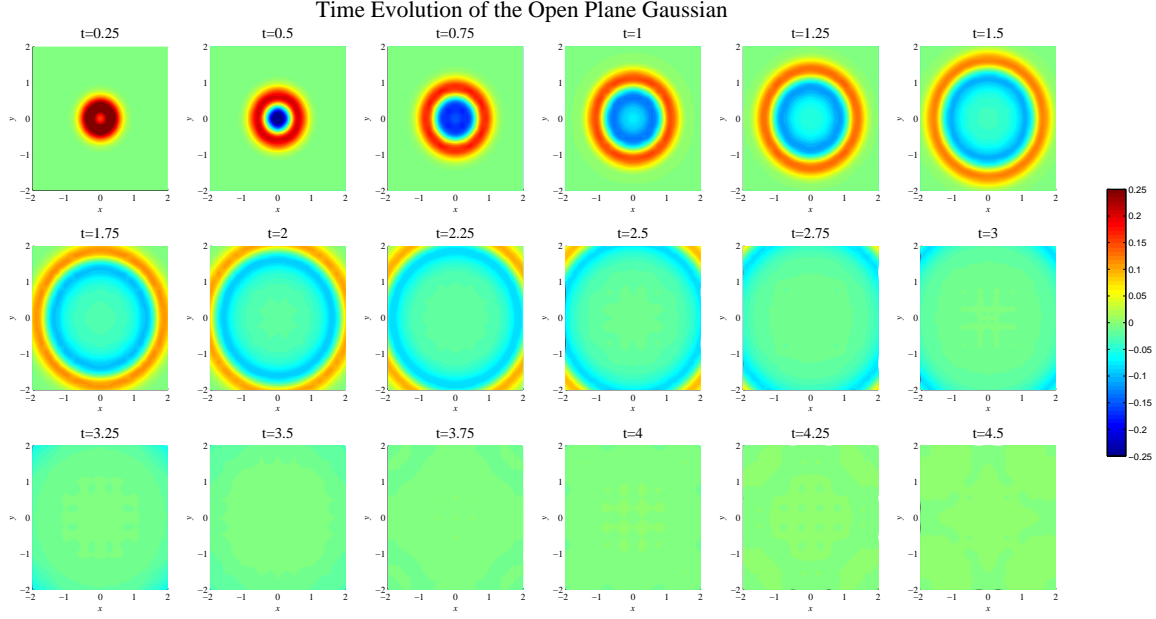


Figure 26: Time Evolution of open plane Gaussian (NRBC on all boundaries) using 4th order spectral elements ($J = 4$) with zero advection.

modest gains made by increasing the spectral element order, once $J = 3$, the errors for all spectral element orders are nearly the same. Second, even though the L^2_Ω results are less impressive than the channel experiments for high-order NRBCs, there is significant improvement from $J = 1$ (Sommerfeld condition) to higher J – even if the improvement is far from exponential.

With this said, one may be concerned with the stability and long term behavior of this NRBC scheme employed in the quarter and open domain planes. Of course, as $t \rightarrow \infty$, one would expect $h \rightarrow 0$. To gain a quantitative handle on this, consider the ∞ -norm defined as follows:

$$||h||_\infty = \max_{1 \leq i \leq N_p} |h_i|$$

where N_p is the number of points in Ω . We choose this norm simply to get an estimate of how much of the initial disturbance is left in the computational domain after a substantial amount of time has passed. Using our now standard test case of 4th order spectral elements

Table 3: L^2_Ω Error as a function of NRBC Order for open plane using various spectral element orders. Gaussian initial condition and zero advection is used.

NRBC Order	L^2_Ω Error Linear Elements	L^2_Ω Error Order 2 Elements	L^2_Ω Error Order 4 Elements
$J = 1$	0.23695	0.21538	0.21102
$J = 2$	0.09145	0.08376	0.04345
$J = 3$	0.06494	0.04056	0.04144
$J = 4$	0.06466	0.03880	0.03837
$J = 5$	0.06454	0.03873	0.03776
$J = 10$	0.06441	0.03794	0.03767
$J = 20$	0.06441	0.03794	0.03767

on a 24×24 element grid with NRBC order $J = 4$, when computed for $t = 1000$ with $J = 10$, it was found that $\|h\|_\infty = 1.03 \times 10^{-17}$ for the quarter plane and $\|h\|_\infty = 5.30 \times 10^{-19}$ for the open domain; in both cases, essentially zero throughout the computational domain. While this is not a rigorous stability analysis, it does experimentally suggest a stable formulation.

4. Corner and Open Plane Domain with Constant Advection Results

It can be shown (see Appendix H for details) that when working in the open plane, to examine the behavior of the KGE under constant advective velocities in various directions, a simple change of coordinate system can recast the problem into a much simpler problem. The simplified problem is one where advection is in only *one* direction aligned with the new coordinate system. This implies that when examining the open plane under advection, it is sufficient to test only cases where advection is in the x or y direction. The benefits of this change of coordinate system include reducing the computational overhead, as well as minimizing various errors due to the more complex formulation if viewed in the original coordinate system. It should be noted, however, that the formulation discussed in VI.D.3 still results in a stable formulation when diagonal advection is applied to the solution. To see this, examine Figure 27 where north-east advection is applied and the $c_{0,y}$ and $c_{0,x}$ terms have been adjusted by advection.

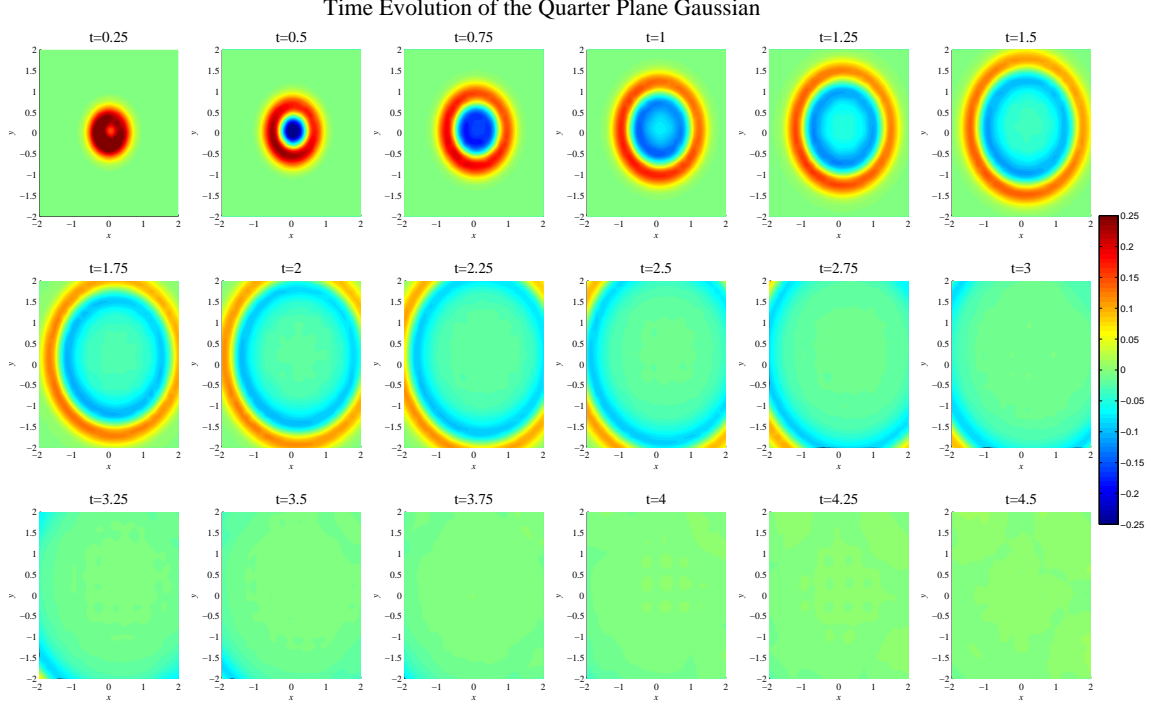


Figure 27: Time Evolution of open plane Gaussian (NRBC on all boundaries) using 4th order spectral elements ($J = 4$) with advection velocities $U = 0.1$ and $V = 0.1$.

The corresponding L^2_{Ω} errors are presented for various SE and NRBC orders in Table 4.

E. EFFECTS OF HIGH-ORDER TIME INTEGRATION

At the outset of this work, it was believed that at some point the improvements realized by increasing the spatial discretization and the order of the NRBC would eventually be limited by the time integration scheme [52]. To this end, the order of the time integration scheme was varied to examine the effects of time integration on accuracy of the solution. As has already been presented, gains made by increasing the order of the NRBC halt for lower order spectral elements after $J = 5$. Early experiments showed that even for high order (order 8 and 16) spectral elements, the gains made by increasing the order of the NRBC are limited at some point using classical RK-4 time integration.

Table 4: L^2_Ω Error as a function of NRBC Order for open plane using various spectral element orders . Gaussian initial condition with advection velocities $U = 0.1$ and $V = 0.1$ used.

NRBC Order	L^2_Ω Error Linear Elements	L^2_Ω Error Order 2 Elements	L^2_Ω Error Order 4 Elements
$J = 1$	0.26914	0.26529	0.16998
$J = 2$	0.09571	0.08642	0.03810
$J = 3$	0.04391	0.02711	0.02631
$J = 4$	0.04061	0.02514	0.02467
$J = 5$	0.04028	0.02413	0.02460
$J = 10$	0.04021	0.02410	0.02460
$J = 20$	0.04018	0.02409	0.02460

For this experiment, we consider the KGE on a semi-infinite channel with $h_{\Gamma_W} = 0$. To ensure that any boundary or time effects are not masked by the interior discretization, 24^{th} order spectral elements are used on a fine mesh consisting of 4,753 global points. The Gaussian initial condition is used and is evaluated until $t = 4$. The reference solution in this case was computed as described previously, except this time using 24^{th} order spectral elements on a fine mesh consisting of 9,457 global points. Time integration was performed with a 10^{th} order Runge-Kutta scheme using a time-step chosen to ensure a Courant number of 0.1.

As can be observed in Figure 28, gains made by improving the time integration matter only if combined with high-order treatment of the boundary. Conversely – gains using high-order treatment of the boundary can only be realized if there is a high-order treatment of the time integration. It should be noted that these results (error on the order of 10^{-10}) cannot be observed unless high-order treatment of the interior also accompanies the high-order treatment of the boundary and time. Several experiments were conducted that varied the order of the interior, boundary and time integration [41, 53]. The clear result was that without high-order treatment of all components in concert, convergence to the reference solution is stalled.

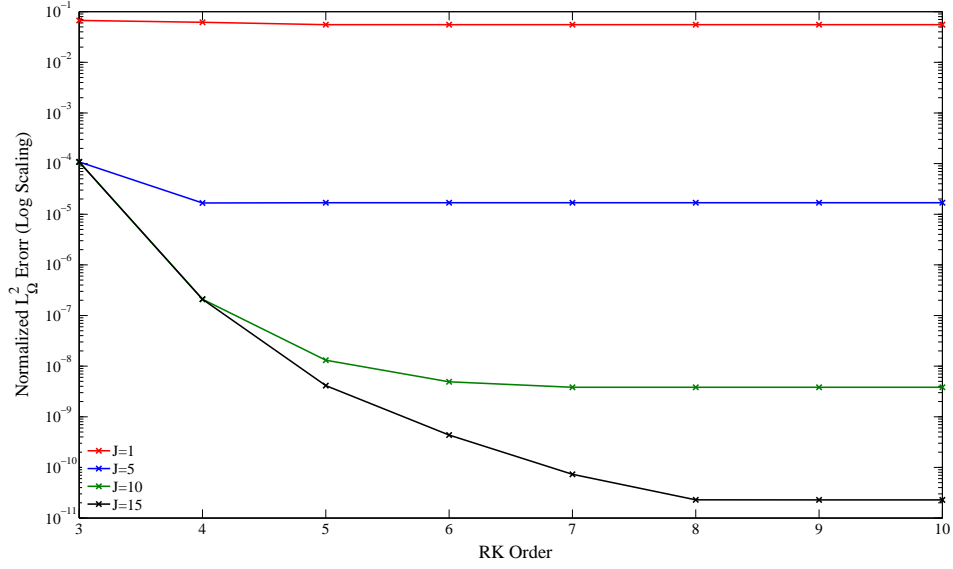


Figure 28: Error in the SE Solution of KGE using NRBCs of various order as a function of time integration order.

We believe as a practical matter that the order of all components of the numerical solution (spatial, boundary and time) should be chosen to ensure that the numerical method is the strongest (in accuracy) component of the model. If high-order treatment of any of the three components is missing, the high-order treatment of the other components is essentially wasted. For models where parameters and data have associated measurement and parameter errors, the numerical method should be chosen to maintain at least the same accuracy.

THIS PAGE INTENTIONALLY LEFT BLANK

VII. TOWARDS ARBITRARY DOMAINS

In the previous chapters, we examined the G-N boundary formulation using spectral elements on unstructured quadrilaterals. The physical boundaries, however were perfectly aligned with the coordinate system axes. This was convenient since it allowed the use of the G-N auxiliary formulation. The power of spectral elements lies not only in its ability to compute high-order accurate solutions, but also in its ability to handle complex geometries. While we demonstrated exponential error convergence in channel experiments when high-order treatment was applied to spatial, boundary and time components of the problem, this exponential convergence broke down when applied to boundary configurations where two NRBCs were adjacent to each other. In short, since there is a discontinuity in the normal at the intersection of adjacent NRBCs, the corner was the problem.

This chapter considers what happens when we completely remove any corners. We first examine an arbitrary domain where the boundary can be of any shape. It will be shown that there are insurmountable complications that arise when using the G-N auxiliary formulation in this context. In this case, results are presented for various domains using a first order non-reflecting boundary condition and high-order G-N when certain simplifying assumptions are made. The chapter concludes by revisiting a boundary condition originally devised in 1998 for the wave equation by Hagstrom and Hariharan and modified in 2003 by vanJoolen et al. to include dispersion.

A. ARBITRARILY SHAPED BOUNDARIES

Ideally, we would like to directly extend the work presented thus far to remove the problematic “corner” configuration and replace it with a continuous, smooth, closed boundary. If this were possible, then a single formulation (instead of four formulations combined in the open domain) for the boundary would result. The benefits to this type of boundary would be that the domain could be “fit” to the area of interest, reducing the

total number of grid points required. A general configuration that demonstrates this idea is shown in Figure 29.

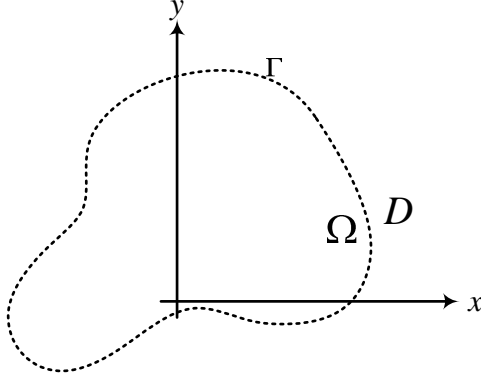


Figure 29: A general domain Ω truncated by artificial boundary Γ

To begin, we again examine the Higdon boundary condition of order J as first presented in Chapter III and the KGE as presented in Chapter II simplified by the assumption of zero advection.

$$H_J : \quad \left[\prod_{j=1}^J \left(\partial_n + \frac{1}{C_j} \partial_t \right) \right] h = 0 \quad \text{on } \Gamma$$

$$\ddot{h} - c_0^2 \nabla^2 h + f^2 h = 0$$

We note that the boundary condition and the KGE are described in two different coordinate systems – namely (n, τ) and (x, y) respectively where n and τ are the normal and tangential directions on the boundary. If we consider an arbitrary part of the boundary (Γ) as shown in Figure 30, we can find a way to express the standard Cartesian derivatives in terms of normal and tangential derivatives.

Of course, in the most general case, the normal and tangential vectors are dependent on the position on the boundary, i.e., $\vec{n} = \vec{n}(x, y)$ and $\vec{\tau} = \vec{\tau}(x, y)$. These normal components can be computed (see Appendix I) for a particular domain by considering a change of coordinates from (x, y) to (n, τ) as defined by the linear transformation and its

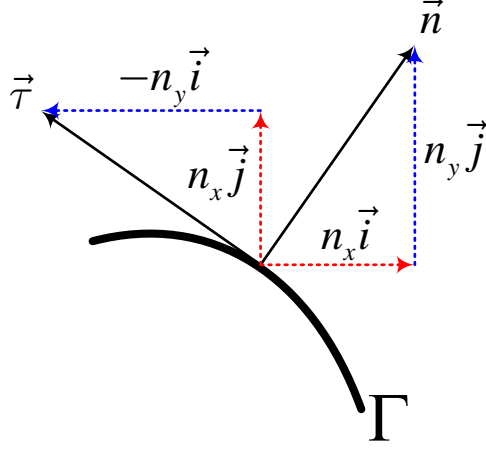


Figure 30: Components of normal and tangential derivatives

associated differentiation operator:

$$\begin{bmatrix} n \\ \tau \end{bmatrix} = \begin{bmatrix} n_x & n_y \\ -n_y & n_x \end{bmatrix} \begin{bmatrix} x \\ y \end{bmatrix} \quad \text{and} \quad \begin{bmatrix} \partial_n \\ \partial_\tau \end{bmatrix} = \begin{bmatrix} n_x & n_y \\ -n_y & n_x \end{bmatrix} \begin{bmatrix} \partial_x \\ \partial_y \end{bmatrix}. \quad (\text{VII.1})$$

Since the transformation is necessarily non-singular, this can also be written as:

$$\begin{bmatrix} \partial_x \\ \partial_y \end{bmatrix} = \frac{1}{n_x^2 + n_y^2} \begin{bmatrix} n_x & -n_y \\ n_y & n_x \end{bmatrix} \begin{bmatrix} \partial_n \\ \partial_\tau \end{bmatrix} = \begin{bmatrix} n_x & -n_y \\ n_y & n_x \end{bmatrix} \begin{bmatrix} \partial_n \\ \partial_\tau \end{bmatrix} \quad (\text{VII.2})$$

Now, if we expand the Higdon boundary condition, for $J = 1$, we get

$$\partial_n h + \frac{1}{C_1} \dot{h} = 0 \Rightarrow \vec{n} \cdot \nabla h = -\frac{1}{C_1} \dot{h}.$$

This is convenient since this boundary condition can be directly applied to the KGE zero advection weak integral form

$$\int_{\Omega} \Psi_i \ddot{h} \, d\Omega - c_0^2 \int_{\Gamma} \Psi_i \vec{n} \cdot \nabla h \, d\Gamma + c_0^2 \int_{\Omega} \nabla \Psi_i \cdot \nabla h \, d\Omega + f^2 \int_{\Omega} \Psi_i h \, d\Omega = 0$$

to yield the first order Sommerfeld formulation

$$\int_{\Omega} \Psi_i \ddot{h} \, d\Omega + \frac{c_0^2}{C_1} \int_{\Gamma} \Psi_i \dot{h} \, d\Gamma + c_0^2 \int_{\Omega} \nabla \Psi_i \cdot \nabla h \, d\Omega + f^2 \int_{\Omega} \Psi_i h \, d\Omega = 0. \quad (\text{VII.3})$$

1. Second Order (and Higher) Higdon Boundary Condition

Recall that the Higdon boundary condition is very general. It can be applied to a variety of wave-type problems and reflection is guaranteed to decrease by simply increasing the order J . They suffer, however, from an implementation point of view since there are increasingly high-order spatial and temporal derivatives. Consider a second order Higdon boundary condition

$$H_2 : \quad \left(\partial_n + \frac{1}{C_2} \partial_t \right) \left(\partial_n h + \frac{1}{C_1} \dot{h} \right) = 0 \quad \text{on } \Gamma.$$

When expanded, this boundary condition takes the form

$$\partial_{nn} h + \left(\frac{1}{C_1} + \frac{1}{C_2} \right) \partial_n \dot{h} + \frac{1}{C_1 C_2} \ddot{h} = 0.$$

Continuing with the expansion to express the boundary condition in terms of the physical coordinate system, we find that $\partial_{nn} h$ is

$$\begin{aligned} \partial_{nn} h &= \frac{\partial}{\partial n} (\partial_n h) = \frac{\partial}{\partial n} (\vec{n} \cdot \nabla h) \\ &= \frac{\partial}{\partial n} (n_x \partial_x h + n_y \partial_y h) = \vec{n} \cdot \nabla (n_x \partial_x h + n_y \partial_y h). \end{aligned} \quad (\text{VII.4})$$

The key point to take away from (VII.4) is that the components of the normal vectors are themselves functions of x and y . The product rule dictates that we must then compute the x and y derivatives of the normals in order to yield an “exact” representation of the higher order Higdon boundary condition. This expansion has two direct consequences that undermine efficient implementation of the formulation.

The first is something that has already been addressed, namely that the ability to implement the model is challenged – especially when dealing with large J . For each order that the Higdon formulation increases, high-order derivatives appear for h as well as the components of the normal vector. The second consequence is even more problematic in that the means to relate the boundary formulation back into the interior formulation has been lost. In the case of the Sommerfeld condition presented, the boundary condition and the boundary integral term (following integration by parts of the Laplacian operator) matched perfectly – thus allowing direct substitution of the boundary condition into the interior formulation.

2. G-N on the Unstructured Boundary

The G-N formulation was designed to remedy this problem of increasingly high-order derivatives by recasting them into a system of low order derivatives. If we try this with the unstructured boundary formulation, a similar auxiliary form to that presented in Chapter III.C) is obtained

$$\left(\partial_n + \frac{1}{C_j} \partial_t \right) \phi_{j-1} = \phi_j \quad j = 1, \dots, J \quad (\text{VII.5})$$

where $\phi_0 \equiv h$ and $\phi_J \equiv 0$. Again, the function h satisfies the KGE and ϕ_1 is obtained by applying the linear (constant coefficient) operator $\left(\partial_n + \frac{1}{C_1} \partial_t \right)$ to h .

Knowing that in the end, we would like to have an auxiliary variable formulation that contains only tangential and time derivatives (so that the boundary formulation can be discretized *only* on the boundary), we must consider the equation that ϕ_j satisfies. It can be shown that when the KGE on the boundary is recast in terms of the normal and tangential coordinate system that it becomes a *variable* coefficient differential equation due to the presence of the normal components $n_x(x, y), n_y(x, y)$. The result of this is that there is no general KGE-like equation that all ϕ_j 's will satisfy. In fact, every time we increase the order of the boundary condition, additional terms such as those encountered in (VII.4) are accumulated. In the end, a separate formulation that contains high-order derivatives will

have to be devised for each auxiliary variable introduced. In short, this implies that the G-N auxiliary variable formulation in its current form is incompatible with an unstructured boundary.

To handle this incompatibility, we consider a simplifying assumption that the curvature on the boundary is small. This replicates the case where in a local region, the boundary “looks” like a straight line to the numerical solution. This assumption allows for all derivatives of normal components to be neglected, i.e.,

$$\frac{\partial}{\partial x}(n_x) = \frac{\partial}{\partial x}(n_y) = \frac{\partial}{\partial y}(n_x) = \frac{\partial}{\partial y}(n_y) = 0.$$

The details of this boundary formulation and how it is integrated into the interior scheme are discussed in Appendix I.

B. RESULTS FOR ADJUSTED G-N NRBCS ON ARBITRARY DOMAINS

Some experiments were performed using the (what turned out to be) convergence limiting assumption of small curvature. While experiments showed stable behavior for the zero advection case, even over long term time integrations, the convergence was again, far from exponential in nature. For the first set of experiments, we consider how the formulation outlined in (VII.3) performs for various boundary shapes. Admittedly, this formulation is only a first order boundary condition, however as has already been shown, a first order condition is *very* easy to implement and has very modest computational overhead. The next set of experiments considers the adjusted G-N formulation. For these experiments, we consider rectangular, circular, and rounded rectangular boundaries where the Gaussian initial condition is used to generate the propagating waves.

Figure 31 shows a series of contour plots for the zero advection case using 4th order spectral elements with $J = 1$ and $J = 4$. Model parameters are set to the standard test case where $c_0^2 = 1$, $f^2 = 0.5$ and initial data as described in (VI.2) is used to generate the waves in the solution. To see the effect of the boundary condition, we compare our solution

to one computed on a larger domain, i.e., $x, y \in [-4, 4]$ where a homogeneous Dirichlet boundary condition $h = 0$ is prescribed for Γ , replacing the NRBC. For this experiment, the discretization is chosen to maintain a mesh of 28,033 grid points for each polynomial order. Time integration is performed with RK-8 to ensure the time discretization is not a limiting factor in computing the reference solution. We then solve the extended domain solution for $t = 3$, ensuring that the disturbance has time to propagate through the artificial boundary, yet has not had time to reach the boundary. The number of elements in each of the NRBC solutions is adjusted to ensure approximately 3,000 global points were used.

What is clear from these plots is that there are trade-offs between accurately representing the G-N NRBC and removing the problematic corners. Specifically, the square domain does not have to make an approximation for small curvature. In fact, with the exception of only 4 points (corners) in the global domain, the G-N NRBC is perfectly represented by the arbitrary domain formulation. This is why there is significant improvement between the $J = 1$ and $J = 4$ cases. The rounded square and circular domains see less dramatic improvement as J is increased. While the problematic corners are removed in these cases, the small curvature assumption induces error in the G-N NRBC, thus imposing a convergence bound that cannot be overcome by simply increasing the order of the NRBC.

A series of experiments was conducted to examine the normalized L^2_{Ω} error as a function of spectral element and NRBC order for each of the NRBC boundary configurations. What is clear from the results shown in Tables 5–7 is that the errors are more a function of the NRBC than of the spectral element order. In short, there is almost no gain observed by using high-order spectral elements since much of the error is generated by the NRBC. When compared with the results shown in Chapter VI.D.3, which used the Sommerfeld approximation for the boundary condition of the auxiliary variables, the results are unimproved.

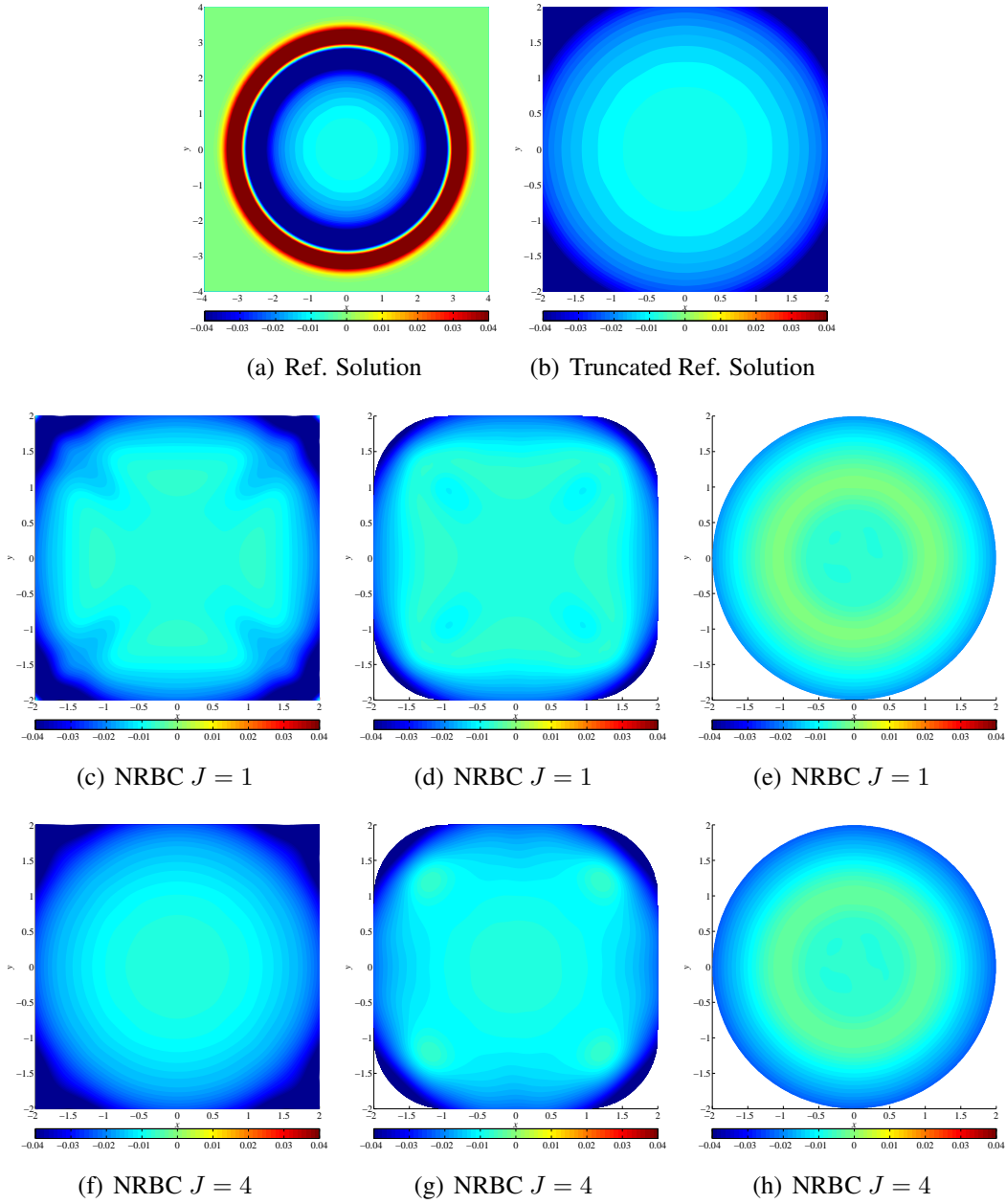


Figure 31: Open Domain, 4^{th} order spectral elements using Gaussian initial condition with zero advection. **Top Plots:** Contour plots of reference solution solved on extended domain. Full and truncated domains shown for comparison. **Center Plots:** Contour plots of various NRBC boundary configurations using $J = 1$. **Bottom Plots:** Contour plots of various NRBC boundary configurations using $J = 4$

Table 5: L^2_Ω Error as a function of NRBC Order for open plane arbitrary domain formulation using various spectral element orders on **square** NRBC domain. Gaussian initial condition and zero advection is used.

NRBC Order	L^2_Ω Error Linear Elements	L^2_Ω Error Order 2 Elements	L^2_Ω Error Order 4 Elements
$J = 1$	0.13632	0.13475	0.13561
$J = 2$	0.09030	0.07383	0.07164
$J = 3$	0.04483	0.04403	0.04293
$J = 4$	0.03996	0.03993	0.03841
$J = 5$	0.03964	0.03984	0.03841
$J = 10$	0.03948	0.03957	0.03841
$J = 20$	0.03948	0.03952	0.03840

Table 6: L^2_Ω Error as a function of NRBC Order for open plane arbitrary domain formulation using various spectral element orders on **rounded square** NRBC domain. Gaussian initial condition and zero advection is used.

NRBC Order	L^2_Ω Error Linear Elements	L^2_Ω Error Order 2 Elements	L^2_Ω Error Order 4 Elements
$J = 1$	0.19805	0.17845	0.17331
$J = 2$	0.08245	0.07027	0.06646
$J = 3$	0.05528	0.04839	0.04458
$J = 4$	0.05246	0.04599	0.04358
$J = 5$	0.05194	0.04547	0.04234
$J = 10$	0.05187	0.04540	0.04203
$J = 20$	0.05186	0.04540	0.04201

C. ALTERNATIVES

Thus far, using the arbitrary boundary idea to remove the problematic corner points, we have not been able to improve results for the open domain problem. While the arbitrary boundary formulation does allow the user to choose a boundary domain of any shape (an advantage in certain contexts), the errors associated with this formulation were on par with alternatives presented in Chapter VI.D. Additionally, neither formulation led to exponential error convergence as the order of the NRBC was increased. With this in mind, we consider an alternative boundary formulation for a circular domain. Hagstrom and Hariharan [6]

Table 7: L^2_Ω Error as a function of NRBC Order for open plane arbitrary domain formulation using various spectral element orders on **circular** NRBC domain. Gaussian initial condition and zero advection is used.

NRBC Order	L^2_Ω Error Linear Elements	L^2_Ω Error Order 2 Elements	L^2_Ω Error Order 4 Elements
$J = 1$	0.26723	0.26615	0.25028
$J = 2$	0.10844	0.10334	0.09448
$J = 3$	0.07584	0.07211	0.06451
$J = 4$	0.07150	0.06788	0.06206
$J = 5$	0.07078	0.06730	0.06151
$J = 10$	0.07070	0.06720	0.06142
$J = 20$	0.07070	0.06711	0.06142

devised high-order NRBCs for the standard time-dependent two-dimensional wave equation in polar coordinates implemented in a finite difference setting. This NRBC follows the ideas pioneered by Bayliss and Turkel [1] with the exception that the NRBC condition does not involve any high-order derivatives after introducing auxiliary variables. Huan and Thompson implemented the same NRBC in a series of papers [54, 55, 56, 57, 58, 59] in a finite element setting. Here, we examine the effect of this work when examined with high-order spectral elements and time integration.

1. Hagstrom Hariharan Polar Boundary Conditions

The boundary condition devised by Hagstrom and Hariharan (hereafter referred as the HH formulation) provides a systematic approach for constructing boundary conditions for standard two-dimensional wave equation. The condition is based on the asymptotic series representation (which does not converge at any fixed radius) for an outgoing solution of the wave equation (in polar coordinates)

$$\frac{1}{c_0^2} \frac{\partial^2 h}{\partial t^2} = \frac{\partial^2 h}{\partial r^2} + \frac{1}{r} \frac{\partial h}{\partial r} + \frac{1}{r^2} \frac{\partial^2 h}{\partial \theta^2}. \quad (\text{VII.6})$$

Since the boundary condition is asymptotic by nature, valid for large radial distances – this implies that larger radial distances should provide better NRBC convergence. Thompson

et al. make the observation that “...for practical problems, truncating the asymptotic expansion after $[J]$ terms provides solutions with errors well below that of the discretization error” [59]. Here, we seek to significantly reduce the discretization error by employing spectral elements to find the true error convergence properties of the NRBC. In developing the boundary condition, Hagstrom and Hariharan construct a sequence of operators that approximately annihilate the residual of the preceding element in the sequence, viewed as a function on the artificial boundary. The sequence begins with a first-order Bayliss-Turkel operator discussed in [1]. The boundary condition takes the form:

$$\frac{\partial h}{\partial r} = \phi_1 - \frac{1}{c_0} \frac{\partial h}{\partial t} - \frac{1}{2r} h, \quad (\text{VII.7})$$

$$\phi_{j+1} = \frac{1}{c_0} \frac{\partial \phi_j}{\partial t} + \frac{j}{r} \phi_j - \frac{(j - \frac{1}{2})^2}{4r^2} \phi_{j-1} - \frac{1}{4r^2} \frac{\partial^2 \phi_{j-1}}{\partial \theta^2}, \quad j = 1, \dots, J-1 \quad (\text{VII.8})$$

where

$$\phi_0 \equiv 2h \quad \text{and} \quad \phi_J \equiv 0.$$

At first glance, this boundary formulation suggests that we should develop a “new” spectral element formulation for the wave equation cast in polar coordinates. If we did this, however, we would then require a polar grid that would introduce additional complications such as the method of dealing with the degenerate quadrilaterals that inevitably occur at the center of the grid. Of course there are ways to overcome these obstacles, but it would be much more convenient to cast the problem in the same framework already developed. In other words, we seek to implement this boundary condition (presented in polar form) in our unstructured quadrilateral formulation of the wave equation (in Cartesian form).

First, consider the two-dimensional wave equation (same formulation as presented in (II.29) with $U = V = f = 0$)

$$\frac{\partial^2 h}{\partial t^2} - c_0^2 \nabla^2 h = 0. \quad (\text{VII.9})$$

Multiplying by the test functions Ψ_i and integrating over the circular domain yields the weak integral form

$$\int_{\Omega} \Psi_i \frac{\partial^2 h}{\partial t^2} d\Omega - c_0^2 \int_{\Omega} \Psi_i \nabla^2 h d\Omega = 0$$

Transferring the second order spatial derivatives from h to the basis functions via integration by parts and applying the divergence theorem to recast one surface integral term as a boundary integral gives us

$$\int_{\Omega} \Psi_i \frac{\partial^2 h}{\partial t^2} d\Omega - c_0^2 \int_{\Gamma} \Psi_i \vec{n} \cdot \nabla h d\Omega + c_0^2 \int_{\Omega} \nabla \Psi_i \cdot \nabla h d\Omega = 0. \quad (\text{VII.10})$$

Of note now is that the boundary condition (VII.7) contains a radial derivatives of h that on the circle is precisely the normal derivative $\vec{n} \cdot \nabla h$. This allows direct implementation of the boundary condition into (VII.10) as follows:

$$\int_{\Omega} \Psi_i \frac{\partial^2 h}{\partial t^2} d\Omega - c_0^2 \int_{\Gamma} \Psi_i \left(\phi_1 - \frac{1}{c_0} \frac{\partial h}{\partial t} - \frac{1}{2r} h \right) d\Omega + c_0^2 \int_{\Omega} \nabla \Psi_i \cdot \nabla h d\Omega = 0. \quad (\text{VII.11})$$

Here, since on the boundary the radius is fixed, the $\frac{1}{2r}$ term may be treated as a constant.

A similar weak form is constructed for the boundary formulation by multiplying (VII.8) by the test functions ζ_i and integrating over Γ yielding (after by integration by parts):

$$\begin{aligned} \frac{1}{c_0} \int_{\Gamma} \zeta_i \frac{\partial \phi_j}{\partial t} d\Gamma + \frac{j}{r} \int_{\Gamma} \zeta_i \phi_j d\Gamma - \frac{(j - \frac{1}{2})^2}{4r^2} \int_{\Gamma} \zeta_i \phi_{j-1} d\Gamma \\ - \frac{1}{4r^2} \zeta_i \frac{\partial \phi_{j-1}}{\partial \theta} \Big|_{start}^{end} + \frac{1}{4r^2} \int_{\Gamma} \frac{\partial \zeta_i}{\partial \theta} \frac{\partial \phi_{j-1}}{\partial \theta} d\Gamma = \int_{\Gamma} \zeta_i \phi_{j+1} d\Gamma. \end{aligned} \quad (\text{VII.12})$$

We now use the fact that the boundary is continuous and closed to surmise that the endpoint evaluation term vanishes. The formal problem statement is then: Find $h \in \mathcal{V}$ and $\phi_j \in \mathcal{V}_{\Gamma}$ where $j = 1, \dots, J-1$, such that Equations (VII.11) and (VII.12) are satisfied $\forall \Psi_i \in \mathcal{V}$ and $\zeta_i \in \mathcal{V}_{\Gamma}$.

2. Results for the HH Formulation

A series of experiments was conducted to determine the effect of the HH boundary condition for various SE and NRBC orders. Since the formulation is designed for circular boundaries, we consider only circular boundaries with unstructured grids. In each case, we choose the number of elements to yield approximately 3,000 global points. Since the Gaussian initial condition described in (VI.2) is perfectly symmetric with respect to the boundary, we introduce asymmetry by adjusting its shape to yield a smooth, two-dimensional “oval-shaped” initial condition with shape parameters $\sigma_x = \frac{1}{2}, \sigma_y = \frac{1}{3}$, further rotated by an angle of $\theta = \frac{\pi}{6}$. The initial condition used here is:

$$h(x, y, 0) = e^{-(ax^2 + 2bxy + cy^2)}, \quad \dot{h}(x, y, 0) = 0. \quad (\text{VII.13})$$

Here, the parameters a, b , and c are defined as follows:

$$a = \frac{\cos^2 \theta}{2\sigma_x^2} + \frac{\sin^2 \theta}{2\sigma_y^2} \quad b = -\frac{\sin 2\theta}{4\sigma_x^2} + \frac{\sin 2\theta}{4\sigma_y^2} \quad c = \frac{\sin^2 \theta}{2\sigma_x^2} + \frac{\cos^2 \theta}{2\sigma_y^2}. \quad (\text{VII.14})$$

Again, the solution is compared to one computed on a larger domain allowing the wave to propagate out of the NRBC domain but not yet impinge on the non-physical boundary used to compute the solution on the larger domain. Qualitative results are shown in Figure 32 and quantitative L_Ω^2 errors are shown for various NRBC orders for SE orders up to 6 in Table 8. No further improvement was observed for SE orders above order 6.

3. Adjustments to HH to Include Mild Dispersion

The unstructured grid representation of the HH formulation has been demonstrated to significantly reduce reflection caused by the boundary for the standard wave equation. The question now arises, can this formulation be extended to include dispersive effects such as Coriolis? In [60], van Joolen et al. presented a method to extend the HH formulation for the standard wave equation under mild dispersion. While this formulation was well grounded mathematically, as far as the author knows, it was never implemented. A brief

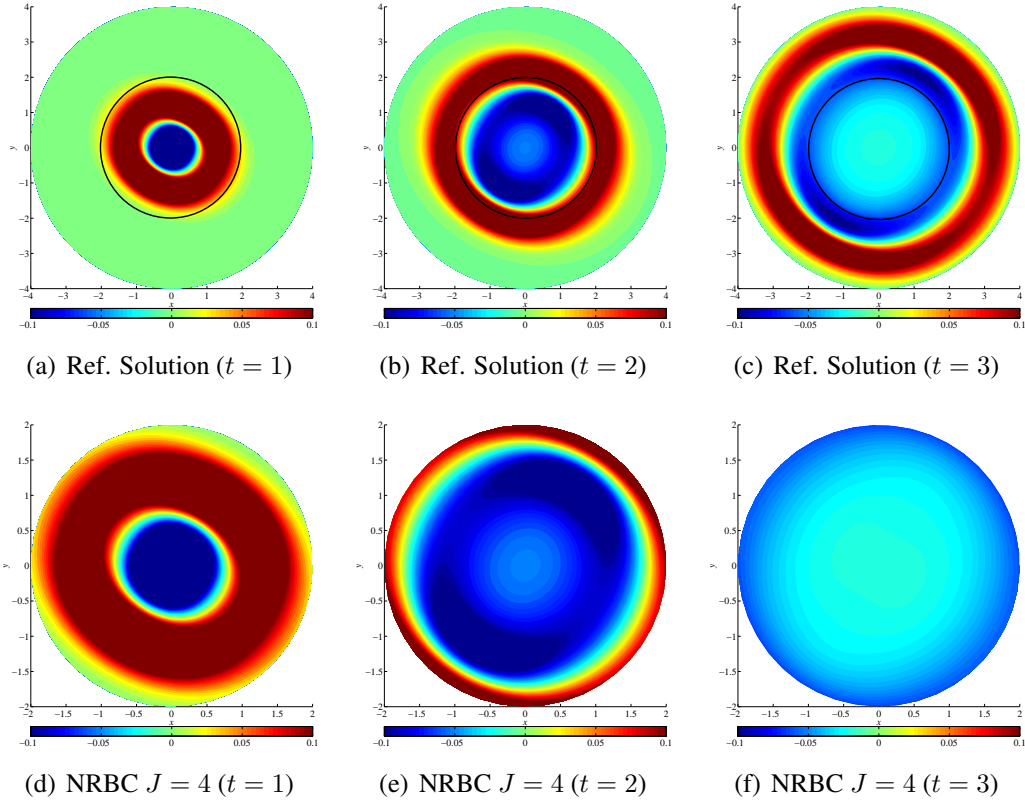


Figure 32: Open Domain, 4^{th} order spectral elements ($J = 4$) using oblique Gaussian initial condition shown for $t = 1, 2, 3$. **Top Plots:** Contour plots of reference solution solved on extended domain. Superimposed black circle indicates NRBC domain. **Bottom Plots:** Contour plots of various NRBC boundary configurations using $J = 4$.

synopsis of their derivation follows with results presented for *mild* dispersion where $f^2 = 0.1$.

We first consider the KGE without advection (in polar coordinates as in the HH derivation):

$$\frac{1}{c_0^2} \frac{\partial^2 h}{\partial t^2} = \frac{\partial^2 h}{\partial r^2} + \frac{1}{r} \frac{\partial h}{\partial r} + \frac{1}{r^2} \frac{\partial^2 h}{\partial \theta^2} - \frac{f^2}{c_0^2} h. \quad (\text{VII.15})$$

As has been previously discussed, in the geophysical context, the dispersion parameter is typically small. We assume here that

$$\frac{f}{c_0 K} \ll 1, \quad (\text{VII.16})$$

Table 8: L^2_Ω Error as a function of NRBC Order for Hagstrom Hariharan NRBC formulation using various spectral element orders on the circular NRBC domain. Oblique Gaussian initial condition is used.

NRBC Order	L^2_Ω Error Linear Elements	L^2_Ω Error Order 2 Elements	L^2_Ω Error Order 4 Elements	L^2_Ω Error Order 6 Elements
$J = 1$	0.09310	0.04772	0.04555	0.04485
$J = 2$	0.03381	0.00465	0.00355	0.00315
$J = 3$	0.02355	0.00324	0.00243	0.00259
$J = 4$	0.02217	0.00305	0.00236	0.00201
$J = 5$	0.02198	0.00302	0.00230	0.00196
$J = 10$	0.02195	0.00302	0.00228	0.00196
$J = 20$	0.02195	0.00302	0.00228	0.00196

where K is a typical wave number appearing in the solution. Now, apply the Fourier transform to (VII.6) and (VII.15) in time to yield:

$$\begin{aligned} \frac{\omega^2}{c_0^2} \hat{h} + \frac{\partial^2 \hat{h}}{\partial r^2} + \frac{1}{r} \frac{\partial \hat{h}}{\partial r} + \frac{1}{r^2} \frac{\partial^2 \hat{h}}{\partial \theta^2} &= 0 & \text{Wave} \\ \left(\frac{\omega^2}{c_0^2} - \frac{f^2}{c_0^2} \right) \hat{h} + \frac{\partial^2 \hat{h}}{\partial r^2} + \frac{1}{r} \frac{\partial \hat{h}}{\partial r} + \frac{1}{r^2} \frac{\partial^2 \hat{h}}{\partial \theta^2} &= 0 & \text{Klein-Gordon} \end{aligned}$$

where ω is the frequency and \hat{h} is the frequency domain representation of h . In both cases, we obtain the Helmholtz equation:

$$\bar{K}^2 \hat{h} + \frac{\partial^2 \hat{h}}{\partial r^2} + \frac{1}{r} \frac{\partial \hat{h}}{\partial r} + \frac{1}{r^2} \frac{\partial^2 \hat{h}}{\partial \theta^2} = 0.$$

In the non-dispersive case, $\bar{K} = \frac{\omega}{c_0} \equiv K$ and $\bar{K} = \sqrt{K^2 - \frac{f^2}{c_0^2}}$ in the dispersive case. In order to facilitate the conversion back to the time domain, we now consider a Taylor series approximation to the square root term found in the dispersive case, i.e.,

$$\sqrt{1-x} = 1 - \frac{1}{2}x + O(x^2).$$

Provided that x is small, we can truncate the $O(x^2)$ terms. In our case, from (VII.16) we can reasonably make this assumption yielding for the dispersive case:

$$\frac{\bar{K}}{K} = \sqrt{1 - \frac{f^2}{c_0^2 K^2}} \approx 1 - \frac{f^2}{2c_0^2 K^2} \Rightarrow \bar{K} \approx K - \frac{f^2}{2c_0^2 K}.$$

We now see that in the frequency domain, an equation valid in the non-dispersive case is valid in the dispersive case if we make the replacement:

$$K \rightarrow \sqrt{K^2 - \frac{f^2}{c_0^2}} \approx K - \frac{f^2}{2c_0^2 K}. \quad (\text{VII.17})$$

We now turn our attention to the boundary condition (VII.7) and (VII.8) that we Fourier transform in time to yield:

$$-iK\hat{h} + \frac{\partial \hat{h}}{\partial r} + \frac{1}{2r}\hat{h} = \hat{\phi}_1 \quad (\text{VII.18})$$

$$-iK\hat{\phi}_j + \frac{j}{r}\hat{\phi}_j - \frac{(j - \frac{1}{2})^2}{4r^2}\hat{\phi}_{j-1} - \frac{1}{4r^2}\frac{\partial^2 \hat{\phi}_{j-1}}{\partial \theta^2} = \hat{\phi}_{j+1}, \quad j = 1, \dots, J-1. \quad (\text{VII.19})$$

Making the substitution (VII.17), we obtain the dispersive version of the HH formulation in the frequency domain, i.e.,

$$\begin{aligned} & -iK\hat{h} + \frac{if^2}{2c_0^2 K}\hat{h} + \frac{\partial \hat{h}}{\partial r} + \frac{1}{2r}\hat{h} = \hat{\phi}_1 \\ & -iK\hat{\phi}_j + \frac{if^2}{2c_0^2 K}\hat{\phi}_j + \frac{j}{r}\hat{\phi}_j - \frac{(j - \frac{1}{2})^2}{4r^2}\hat{\phi}_{j-1} - \frac{1}{4r^2}\frac{\partial^2 \hat{\phi}_{j-1}}{\partial \theta^2} = \hat{\phi}_{j+1}, \quad j = 1, \dots, J-1. \end{aligned}$$

Transforming these equations back into the time domain results in the final HH boundary formulation for the KGE:

$$\frac{1}{c_0} \frac{\partial h}{\partial t} + \frac{f^2}{2c_0} \underbrace{\int_0^t h(\tau) d\tau}_{m(t)} + \frac{\partial h}{\partial r} + \frac{1}{2r} h = \phi_1 \quad (\text{VII.20})$$

$$\frac{1}{c_0} \frac{\partial \phi_j}{\partial t} + \frac{f^2}{2c_0} \underbrace{\int_0^t \phi_j(\tau) d\tau}_{n(t)} + \frac{j}{r} \phi_j - \frac{(j - \frac{1}{2})^2}{4r^2} \phi_{j-1} - \frac{1}{4r^2} \frac{\partial^2 \phi_{j-1}}{\partial \theta^2} = \phi_{j+1} \quad (\text{VII.21})$$

where

$$j = 1, \dots, J-1, \quad \phi_0 \equiv 2h \quad \text{and} \quad \phi_J \equiv 0.$$

It should be noted that van Joolen et al. [60] show how $m(t)$ and $n(t)$ can be calculated in each time-step to keep the boundary condition local in time without having to store and operate on the history of the solution. For this analysis, a simple trapezoidal approximation was used to approximate the integral.

The weak form of the formulation is now constructed. We consider the KGE in its general form:

$$\frac{\partial^2 h}{\partial t^2} - c_0^2 \nabla^2 h + f^2 h = 0.$$

Multiplying by the test functions Ψ_i and integrating over the circular domain yields the weak integral form

$$\int_{\Omega} \Psi_i \frac{\partial^2 h}{\partial t^2} d\Omega - c_0^2 \int_{\Omega} \Psi_i \nabla^2 h d\Omega + f^2 \int_{\Omega} \Psi_i h d\Omega = 0.$$

Transferring the second order spatial derivatives from h to the basis functions via integration by parts and applying the divergence theorem to recast one surface integral term as a boundary integral gives us

$$\int_{\Omega} \Psi_i \frac{\partial^2 h}{\partial t^2} d\Omega - c_0^2 \int_{\Gamma} \Psi_i \vec{n} \cdot \nabla h d\Omega + c_0^2 \int_{\Omega} \nabla \Psi_i \cdot \nabla h d\Omega + f^2 \int_{\Omega} \Psi_i h d\Omega = 0. \quad (\text{VII.22})$$

Of note now is that the boundary condition (VII.20) contains a radial derivatives of h that on the circle is precisely the normal derivative $\vec{n} \cdot \nabla h$. This allows direct implementation of the boundary condition into (VII.22) as follows:

$$\begin{aligned} \int_{\Omega} \Psi_i \frac{\partial^2 h}{\partial t^2} d\Omega - c_0^2 \int_{\Gamma} \Psi_i \left(\phi_1 - \frac{1}{c_0} \frac{\partial h}{\partial t} - \frac{1}{2r} h - \frac{f^2}{2c_0} m(t) \right) d\Omega \\ + c_0^2 \int_{\Omega} \nabla \Psi_i \cdot \nabla h d\Omega + f^2 \int_{\Omega} \Psi_i h d\Omega = 0. \end{aligned} \quad (\text{VII.23})$$

Here, since on the boundary the radius is fixed, the $\frac{1}{2r}$ term may be treated as a constant.

A similar weak form is constructed for the boundary formulation by multiplying (VII.21) by the test functions ζ_i and integrating over Γ yielding (after by integration by parts):

$$\begin{aligned} \frac{1}{c_0} \int_{\Gamma} \zeta_i \frac{\partial \phi_j}{\partial t} d\Gamma + \frac{f^2}{2c_0} \int_{\Gamma} \zeta_i n(t) d\Gamma + \frac{j}{r} \int_{\Gamma} \zeta_i \phi_j d\Gamma - \frac{(j - \frac{1}{2})^2}{4r^2} \int_{\Gamma} \zeta_i \phi_{j-1} d\Gamma \\ - \frac{1}{4r^2} \zeta_i \frac{\partial \phi_{j-1}}{\partial \theta} \Big|_{start}^{end} + \frac{1}{4r^2} \int_{\Gamma} \frac{\partial \zeta_i}{\partial \theta} \frac{\partial \phi_{j-1}}{\partial \theta} d\Gamma = \int_{\Gamma} \zeta_i \phi_{j+1} d\Gamma. \end{aligned} \quad (\text{VII.24})$$

We now use the fact that the boundary is continuous and closed to surmise that the endpoint evaluation term vanishes. The formal problem statement is then: Find $h \in \mathcal{V}$ and $\phi_j \in \mathcal{V}_{\Gamma}$ where $j = 1, \dots, J-1$, such that Equations (VII.23) and (VII.24) are satisfied $\forall \Psi_i \in \mathcal{V}$ and $\zeta_i \in \mathcal{V}_{\Gamma}$.

4. Results for HH with Dispersion

A series of experiments was conducted to determine the effect of the HH boundary condition extended to include mild dispersion for various SE and NRBC orders. The set-up is identical to the experiments without dispersion, except the dispersion parameter is set to $f^2 = 0.1$. Qualitative results are shown in Figure 33 and quantitative L_{Ω}^2 errors are shown for various NRBC orders for SE orders up to 6 in Table 9. As in the non-dispersive case, no improvement was observed for SE orders above order 6.

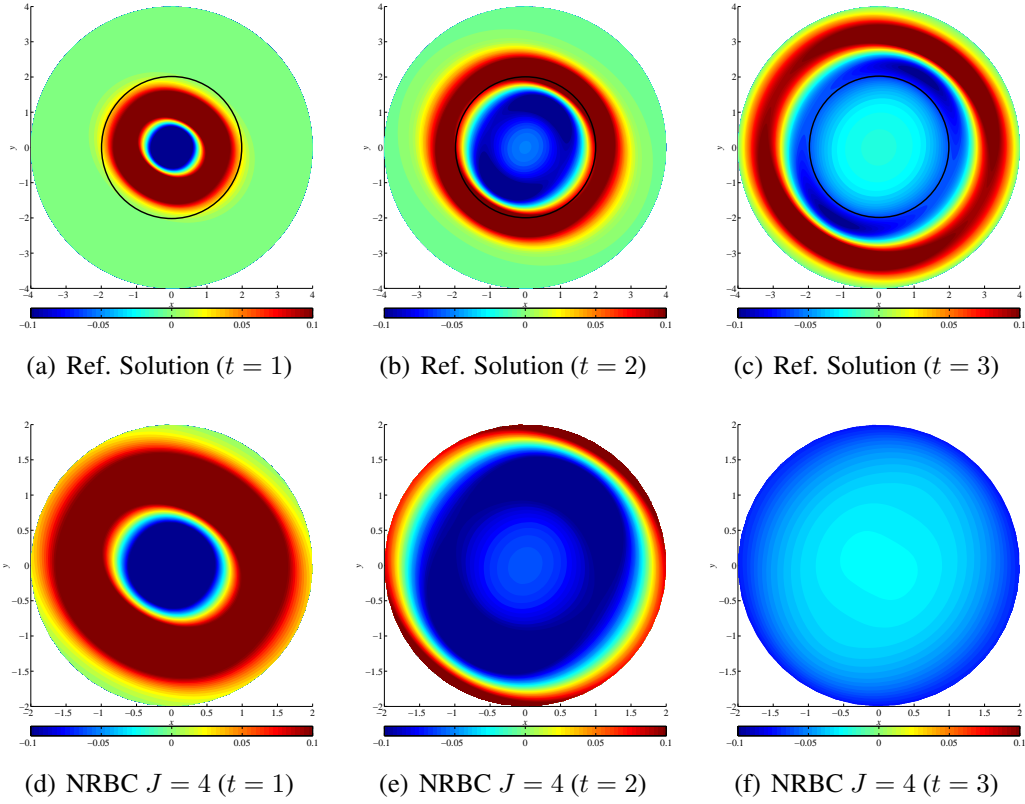


Figure 33: Open Domain, 4^{th} order spectral elements ($J = 4$) using oblique Gaussian initial condition shown for $t = 1, 2, 3$ under dispersion $f^2 = 0.1$. **Top Plots:** Contour plots of reference solution solved on extended domain. Superimposed black circle indicates NRBC domain. **Bottom Plots:** Contour plots of various NRBC boundary configurations using $J = 4$.

Table 9: L^2_Ω Error as a function of NRBC Order for Hagstrom Hariharan NRBC formulation using various spectral element orders on the circular NRBC domain. Oblique Gaussian initial condition is used with dispersion parameter set to $f^2 = 0.1$.

NRBC Order	L^2_Ω Error Linear Elements	L^2_Ω Error Order 2 Elements	L^2_Ω Error Order 4 Elements	L^2_Ω Error Order 6 Elements
$J = 1$	0.07290	0.03555	0.03369	0.03293
$J = 2$	0.02684	0.00371	0.00283	0.00248
$J = 3$	0.01869	0.00258	0.00192	0.00204
$J = 4$	0.01759	0.00243	0.00186	0.00157
$J = 5$	0.01744	0.00240	0.00181	0.00154
$J = 10$	0.01742	0.00240	0.00180	0.00153
$J = 20$	0.01742	0.00240	0.00180	0.00153

VIII. CONCLUSIONS AND AREAS FOR FUTURE RESEARCH

In this dissertation, we considered a reduced form of the shallow water equations in various (semi-infinite and infinite channels as well as open domain) configurations. Using the Givoli-Neta auxiliary variable formulation of the Higdon non-reflecting boundary conditions, we truncated the original infinite domain and developed the boundary conditions specific to the problem at hand. Using a high-order approach to the spatial discretization (spectral elements), time integration (high-order Runge-Kutta) in concert with high-order boundary treatment, we showed *exponential* convergence to the reference solution in channel configurations. These results suggest a balanced approach to dealing with truncation errors – namely, to make improvements in *all* components of the problem to see improved accuracy.

In open domain problems, we considered various ways to handle corner compatibility concerns when using the Givoli-Neta auxiliary variable formulation. Using a physical argument that the auxiliary variables themselves should be non-reflecting at a boundary, we formulated a spectral element formulation that yielded stable solutions (even for long term time integrations) using first order NRBCs for the auxiliary variables. This formulation showed significant improvement from the first order ($J = 1$ Sommerfeld condition) to higher order J , although the improvement was far from exponential. Besides the low order method of handling the auxiliary variable boundaries, the “node-splitting” method of handling double-counting corner nodes turned out to be convergence limiting.

Recognizing that any formulation that included corners would be problematic, we sought a boundary condition that would be valid for an arbitrarily shaped domain. The Givoli-Neta formulation was shown to have insurmountable implementation issues without the simplifying assumption of small curvature on the boundary. When the small curvature assumption was made, the formulation was shown to have stable, improved results from the first order ($J = 1$) Sommerfeld condition. It was clear, however, that there are trade-offs associated between accurately representing the Givoli-Neta formulation and removing

the problematic corners. Specifically, using a square domain (where the small curvature assumption affects only the four corner points) errors were shown to be improved over alternative domains (rounded square and circle).

The final experiments conducted considered a boundary condition originally devised by Hagstrom and Hariharan and extended to the dispersive wave equation by van Joolen et al. This boundary condition is based on the asymptotic series representation of the wave equation in polar coordinates, valid for large radial distances. Results were improved over the alternative arbitrary domain formulations although valid only for large radial distances and restricted to circular boundary domains in this analysis.

This research has demonstrated exponential convergence in channel experiments, only hypothesized in previous low-order settings. Additionally, it has developed several alternatives to handling open domains which improve performance to first-order NRBC schemes at a very moderate computational cost. What remains is to extend this high-order numerical formulation to more complex linear and non-linear systems of fluid motion such as the Euler equations. Additionally, better alternatives to dealing with corner compatibility concerns remains an open problem.

APPENDIX A. DEPTH INTEGRATING THE CONTINUITY EQUATION

In order to arrive at the final form of the shallow water equations, we depth integrated our shallow water continuity equation. The details follow. Given

$$0 = \nabla \cdot \mathbf{u}$$

we integrate in z

$$\begin{aligned} 0 &= \int_{-h_B}^h \nabla \cdot \mathbf{u} dz \\ &= \int_{-h_B}^h \left(\frac{\partial u}{\partial x} + \frac{\partial v}{\partial y} \right) dz + w|_{z=h} - w|_{z=-h_B} \end{aligned} \quad (\text{A.1})$$

Since both h and h_B depend on x and y (and t for h), we apply the Leibniz integral rule, which allows us to write:

$$\begin{aligned} \frac{\partial}{\partial x} \int_{z=-h_B}^{z=h} u dz &= \int_{z=-h_B}^{z=h} \frac{\partial u}{\partial x} dz + u \Big|_h \frac{\partial h}{\partial x} - u \Big|_{h_B} \frac{\partial (-h_B)}{\partial x} \\ \frac{\partial}{\partial y} \int_{z=-h_B}^{z=h} v dz &= \int_{z=-h_B}^{z=h} \frac{\partial v}{\partial y} dz + v \Big|_h \frac{\partial h}{\partial y} - v \Big|_{h_B} \frac{\partial (-h_B)}{\partial y}. \end{aligned}$$

Substituting these into (A.1) we have

$$\begin{aligned} 0 &= \frac{\partial}{\partial x} \int_{-h_B}^h u dz - \left(u \Big|_{z=h} \frac{\partial h}{\partial x} - u \Big|_{z=-h_B} \frac{\partial (-h_B)}{\partial x} \right) \\ &\quad + \frac{\partial}{\partial y} \int_{-h_B}^h v dz - \left(v \Big|_{z=h} \frac{\partial h}{\partial y} - v \Big|_{z=-h_B} \frac{\partial (-h_B)}{\partial y} \right) + w \Big|_{z=h} - w \Big|_{z=-h_B}. \end{aligned}$$

Now, using the appropriate boundary conditions

$$w(x, y, -h_B) = -u \frac{\partial h_B}{\partial x} - v \frac{\partial h_B}{\partial y}$$

$$w(x, y, h, t) = \frac{\partial h}{\partial t} + u \frac{\partial h}{\partial x} + v \frac{\partial h}{\partial y}$$

we substitute to find

$$0 = \frac{\partial}{\partial x} \int_{-h_B}^h u dz + \frac{\partial}{\partial y} \int_{-h_B}^h v dz - u \Big|_{z=h} \frac{\partial h}{\partial x} - v \Big|_{z=h} \frac{\partial h}{\partial y} - u \Big|_{z=-h_B} \frac{\partial h_B}{\partial x} - v \Big|_{z=-h_B} \frac{\partial h_B}{\partial y} + \frac{\partial h}{\partial t} + u \Big|_{z=h} \frac{\partial h}{\partial x} + v \Big|_{z=h} \frac{\partial h}{\partial y} + u \Big|_{z=-h_B} \frac{\partial h_B}{\partial x} + v \Big|_{z=-h_B} \frac{\partial h_B}{\partial y}.$$

Which simplifies to

$$\frac{\partial h}{\partial t} + \frac{\partial}{\partial x} \int_{-h_B}^h u dz + \frac{\partial}{\partial y} \int_{-h_B}^h v dz.$$

The construction of the shallow water model as shown in Figure 3 has $H = h + h_B$ where H is the depth of the fluid. Since a previous argument showed that u and v are independent of depth, we are left with our final, depth integrated continuity equation

$$\frac{\partial h}{\partial t} + \frac{\partial}{\partial x} (Hu) + \frac{\partial}{\partial y} (Hv) = 0$$

APPENDIX B. LINEARIZING THE SHALLOW WATER EQUATIONS

The non-linear version of the shallow water equations are:

$$\partial_t u + u \partial_x u + v \partial_y u - f v = -g \partial_x h$$

$$\partial_t v + u \partial_x v + v \partial_y v + f u = -g \partial_y h$$

$$\partial_t h + \partial_x (H u) + \partial_y (H v) = 0.$$

We wish to find a linear version of these equations. Suppose the bottom topography is flat such that h_B is constant and u and v can be described by a constant *mean* term and a small $O(\delta)$ deviation from that value, i.e.,

$$u = U + u^* \quad v = V + v^* \quad H = h_B + h$$

To be clear, U and V are the mean velocities and h_B is the mean water depth. We now make these perturbation substitutions.

$$\partial_t (U + u^*) + (U + u^*) \partial_x (U + u^*) + (V + v^*) \partial_y (U + u^*) - f (V + v^*) = -g \partial_x h$$

$$\partial_t (V + v^*) + (U + u^*) \partial_x (V + v^*) + (V + v^*) \partial_y (V + v^*) + f (U + u^*) = -g \partial_y h$$

$$\partial_t h + \partial_x ((h_B + h) (U + u^*)) + \partial_y ((h_B + h) (V + v^*)) = 0.$$

Now, recalling that U, V and h_B are constants, we simplify to find:

$$\partial_t u^* + (U + u^*) \partial_x u^* + (V + v^*) \partial_y u^* - f (V + v^*) = -g \partial_x h$$

$$\partial_t v^* + (U + u^*) \partial_x v^* + (V + v^*) \partial_y v^* + f (U + u^*) = -g \partial_y h$$

$$\partial_t h + h_B (\partial_x u^* + \partial_y v^*) + \partial_x h (U + u^*) + \partial_y h (V + v^*) + h (\partial_x u^* + \partial_y v^*) = 0.$$

If we expand each term, the result is:

$$\begin{aligned}
\partial_t u^* + U \partial_x u^* + u^* \partial_x u^* + V \partial_y u^* + v^* \partial_y u^* - f(V + v^*) &= -g \partial_x h \\
\partial_t v^* + U \partial_x v^* + u^* \partial_x v^* + V \partial_y v^* + v^* \partial_y v^* + f(U + u^*) &= -g \partial_y h \\
\partial_t h + h_B \partial_x u^* + h_B \partial_y v^* + U \partial_x h + u^* \partial_x h + V \partial_y h + v^* \partial_y h + h \partial_x u^* + h \partial_y v^* &= 0.
\end{aligned}$$

We now neglect any terms of $O(\delta^2)$ to arrive at our final form of the linearized shallow water equations:

$$\begin{aligned}
\partial_t u^* + U \partial_x u^* + V \partial_y u^* - f(V + v^*) &= -g \partial_x h \\
\partial_t v^* + U \partial_x v^* + V \partial_y v^* + f(U + u^*) &= -g \partial_y h \\
\partial_t h + U \partial_x h + V \partial_y h + h_B (\partial_x u^* + \partial_y v^*) &= 0.
\end{aligned}$$

APPENDIX C. ADJUSTING HIGDON'S CONDITION FOR ADVECTION

Suppose that we have a wave that moves according to

$$(\partial_t + U \partial_x)^2 h - c_0^2 \partial_x^2 h = 0. \quad (\text{C.1})$$

This equation can be “factored” as follows:

$$0 = \left(\partial_t + (U - c_0) \partial_x \right) \left(\partial_t + (U + c_0) \partial_x \right) h$$

Following a standard method of characteristics derivation, we define functions w and v as

$$w(x, t) = \partial_t h + (U - c_0) \partial_x h$$

$$v(x, t) = \partial_t h + (U + c_0) \partial_x h.$$

It can be verified that both

$$\partial_t w + (U - c_0) \partial_x w = 0$$

$$\partial_t v + (U + c_0) \partial_x v = 0$$

satisfy (C.1) exactly. If we then solve w along its characteristic $x = (U - c_0) t + x_0$ and v along its characteristic $x = (U + c_0) t + x_0$, with initial data $w(x_0, 0) = P(x_0)$ and $v(x_0, 0) = Q(x_0)$, then the solutions for w and v are respectively

$$w(x, t) = P\left(x - (U - c_0)t\right) = \partial_t h + (U - c_0) \partial_x h \quad (\text{C.2})$$

$$v(x, t) = Q\left(x - (U + c_0)t\right) = \partial_t h + (U + c_0) \partial_x h \quad (\text{C.3})$$

We subtract (C.3) from (C.2) to find

$$\begin{aligned}
P\left(x - (U - c_0)t\right) &= \partial_t h + (U + c_0)\partial_x h \\
- Q\left(x - (U + c_0)t\right) &= \partial_t h + (U - c_0)\partial_x h \\
\hline
P\left(x - (U - c_0)t\right) - Q\left(x - (U + c_0)t\right) &= 2c_0\partial_x h.
\end{aligned} \tag{C.4}$$

Further, if we combine (C.2) and (C.3) as

$$\begin{aligned}
(U - c_0)P\left(x - (U - c_0)t\right) &= (U - c_0)\left(\partial_t h + (U + c_0)\partial_x h\right) \\
- (U + c_0)Q\left(x - (U + c_0)t\right) &= (U + c_0)\left(\partial_t h + (U - c_0)\partial_x h\right) \\
\hline
(U - c_0)P\left(x - (U - c_0)t\right) - (U + c_0)Q\left(x - (U + c_0)t\right) &= -2c_0\partial_t h.
\end{aligned} \tag{C.5}$$

This implies that the solution takes the form $h(x, t) = F\left(x - (U + c_0)t\right) + G\left(x - (U - c_0)t\right)$.

Here, F and G are arbitrary functions of the initial data. To see this, consider

$$\partial_t h = -(U + c_0)F'\left(x - (U + c_0)t\right) - (U - c_0)G'\left(x - (U - c_0)t\right) \tag{C.6}$$

$$\partial_x h = F'\left(x - (U + c_0)t\right) + G'\left(x - (U - c_0)t\right). \tag{C.7}$$

Equating coefficients with (C.4) and (C.5) this yields a relation between the initial data and the functions F and G

$$P\left(x - (U - c_0)t\right) = 2c_0G'\left(x - (U - c_0)t\right) \tag{C.8}$$

$$Q\left(x - (U + c_0)t\right) = -2c_0F'\left(x - (U + c_0)t\right). \tag{C.9}$$

This solution can be rewritten as

$$h(x, t) = F\left(x - (c_0 + U)t\right) + G\left(x + (c_0 - U)t\right) \tag{C.10}$$

with the interpretation that the general solution is the sum of $F\left(x - (c_0 + U)t\right)$, a wave of fixed shape moving to the right with velocity $(c_0 + U)$ and $G\left(x + (c_0 - U)t\right)$ a wave of fixed shape moving to the left with velocity $(c_0 - U)$.

THIS PAGE INTENTIONALLY LEFT BLANK

APPENDIX D. NORMAL TO TANGENTIAL DERIVATIVE TRANSFORMATION FOR EASTERN NRBC

The function h satisfies the dispersive, advective wave equation (II.29) in D . Since the function ϕ_1 is obtained by applying the linear (constant coefficient) operator $\left(\partial_x + \frac{1}{C_1}\partial_t\right)$ to h , it can be shown that ϕ_1 should also satisfy the same equation in D ⁹. Further, since ϕ_j is obtained by applying the same linear operator $j - 1$ times to ϕ_1 , the functions ϕ_j should satisfy an equation like (II.29), namely,

$$\begin{aligned} &\left(\partial_{tt} + (U^2 - c_0^2)\partial_{xx} + (V^2 - c_0^2)\partial_{yy} + \right. \\ &\quad \left. 2U\partial_{xt} + 2V\partial_{yt} + 2UV\partial_{xy} + f^2\right)\phi_j = 0 \end{aligned} \quad (\text{D.1})$$

Now, use the following identities:

$$\partial_{xx}\phi_j = \left(\partial_x - \frac{1}{C_{j+1}}\partial_t\right)\left(\partial_x + \frac{1}{C_{j+1}}\partial_t\right)\phi_j + \frac{1}{C_{j+1}^2}\ddot{\phi}_j \quad (\text{D.2})$$

$$\partial_{xt}\phi_j = \partial_t(\partial_x\phi_j) \quad (\text{D.3})$$

$$\partial_{xy}\phi_j = \partial_y(\partial_x\phi_j) \quad (\text{D.4})$$

and

$$\left(\partial_x + \frac{1}{C_j}\partial_t\right)\phi_{j-1} = \phi_j \quad j = 1, \dots, J. \quad (\text{D.5})$$

⁹Here we must use the assumption that c_0 and f are constants. By applying the differential operator to (II.29), computing each of the ϕ_j derivatives present in (III.17) using the differential operator and simplifying, a simple induction argument shows that the ϕ_j 's must satisfy (III.17)

Now, if we substitute (D.2) - (D.4) into (D.1), and replace j with $j - 1$ everywhere yields, for $j = 1, \dots, J$

$$\ddot{\phi}_{j-1} + (U^2 - c_0^2) \left[\left(\partial_x - \frac{1}{C_j} \partial_t \right) \left(\partial_x + \frac{1}{C_j} \partial_t \right) \phi_{j-1} + \frac{1}{C_j^2} \ddot{\phi}_{j-1} \right] + (V^2 - c_0^2) \partial_{yy} \phi_{j-1} + 2U \partial_t (\partial_x \phi_{j-1}) + 2V \partial_{yt} \phi_{j-1} + 2UV \partial_y (\partial_x \phi_{j-1}) + f^2 \phi_{j-1} = 0 \quad (\text{D.6})$$

From this and (D.5) one gets, for $j = 1, \dots, J$

$$\ddot{\phi}_{j-1} + (U^2 - c_0^2) \left[\left(\partial_x - \frac{1}{C_j} \partial_t \right) \phi_j + \frac{1}{C_j^2} \ddot{\phi}_{j-1} \right] + (V^2 - c_0^2) \partial_{yy} \phi_{j-1} + 2U \partial_t (\partial_x \phi_{j-1}) + 2V \partial_{yt} \phi_{j-1} + 2UV \partial_y (\partial_x \phi_{j-1}) + f^2 \phi_{j-1} = 0 \quad (\text{D.7})$$

Now, we shift indices on (D.5) and multiply both sides by $(U^2 - c_0^2)$ as:

$$(U^2 - c_0^2) \left(\partial_x + \frac{1}{C_{j+1}} \partial_t \right) \phi_j = (U^2 - c_0^2) \phi_{j+1} \quad j = 0, \dots, J - 1. \quad (\text{D.8})$$

Subtract (D.7) from (D.8)

$$-\ddot{\phi}_{j-1} + (U^2 - c_0^2) \left(\frac{1}{C_j} + \frac{1}{C_{j+1}} \right) \dot{\phi}_j - (U^2 - c_0^2) \frac{1}{C_j^2} \ddot{\phi}_{j-1} - (V^2 - c_0^2) \partial_{yy} \phi_{j-1} - 2U \partial_t (\partial_x \phi_{j-1}) - 2V \partial_{yt} \phi_{j-1} - 2UV \partial_y (\partial_x \phi_{j-1}) - f^2 \phi_{j-1} = (U^2 - c_0^2) \phi_{j+1} \quad (\text{D.9})$$

Now, consider (D.5). Expanding and solving for $\partial_x \phi_{j-1}$, we get:

$$\partial_x \phi_{j-1} = \phi_j - \frac{1}{C_j} \dot{\phi}_{j-1} \quad j = 1, \dots, J. \quad (\text{D.10})$$

Substitute (D.10) into (D.9)

$$\begin{aligned}
& -\ddot{\phi}_{j-1} + (U^2 - c_0^2) \left(\frac{1}{C_j} + \frac{1}{C_{j+1}} \right) \dot{\phi}_j - (U^2 - c_0^2) \frac{1}{C_j^2} \ddot{\phi}_{j-1} - \\
& (V^2 - c_0^2) \partial_{yy} \phi_{j-1} - 2U \partial_t \left(\phi_j - \frac{1}{C_j} \dot{\phi}_{j-1} \right) - 2V \partial_{yt} \phi_{j-1} - \\
& 2UV \partial_y \left(\phi_j - \frac{1}{C_j} \dot{\phi}_{j-1} \right) - f^2 \phi_{j-1} = (U^2 - c_0^2) \phi_{j+1}
\end{aligned} \tag{D.11}$$

Simplify:

$$\begin{aligned}
& \left(\frac{2U}{C_j} - 1 - \frac{U^2 - c_0^2}{C_j^2} \right) \ddot{\phi}_{j-1} + \left(\frac{2UV}{C_j} - 2V \right) \dot{\phi}'_{j-1} - (V^2 - c_0^2) \phi''_{j-1} + \\
& \left((U^2 - c_0^2) \left(\frac{1}{C_j} + \frac{1}{C_{j+1}} \right) - 2U \right) \dot{\phi}_j - 2UV \phi'_j - f^2 \phi_{j-1} = (U^2 - c_0^2) \phi_{j+1} \tag{D.12}
\end{aligned}$$

for $j = 1, \dots, J - 1$

In (D.12) and elsewhere, a prime indicates differentiation with respect to y along Γ_E , i.e. the tangential derivative along those boundaries.

THIS PAGE INTENTIONALLY LEFT BLANK

APPENDIX E. METRIC TERMS DERIVATION

To facilitate interpolation and integration required for the SE method, we transform all terms of the weak integral form in physical space $\mathbf{x} = (x, y)^T$ to a canonical space $\boldsymbol{\xi} = (\xi, \eta)^T$. This nonsingular mapping assumes $\mathbf{x} = \mathbf{x}(\xi, \eta)$ and conversely $\boldsymbol{\xi} = \boldsymbol{\xi}(x, y)$.

A. DERIVATION OF METRIC TERMS

Using the chain rule, we find

$$d\mathbf{x} = \frac{\partial \mathbf{x}}{\partial \xi} d\xi + \frac{\partial \mathbf{x}}{\partial \eta} d\eta,$$

which can be written in matrix form

$$\begin{pmatrix} dx \\ dy \end{pmatrix} = J^e \begin{pmatrix} d\xi \\ d\eta \end{pmatrix}. \quad (\text{E.1})$$

Here J^e is the transformation Jacobian with associated determinant $|J^e|$ defined as

$$J^e = \begin{pmatrix} \frac{\partial x}{\partial \xi} & \frac{\partial x}{\partial \eta} \\ \frac{\partial y}{\partial \xi} & \frac{\partial y}{\partial \eta} \end{pmatrix}, \quad |J^e| = \frac{\partial x}{\partial \xi} \frac{\partial y}{\partial \eta} - \frac{\partial y}{\partial \xi} \frac{\partial x}{\partial \eta}. \quad (\text{E.2})$$

Similarly, we can find the inverse transformation

$$d\boldsymbol{\xi} = \frac{\partial \boldsymbol{\xi}}{\partial x} dx + \frac{\partial \boldsymbol{\xi}}{\partial y} dy$$

and write the derivatives of $\boldsymbol{\xi}(x, y)$ in matrix form as

$$\begin{pmatrix} d\xi \\ d\eta \end{pmatrix} = J_{\boldsymbol{\xi}}^e \begin{pmatrix} dx \\ dy \end{pmatrix} \quad (\text{E.3})$$

where

$$J_{\xi}^e = \begin{pmatrix} \frac{\partial \xi}{\partial x} & \frac{\partial \xi}{\partial y} \\ \frac{\partial \eta}{\partial x} & \frac{\partial \eta}{\partial y} \end{pmatrix} \quad (\text{E.4})$$

is the Jacobian of the inverse transformation. Since the Jacobian described by (E.2) is non-singular, we can write the transformation described by (E.1) as

$$\begin{pmatrix} d\xi \\ d\eta \end{pmatrix} = (J^e)^{-1} \begin{pmatrix} dx \\ dy \end{pmatrix}. \quad (\text{E.5})$$

Here $(J^e)^{-1}$ is the standard matrix inverse defined by

$$(J^e)^{-1} = \frac{1}{|J^e|} \begin{pmatrix} \frac{\partial y}{\partial \eta} & -\frac{\partial x}{\partial \eta} \\ -\frac{\partial y}{\partial \xi} & \frac{\partial x}{\partial \xi} \end{pmatrix} \quad (\text{E.6})$$

We now note that the formulations described by (E.3) and (E.5) are identical, therefore, equating coefficients from the two Jacobian terms (E.4) and (E.6) yields the metric terms

$$\frac{\partial \xi}{\partial x} = \frac{1}{|J^e|} \frac{\partial y}{\partial \eta}, \quad \frac{\partial \xi}{\partial y} = -\frac{1}{|J^e|} \frac{\partial x}{\partial \eta}, \quad \frac{\partial \eta}{\partial x} = -\frac{1}{|J^e|} \frac{\partial y}{\partial \xi}, \quad \frac{\partial \eta}{\partial y} = \frac{1}{|J^e|} \frac{\partial x}{\partial \xi}. \quad (\text{E.7})$$

This formulation is convenient since all metric terms are defined in terms of terms that are readily calculated via basis function expansions of $\mathbf{x}(\xi, \eta)$.

B. CONSEQUENCES OF QUADRILATERAL GRID DEGENERATION

Given the discussion of metric terms, we see that there is a common term in that has the potential to cause numerical instability – namely $\frac{1}{|J^e|}$. If the elemental Jacobian tends to zero, then all metric terms associated with that Jacobian will tend toward infinity. In fact, if the element Jacobian is small at certain points on the global domain compared with other locations on the global domain, experiments in this dissertation have shown that they tend

to corrupt the entire solution. The question then arises, what element geometries have the potential to cause numerical instabilities?

Since the global problem is discretized into smaller elements, this question must be answered in the context of grid generation. There is general agreement in literature [45, 61, 62, 63, 64, 65, 66] concerning quadrilateral grid generation that convex elements with maximum internal angles $\approx 135^\circ$ constitute a *quality* mesh. Li et al. in [67] describe procedures to adjust quadrilateral basis functions to deal with elements that have large interior angles or, in fact completely degenerate into triangles, although with these adjustments, computational overhead is increased to deal with alternate canonical geometries. In this analysis, we seek a quality **all quadrilateral** mesh.

To demonstrate how a poorly generated mesh can taint a solution, we consider an extreme example where a quadrilateral element is degenerated into a triangle as shown in Figure 34. In this case, one of the internal angles of the “*quadrilateral*” is 180° .

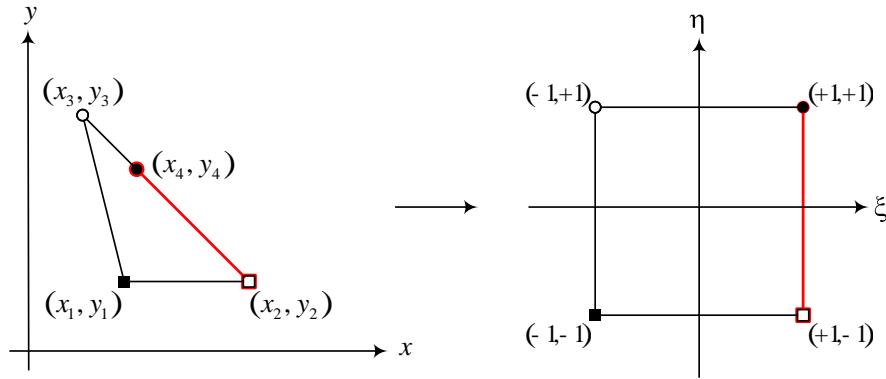


Figure 34: Degenerate quadrilateral mapped to a canonical reference element.

Now, consider the linear basis function expansion (similar argument for higher order expansions) of the physical coordinates and their derivatives

$$\begin{aligned}\mathbf{x}_N(\xi, \eta) &= \sum_{k=1}^4 \psi_k(\xi, \eta) \mathbf{x}_k \\ \frac{\partial \mathbf{x}_N}{\partial \xi}(\xi, \eta) &= \sum_{k=1}^4 \frac{\partial \psi_k}{\partial \xi}(\xi, \eta) \mathbf{x}_k\end{aligned}$$

where the linear Lagrange basis functions are defined as

$$\begin{aligned}\psi_1(\xi, \eta) &= \frac{1}{4}(1 - \xi)(1 - \eta), & \psi_2(\xi, \eta) &= \frac{1}{4}(1 + \xi)(1 - \eta), \\ \psi_3(\xi, \eta) &= \frac{1}{4}(1 - \xi)(1 + \eta), & \psi_4(\xi, \eta) &= \frac{1}{4}(1 + \xi)(1 + \eta).\end{aligned}$$

We consider the degenerate vertex located at $(\xi, \eta) = (1, 1)$ and compute each term required for computation of the Jacobian.

$$\begin{aligned}\frac{\partial x}{\partial \xi}(1, 1) &= \frac{1}{2}(-x_3 + x_4), & \frac{\partial x}{\partial \eta}(1, 1) &= \frac{1}{2}(-x_2 + x_4), \\ \frac{\partial y}{\partial \xi}(1, 1) &= \frac{1}{2}(-y_3 + y_4), & \frac{\partial y}{\partial \eta}(1, 1) &= \frac{1}{2}(-y_2 + y_4).\end{aligned}$$

Using the fact that $(x_2, y_2), (x_3, y_3), (x_4, y_4)$ are collinear, we put x_4 in terms of the other two points yielding

$$x_4 = \left(y_4 - y_3 + x_3 \left(\frac{y_3 - y_2}{x_3 - x_2} \right) \right) \left(\frac{x_3 - x_2}{y_3 - y_2} \right). \quad (\text{E.8})$$

Computing the determinant of the Jacobian (E.2) and simplifying using (E.8) yields

$$|J^e| = \frac{1}{4} \left((-x_3 + x_4)(-y_2 + y_4) - (-y_3 + y_4)(-x_2 + x_4) \right) = 0 \quad (\text{E.9})$$

This degenerate quadrilateral will have infinite metric terms. Even if the quadrilateral element does not completely degenerate into a triangle, but has a large angle – the metric

terms will be very large in comparison to other element metric terms and will have a destabilizing effect. Therefore, all meshes in this analysis were generated with internal angles less than 135° choosing to add additional elements (and degrees of freedom) to ensure that this happens.

THIS PAGE INTENTIONALLY LEFT BLANK

APPENDIX F. NON-DIMENSIONALIZATION OF THE KGE

Consider the KGE

$$(\partial_t + U\partial_x + V\partial_y)^2 h - c_0^2 \nabla^2 h + f^2 h = 0$$

that we wish to study in a non-dimensional context. For simplicity in derivation, we assume that there is no advection ($U = V = 0$), yielding:

$$\frac{\partial^2 h}{\partial t^2} - c_0^2 \nabla^2 h + f^2 h = 0.$$

Now, as outlined in [51], we examine typical scales of motion in the ocean so as to recast the problem in a dimensionless way (can substitute typical scales for atmosphere or other medium as well with the same process that follows). For this analysis, the length scales were chosen $O(100 \text{ km})$, vertical depth scales $O(100 \text{ m})$, scales for h $O(1 \text{ m})$ and the dispersion parameter f for Coriolis $O(10^{-4} \text{ s}^{-1})$. Given these choices, we know from the discussion in Chapter II that

$$c_0^2 = gh_B = \left(10 \frac{\text{m}}{\text{s}^2}\right) (100 \text{ m}) = 1000 \frac{\text{m}^2}{\text{s}^2}$$

that makes our specific problem:

$$\frac{\partial^2 h}{\partial t^2} - 1000 \frac{\text{m}^2}{\text{s}^2} \nabla^2 h + \frac{10^{-8}}{\text{s}^2} h = 0.$$

Now, we follow the details as outlined in [68] to scale out any dimensions. In particular, we define the following:

$$\bar{x} = \frac{x}{10^5} \frac{\text{m}}{\text{m}} \quad \bar{y} = \frac{y}{10^5} \frac{\text{m}}{\text{m}} \quad \bar{h} = \frac{h}{1} \frac{\text{m}}{\text{m}}$$

where the typical length scale is 100 km (10^5 m). Now, we note via the chain rule that:

$$\begin{aligned}\frac{\partial h}{\partial x} &= \frac{\partial h}{\partial \bar{x}} \frac{d\bar{x}}{dx} = \frac{\partial h}{\partial \bar{x}} \frac{1}{10^5 \text{m}} \\ \frac{\partial^2 h}{\partial x^2} &= \frac{\partial}{\partial x} \left(\frac{\partial h}{\partial x} \right) = \frac{1}{10^5 \text{m}} \frac{\partial}{\partial x} \left(\frac{\partial h}{\partial \bar{x}} \right) = \frac{1}{10^5 \text{m}} \frac{\partial}{\partial \bar{x}} \left(\frac{\partial h}{\partial x} \right) = \frac{1}{10^{10} \text{m}^2} \frac{\partial^2 h}{\partial \bar{x}^2}\end{aligned}$$

similarly,

$$\frac{\partial^2 h}{\partial y^2} = \frac{1}{10^{10} \text{m}^2} \frac{\partial^2 h}{\partial \bar{y}^2}.$$

Using this information in (F) yields:

$$\begin{aligned}\frac{\partial^2 h}{\partial t^2} - \frac{1000 \text{m}^2}{\text{s}^2} \left[\frac{1}{10^{10} \text{m}^2} (\nabla^2 h) \right] + \frac{10^{-8}}{\text{s}^2} h &= 0 \\ \Rightarrow \frac{\partial^2 h}{\partial t^2} - \frac{1}{10^7 \text{s}^2} \nabla^2 h + \frac{10^{-8}}{\text{s}^2} h &= 0 \\ \Rightarrow 10^7 \text{s}^2 \frac{\partial^2 h}{\partial t^2} - \nabla^2 h + 0.1 h &= 0\end{aligned}$$

Now, we remove the dimensions from our variable h to get

$$10^7 \text{s}^2 \frac{\partial^2 \bar{h}}{\partial t^2} - \nabla^2 \bar{h} + 0.1 \bar{h} = 0.$$

Letting $\bar{t} = \frac{t}{10^{3.5} \text{s}}$ and noting via a similar argument as above that

$$\frac{\partial^2 \bar{h}}{\partial t^2} = \frac{1}{10^7 \text{s}^2} \frac{\partial^2 \bar{h}}{\partial \bar{t}^2}$$

we arrive at our final, non-dimensional form of the Klein-Gordon Equation,

$$\frac{\partial^2 \bar{h}}{\partial \bar{t}^2} - \nabla^2 \bar{h} + 0.1 \bar{h} = 0$$

where $t = (10^{3.5} \text{s}) \bar{t}$, $h = (1 \text{ m}) \bar{h}$, $x = (10^5 \text{ m}) \bar{x}$ and $y = (10^5 \text{ m}) \bar{y}$.

APPENDIX G. AUXILIARY VARIABLE FORMULATIONS FOR WESTERN, NORTHERN AND SOUTHERN BOUNDARIES

For configurations studied in this dissertation, G-N auxiliary variable formulations are required for boundaries other than Γ_E , explicitly derived in Chapter III. What follows here are the details of the formulation for each of the other boundaries.

A. FORMULATION FOR THE WESTERN BOUNDARY

We begin by stating the Higdon boundary condition for Γ_W given by:

$$H_J : \left[\prod_{j=1}^J \left(\partial_x - \frac{1}{C_j} \partial_t \right) \right] h = 0 \text{ on } \Gamma_W. \quad (\text{G.1})$$

When imposed as a boundary condition on Γ_W , we can recast this formulation in terms of auxiliary variables as outlined in Chapter III equivalent to the single boundary condition (G.1) as:

$$\begin{aligned} \left(\partial_x - \frac{1}{C_j} \partial_t \right) \phi_{j-1} &= \phi_j & j = 1, \dots, J \\ \text{where: } \phi_0 &\equiv h & \phi_J \equiv 0 \end{aligned} \quad (\text{G.2})$$

This set of conditions involves only first-order derivatives. However, due to the appearance of the x -derivative in (G.2), one cannot discretize the ϕ_j on the boundary Γ_W alone. Therefore, we shall manipulate (G.2) in order to get rid of the x -derivative.

The function h satisfies the dispersive, advective wave equation (II.29) in D . Since the function ϕ_1 is obtained by applying the linear (constant coefficient) operator $\left(\partial_x - \frac{1}{C_1} \partial_t \right)$ to h , it is clear that ϕ_1 should also satisfy the same equation in D . Further, since ϕ_j is obtained by applying the same linear operator $j-1$ times to ϕ_1 , the functions ϕ_j should satisfy

an equation like (II.29), namely,

$$\begin{aligned} & \left(\partial_{tt} + (U^2 - c_0^2) \partial_{xx} + (V^2 - c_0^2) \partial_{yy} + \right. \\ & \left. 2U \partial_{xt} + 2V \partial_{yt} + 2UV \partial_{xy} + f^2 \right) \phi_j = 0 \end{aligned} \quad (\text{G.3})$$

Using the following identities:

$$\begin{aligned} \partial_{xx} \phi_j &= \left(\partial_x + \frac{1}{C_{j+1}} \partial_t \right) \left(\partial_x - \frac{1}{C_{j+1}} \partial_t \right) \phi_j + \frac{1}{C_{j+1}^2} \ddot{\phi}_j \\ \partial_{xt} \phi_j &= \partial_t (\partial_x \phi_j) \\ \partial_{xy} \phi_j &= \partial_y (\partial_x \phi_j) \end{aligned}$$

and combining with (G.2) allows us to write (G.3) as:

$$\begin{aligned} & \left(-\frac{2U}{C_j} - 1 - \frac{U^2 - c_0^2}{C_j^2} \right) \ddot{\phi}_{j-1} - \left(\frac{2UV}{C_j} + 2V \right) \dot{\phi}'_{j-1} - (V^2 - c_0^2) \phi''_{j-1} - \\ & \left((U^2 - c_0^2) \left(\frac{1}{C_j} + \frac{1}{C_{j+1}} \right) + 2U \right) \dot{\phi}_j - 2UV \phi'_j - f^2 \phi_{j-1} = (U^2 - c_0^2) \phi_{j+1} \\ & \text{for } j = 1, \dots, J-1 \end{aligned} \quad (\text{G.4})$$

In (G.4) and elsewhere, a prime indicates differentiation with respect to y along Γ_W , i.e., the tangential derivative along Γ_W . As desired, the new boundary condition (G.4) does not involve x -derivatives. In addition, there are no high- y or t derivatives beyond second order. The new formulation of the J^{th} -order NRBC on Γ_W can be summarized as follows:

$$\begin{aligned} & \beta_0 \dot{h} + \partial_x h = \phi_1, \\ & \alpha_j \ddot{\phi}_{j-1} + \kappa_j \dot{\phi}'_{j-1} - \lambda_y \phi''_{j-1} + \beta_j \dot{\phi}_j - \gamma \phi'_j - f^2 \phi_{j-1} = \lambda_x \phi_{j+1} \\ & \phi_0 \equiv h \quad \phi_J \equiv 0 \end{aligned} \quad (\text{G.5})$$

where

$$\begin{aligned}\beta_0 &= -\frac{1}{C_1}, & \alpha_j &= -\frac{2U}{C_j} - 1 - \frac{U^2 - c_0^2}{C_j^2}, & \kappa_j &= -\frac{2UV}{C_j} - 2V, & \lambda_y &= V^2 - c_0^2, \\ \beta_j &= -(U^2 - c_0^2) \left(\frac{1}{C_j} \frac{1}{C_{j+1}} \right) - 2U, & \gamma &= 2UV, & \lambda_x &= U^2 - c_0^2\end{aligned}$$

B. FORMULATION FOR THE NORTHERN BOUNDARY

The Higdon boundary condition for Γ_N is given by:

$$H_J : \left[\prod_{j=1}^J \left(\partial_y + \frac{1}{C_j} \partial_t \right) \right] h = 0 \text{ on } \Gamma_N. \quad (\text{G.6})$$

When imposed as a boundary condition on Γ_N , we can recast this formulation in terms of auxiliary variables as outlined in Chapter III equivalent to the single boundary condition (G.6) as:

$$\begin{aligned} \left(\partial_y + \frac{1}{C_j} \partial_t \right) \phi_{j-1} &= \phi_j & j &= 1, \dots, J & (\text{G.7}) \\ \text{where: } \phi_0 &\equiv h & \phi_J &\equiv 0 \end{aligned}$$

This set of conditions involves only first-order derivatives. However, due to the appearance of the y -derivative in (G.7), one cannot discretize the ϕ_j on the boundary Γ_N alone. Therefore we shall manipulate (G.7) in order to get rid of the y -derivative.

The function h satisfies the dispersive, advective wave equation (II.29) in D . Since the function ϕ_1 is obtained by applying the linear (constant coefficient) operator $\left(\partial_y + \frac{1}{C_1} \partial_t \right)$ to h , it is clear that ϕ_1 should also satisfy the same equation in D . Further, since ϕ_j is obtained by applying the same linear operator $j-1$ times to ϕ_1 , the functions ϕ_j should satisfy

an equation like (G.3). Using the following identities:

$$\begin{aligned}\partial_{yy}\phi_j &= \left(\partial_y - \frac{1}{C_{j+1}}\partial_t\right) \left(\partial_y + \frac{1}{C_{j+1}}\partial_t\right) \phi_j + \frac{1}{C_{j+1}^2}\ddot{\phi}_j \\ \partial_{yt}\phi_j &= \partial_t(\partial_y\phi_j) \\ \partial_{xy}\phi_j &= \partial_x(\partial_y\phi_j)\end{aligned}$$

and combining with (G.3) and (G.7) allows us to formulate the boundary as:

$$\begin{aligned}\left(\frac{2V}{C_j} - 1 - \frac{V^2 - c_0^2}{C_j^2}\right) \ddot{\phi}_{j-1} + \left(\frac{2UV}{C_j} - 2U\right) \dot{\phi}'_{j-1} - (U^2 - c_0^2) \phi''_{j-1} + \\ \left((V^2 - c_0^2) \left(\frac{1}{C_j} + \frac{1}{C_{j+1}}\right) - 2V\right) \dot{\phi}_j - 2UV\phi'_j - f^2\phi_{j-1} = (V^2 - c_0^2) \phi_{j+1}\end{aligned}$$

for $j = 1, \dots, J-1$ (G.8)

In (G.8) and elsewhere, a prime indicates differentiation with respect to x along Γ_N , i.e., the tangential derivative along Γ_N . As desired, the new boundary condition (G.8) does not involve y -derivatives. In addition, there are no high- x or t derivatives beyond second order. The new formulation of the J^{th} -order NRBC on Γ_N can be summarized as follows:

$$\begin{aligned}\beta_0 \dot{h} + \partial_y h &= \phi_1, \\ \alpha_j \ddot{\phi}_{j-1} + \kappa_j \dot{\phi}'_{j-1} - \lambda_x \phi''_{j-1} + \beta_j \dot{\phi}_j - \gamma \phi'_j - f^2 \phi_{j-1} &= \lambda_y \phi_{j+1} \\ \phi_0 &\equiv h \quad \phi_J \equiv 0\end{aligned}$$

(G.9)

where

$$\begin{aligned}\beta_0 &= \frac{1}{C_1}, \quad \alpha_j = \frac{2V}{C_j} - 1 - \frac{V^2 - c_0^2}{C_j^2}, \quad \kappa_j = \frac{2UV}{C_j} - 2U, \quad \lambda_y = V^2 - c_0^2, \\ \beta_j &= (V^2 - c_0^2) \left(\frac{1}{C_j} + \frac{1}{C_{j+1}}\right) - 2V, \quad \gamma = 2UV, \quad \lambda_x = U^2 - c_0^2\end{aligned}$$

C. FORMULATION FOR THE SOUTHERN BOUNDARY

The Higdon boundary condition for Γ_S is given by:

$$H_J : \left[\prod_{j=1}^J \left(\partial_y - \frac{1}{C_j} \partial_t \right) \right] h = 0 \text{ on } \Gamma_S. \quad (\text{G.10})$$

When imposed as a boundary condition on Γ_S , we can recast this formulation in terms of auxiliary variables as outlined in Chapter III equivalent to the single boundary condition (G.10) as:

$$\begin{aligned} \left(\partial_y - \frac{1}{C_j} \partial_t \right) \phi_{j-1} &= \phi_j & j = 1, \dots, J \\ \text{where: } \phi_0 &\equiv h & \phi_J \equiv 0 \end{aligned} \quad (\text{G.11})$$

This set of conditions involves only first-order derivatives. However, due to the appearance of the y -derivative in (G.11), one cannot discretize the ϕ_j on the boundary Γ_S alone. Therefore we shall manipulate (G.11) in order to get rid of the y -derivative.

The function h satisfies the dispersive, advective wave equation (II.29) in D . Since the function ϕ_1 is obtained by applying the linear (constant coefficient) operator $\left(\partial_y - \frac{1}{C_1} \partial_t \right)$ to h , it is clear that ϕ_1 should also satisfy the same equation in D . Further, since ϕ_j is obtained by applying the same linear operator $j-1$ times to ϕ_1 , the functions ϕ_j should satisfy an equation like (G.3). Using the following identities:

$$\begin{aligned} \partial_{yy} \phi_j &= \left(\partial_y + \frac{1}{C_{j+1}} \partial_t \right) \left(\partial_y - \frac{1}{C_{j+1}} \partial_t \right) \phi_j + \frac{1}{C_{j+1}^2} \ddot{\phi}_j \\ \partial_{yt} \phi_j &= \partial_t (\partial_y \phi_j) \\ \partial_{xy} \phi_j &= \partial_x (\partial_y \phi_j) \end{aligned}$$

and combining with (G.3) and (G.11) allows us to formulate the boundary as:

$$\begin{aligned} \left(-\frac{2V}{C_j} - 1 - \frac{V^2 - c_0^2}{C_j^2}\right) \ddot{\phi}_{j-1} - \left(\frac{2UV}{C_j} + 2U\right) \dot{\phi}'_{j-1} - (U^2 - c_0^2) \phi''_{j-1} - \\ \left((V^2 - c_0^2) \left(\frac{1}{C_j} + \frac{1}{C_{j+1}}\right) + 2V\right) \dot{\phi}_j - 2UV \phi'_j - f^2 \phi_{j-1} = (V^2 - c_0^2) \phi_{j+1} \end{aligned}$$

for $j = 1, \dots, J-1$ (G.12)

In (G.12) and elsewhere, a prime indicates differentiation with respect to x along Γ_S , i.e., the tangential derivative along Γ_S . As desired, the new boundary condition (G.12) does not involve y -derivatives. In addition, there are no high- x or t derivatives beyond second order. The new formulation of the J^{th} -order NRBC on Γ_S can be summarized as follows:

$$\begin{aligned} \beta_0 \dot{h} - \partial_y h &= \phi_1, \\ \alpha_j \ddot{\phi}_{j-1} + \kappa_j \dot{\phi}'_{j-1} - \lambda_x \phi''_{j-1} + \beta_j \dot{\phi}_j - \gamma \phi'_j - f^2 \phi_{j-1} &= \lambda_y \phi_{j+1} \end{aligned} \quad (G.13)$$

$$\phi_0 \equiv h \quad \phi_J \equiv 0$$

where

$$\begin{aligned} \beta_0 &= -\frac{1}{C_1}, & \alpha_j &= -\frac{2V}{C_j} - 1 - \frac{V^2 - c_0^2}{C_j^2}, & \kappa_j &= -\frac{2UV}{C_j} - 2U, & \lambda_y &= V^2 - c_0^2, \\ \beta_j &= -(V^2 - c_0^2) \left(\frac{1}{C_j} + \frac{1}{C_{j+1}}\right) - 2V, & \gamma &= 2UV, & \lambda_x &= U^2 - c_0^2 \end{aligned}$$

APPENDIX H. OPEN PLANE DOMAIN ROTATION IN THE DIRECTION OF ADVECTION

Here, we consider the effects of diagonal advection and how our formulation may be simplified. Suppose we have an open plane domain where NRBCs are specified on all four cardinal boundaries. The question arises – since we are dealing with an infinite domain, can the problem be simplified by a change in coordinates? If so, how would this adjust the problem, and would it make the problem any easier?

To examine this question, recall our PDE in its standard $x - y$ plane:

$$(\partial_t + U\partial_x + V\partial_y)^2 h - c_0^2 \nabla^2 h + f^2 h = 0 \quad (\text{H.1})$$

Further, suppose that the advection velocities U and V are non-zero in both directions resulting in activation of all components of (H.1). To fix some ideas, let $U > 0$ and $V > 0$. The goal is to convert (H.1) in its current coordinate system to one that is in the direction of the advection velocity. To see this, consider Figure 35.

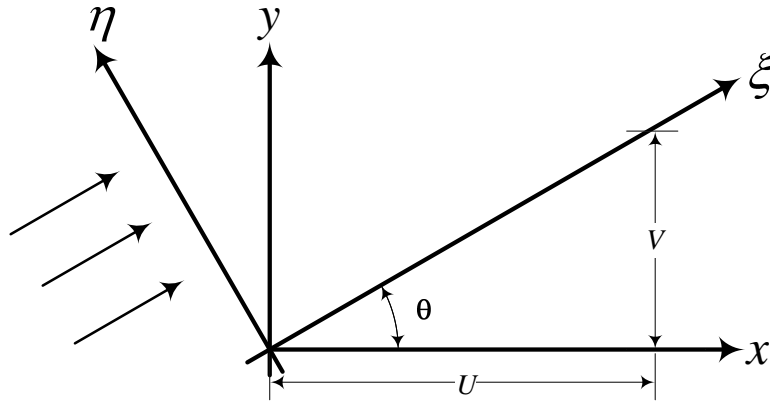


Figure 35: Generation of a new coordinate system in the direction of advection

The new coordinate system (ξ, η) places the ξ axis in the direction of advection. This transformation is a simple rotation that can be described by:

$$\begin{aligned}x &= \cos(\theta)\xi - \sin(\theta)\eta \\y &= \sin(\theta)\xi + \cos(\theta)\eta\end{aligned}$$

or:

$$\begin{aligned}\xi &= \cos(\theta)x + \sin(\theta)y \\ \eta &= -\sin(\theta)x + \cos(\theta)y\end{aligned}$$

Clearly U and V are also related by the geometry of the problem.

$$\begin{aligned}\sin(\theta) &= \frac{V}{\sqrt{U^2 + V^2}} \\ \cos(\theta) &= \frac{U}{\sqrt{U^2 + V^2}}\end{aligned}\tag{H.2}$$

We note now that we can express h in terms of the new coordinate system as $h(x, y, t) = h(\xi(x, y), \eta(x, y), t)$. Since (H.1) is developed in the (x, y) system, we use the chain rule to expand (H.1) in terms of (ξ, η) . We adopt the shorthand convention

$$h_a = \frac{\partial h}{\partial a} \quad h_{ab} = \frac{\partial^2 h}{\partial a \partial b}$$

to yield the following expansions

$$\begin{aligned}
h_x &= h_\xi \xi_x + h_\eta \eta_x \\
h_y &= h_\xi \xi_y + h_\eta \eta_y \\
h_{xy} &= h_{\xi\xi} \xi_x \xi_y + h_{\xi\eta} (\xi_x \eta_y + \xi_y \eta_x) + h_{\eta\eta} \eta_x \eta_y + h_\xi \xi_{xy} + h_\eta \eta_{xy} \\
h_{xx} &= h_{\xi\xi} \xi_x^2 + 2h_{\xi\eta} \xi_x \eta_x + h_{\eta\eta} \eta_x^2 + h_\xi \xi_{xx} + h_\eta \eta_{xx} \\
h_{yy} &= h_{\xi\xi} \xi_y^2 + 2h_{\xi\eta} \xi_y \eta_y + h_{\eta\eta} \eta_y^2 + h_\xi \xi_{yy} + h_\eta \eta_{yy}.
\end{aligned} \tag{H.3}$$

Since the coordinate transformation is linear, the problem is simplified even more as the second order metric terms vanish.

$$\begin{aligned}
\xi_x &= \cos \theta & \eta_x &= -\sin \theta & \xi_y &= \sin \theta & \eta_y &= \cos(\theta) \\
\xi_{xx} &= \xi_{yy} = \xi_{xy} = \eta_{xx} = \eta_{yy} = \eta_{xy} = 0
\end{aligned} \tag{H.4}$$

Now, looking term by term at (H.1), in light of (H.3), we consolidate terms to see the result of the transformation.

$$\ddot{h} + \mathbb{A} h_{\xi\xi} + \mathbb{B} h_{\eta\eta} + \mathbb{C} h_{\xi t} + \mathbb{D} h_{\eta t} + \mathbb{E} h_{\xi\eta} + f^2 h = 0 \tag{H.5}$$

where $h = h(\xi, \eta, t)$ and:

$$\begin{aligned}
\mathbb{A} &= (U^2 - c_0^2) \xi_x^2 + (V^2 - c_0^2) \xi_y^2 + 2UV \xi_x \xi_y \\
\mathbb{B} &= (U^2 - c_0^2) \eta_x^2 + (V^2 - c_0^2) \eta_y^2 + 2UV \eta_x \eta_y \\
\mathbb{C} &= 2(U \xi_x + V \xi_y) \\
\mathbb{D} &= 2(U \eta_x + V \eta_y) \\
\mathbb{E} &= (U^2 - c_0^2) 2\xi_x \eta_x + (V^2 - c_0^2) 2\xi_y \eta_y + 2UV (\xi_x \eta_y + \xi_y \eta_x)
\end{aligned} \tag{H.6}$$

We continue by using the information provided by the geometry of the transformation in (H.2) and the metric terms found in (H.4). Specifically, if we define the adjusted

advection velocities \bar{U} and \bar{V} corresponding to the ξ and η directions respectively as:

$$\bar{U} = U\xi_x + V\xi_y$$

$$\bar{V} = U\eta_x + V\eta_y$$

then each of the terms in (H.6) simplify to:

$$\begin{aligned}\mathbb{A} &= \bar{U}^2 - C_0^2 \\ \mathbb{B} &= \bar{V}^2 - C_0^2 \\ \mathbb{C} &= 2\bar{U} \\ \mathbb{D} &= 2\bar{V} \\ \mathbb{E} &= 2\bar{U}\bar{V} - 2c_0^2 \underbrace{(2\xi_x\eta_x + \xi_y\eta_y)}_{=0}\end{aligned}\tag{H.7}$$

Of course, if one examines \bar{V} we find:

$$\bar{V} = U\eta_x + V\eta_y = -U \sin(\theta) + V \cos(\theta) = -U \frac{V}{\sqrt{U^2 + V^2}} + V \frac{U}{\sqrt{U^2 + V^2}} = 0 \tag{H.8}$$

This significantly simplifies the problem to:

$$h_{tt} + (\bar{U}^2 - C_0^2) h_{\xi\xi} - c_0^2 h_{\eta\eta} + 2\bar{U} h_{\xi t} + f^2 h = 0 \tag{H.9}$$

This procedure shows that for the open plane domain, any constant advection velocity not in a cardinal direction in the standard $x - y$ coordinate system can be converted to an equivalent problem where the advection velocity is in a cardinal direction in an alternate $\xi - \eta$ coordinate system. The result is that when examining the open plane domain, one only needs to examine advections in one cardinal direction since a problem with diagonal advection could be recast into a cardinal direction advection problem in another coordinate system.

APPENDIX I. ARBITRARILY SHAPED BOUNDARY FORMULATION

Recall the KGE

$$(\partial_t + U\partial_x + V\partial_y)^2 h - c_0^2 \nabla^2 h + f^2 h = 0 \quad (\text{I.1})$$

for which we wish to formulate the G-N auxiliary variable formulation for an arbitrarily shaped boundary. The Higdon boundary condition of order J is given by

$$H_J : \quad \left[\prod_{j=1}^J \left(\partial_n + \frac{1}{C_j} \partial_t \right) \right] h = 0 \quad \text{on } \Gamma \quad (\text{I.2})$$

Now, we introduce the auxiliary functions $\phi_1, \dots, \phi_{J-1}$, which are defined on Γ as well as in the exterior domain D (see Figure 29). Eventually, we shall use these functions only on Γ , but the derivation requires that they be defined in D as well, or at least in a non-vanishing region adjacent to Γ . The functions ϕ_j are defined via the relations

$$\left(\partial_n + \frac{1}{C_1} \partial_t \right) h = \phi_1, \quad (\text{I.3})$$

$$\left(\partial_n + \frac{1}{C_2} \partial_t \right) \phi_1 = \phi_2, \quad (\text{I.4})$$

$$\vdots$$

$$\left(\partial_n + \frac{1}{C_J} \partial_t \right) \phi_{J-1} = 0. \quad (\text{I.5})$$

By definition, these relations hold in D , and also on Γ . It is easy to see that (I.3 - I.5), when imposed as boundary conditions on Γ , are equivalent to the single boundary condition (I.2).

If we also define

$$\phi_0 \equiv h \quad \phi_J \equiv 0, \quad (\text{I.6})$$

then we can write (I.3 - I.5) concisely as

$$\left(\partial_n + \frac{1}{C_j}\partial_t\right)\phi_{j-1} = \phi_j \quad j = 1, \dots, J. \quad (\text{I.7})$$

This set of conditions involves only first-order derivatives. However, due to the appearance of the normal derivative in (I.7), one cannot discretize the ϕ_j on the boundary Γ alone. Therefore, we shall manipulate (I.7) in order to get rid of the normal derivative $\partial_n = n_x\partial_x + n_y\partial_y$ where $n_x = n_x(x, y)$ and $n_y = n_y(x, y)$.

The function h satisfies the KGE in D . Since the function ϕ_1 is obtained by applying the linear operator $\left(\partial_n + \frac{1}{C_1}\partial_t\right)$ to h , we must consider what equation that ϕ_1 satisfies. We begin by applying this operator to the KGE to yield

$$\begin{aligned} \left(\partial_n + \frac{1}{C_1}\partial_t\right) \left(\ddot{h} + \lambda_x\partial_{xx}h + \lambda_y\partial_{yy}h + 2U\partial_{xt}h + 2V\partial_{yt}h + 2UV\partial_{xy}h + f^2h\right) &= 0 \\ n_x \left(\partial_{xtt}h + \lambda_x\partial_{xxx}h + \lambda_y\partial_{xyy}h + 2U\partial_{xxt}h + 2V\partial_{xyt}h + \lambda_x\partial_{xxy}h + f^2\partial_xh\right) & \\ n_y \left(\partial_{ytt}h + \lambda_x\partial_{xxy}h + \lambda_y\partial_{yyy}h + 2U\partial_{xyt}h + 2V\partial_{yyt}h + \lambda_x\partial_{xyy}h + f^2\partial_yh\right) & \quad (\text{I.8}) \\ \frac{1}{C_1} \left(\partial_{ttt}h + \lambda_x\partial_{xxt}h + \lambda_y\partial_{yyt}h + 2U\partial_{xtt}h + 2V\partial_{ytt}h + \lambda_x\partial_{xyt}h + f^2\partial_th\right) &= 0 \end{aligned}$$

Now, consider the first order derivatives for the ϕ_1 boundary condition

$$\begin{aligned} \partial_x\phi_1 &= \frac{\partial}{\partial x}(n_x)\partial_xu + n_x\partial_{xx}h + \frac{\partial}{\partial x}(n_y)\partial_yu + n_y\partial_{xy}h + \frac{1}{C_1}\partial_{xt}h \\ \partial_y\phi_1 &= \frac{\partial}{\partial y}(n_x)\partial_xu + n_x\partial_{xy}h + \frac{\partial}{\partial y}(n_y)\partial_yu + n_y\partial_{yy}h + \frac{1}{C_1}\partial_{yt}h \\ \partial_t\phi_1 &= \frac{\partial}{\partial t}(n_x)\partial_xu + n_x\partial_{xt}h + \frac{\partial}{\partial t}(n_y)\partial_yu + n_y\partial_{yt}h + \frac{1}{C_1}\partial_{tt}h \end{aligned}$$

Since the components of the normal vector are themselves functions of x and y , we incur additional terms for the derivatives of those components. If the boundary is fixed in time, clearly the time derivatives of the normal components will vanish, however, the spatial derivatives will not. We now consider a simplifying assumption that the curvature on the boundary is negligible. In other words, the spatial rate of change of the components of the

normal vector are very small in comparison to the other terms. This allows us to neglect the following terms:

$$\frac{\partial}{\partial x}(n_x) = \frac{\partial}{\partial x}(n_y) = \frac{\partial}{\partial y}(n_x) = \frac{\partial}{\partial y}(n_y) = 0.$$

Using this assumption, the second order derivatives of ϕ_1 are

$$\begin{aligned}\partial_{xx}\phi_1 &= n_x\partial_{xxx}h + n_y\partial_{xxy}h + \frac{1}{C_1}\partial_{xxt}h \\ \partial_{xy}\phi_1 &= n_x\partial_{xxy}h + n_y\partial_{xyy}h + \frac{1}{C_1}\partial_{xyt}h \\ \partial_{yy}\phi_1 &= n_x\partial_{xyy}h + n_y\partial_{yyy}h + \frac{1}{C_1}\partial_{yyt}h \\ \partial_{tt}\phi_1 &= n_x\partial_{xtt}h + n_y\partial_{ytt}h + \frac{1}{C_1}\partial_{ttt}h \\ \partial_{xt}\phi_1 &= n_x\partial_{xxt}h + n_y\partial_{xyt}h + \frac{1}{C_1}\partial_{xtt}h \\ \partial_{yt}\phi_1 &= n_x\partial_{xyt}h + n_y\partial_{yyt}h + \frac{1}{C_1}\partial_{ytt}h\end{aligned}\tag{I.9}$$

We can now use (I.9) in (I.8) to find that ϕ_1 should also satisfy the KGE in D . Further, since ϕ_j is obtained by applying the same operator to ϕ_{j-1} , the functions ϕ_j should satisfy a similar equation, namely,

$$\left[\partial_{tt} + (U^2 - c_0^2)\partial_{xx} + (V^2 - C_0^2)\partial_{yy} + 2U\partial_{xt} + 2V\partial_{yt} + 2UV\partial_{xy} + f^2\right]\phi_j = 0 \tag{I.10}$$

We now note that the boundary condition and the PDE that ϕ_j satisfies are described in two different coordinate systems – namely (n, τ) and (x, y) respectively. Consider an arbitrary part of the boundary (Γ) shown in Figure 30. Of course, in the most general case, the normal and tangential vectors are dependent on the position on the boundary, but can be computed given a particular domain. Since these components then are “known,” we consider a change of coordinates from x and y to n and τ as defined by the linear transformation and its associated differentiation operator (VII.2). Rewriting each operator

in (I.10) and again using the small curvature assumption yields:

$$\begin{aligned}
\partial_{tt} &= \partial_{tt} \\
\partial_{xx} &= n_x^2 \partial_{nn} - 2n_x n_y \partial_{n\tau} + n_y^2 \partial_{\tau\tau}^2 \\
\partial_{yy} &= n_y^2 \partial_{nn} + 2n_x n_y \partial_{n\tau} + n_x^2 \partial_{\tau\tau}^2 \\
\partial_{xt} &= n_x \partial_{nt} - n_y \partial_{\tau t} \\
\partial_{yt} &= n_y \partial_{nt} + n_x \partial_{\tau t} \\
\partial_{xy} &= n_x n_y \partial_{nn} + (n_x^2 - n_y^2) \partial_{n\tau}^2 - n_x n_y \partial_{\tau\tau}^2.
\end{aligned}$$

Substituting these terms back into (I.10) and organizing this simplifies to:

$$\left[\partial_{tt} + \mathbf{A} \partial_{nn} + \mathbf{B} \partial_{\tau\tau} + \mathbf{C} \partial_{n\tau}^2 + 2 \mathbf{D} \partial_{nt} + 2 \mathbf{E} \partial_{\tau t} + f^2 \right] \phi_j = 0 \quad (\text{I.11})$$

where:

$$\begin{aligned}
\mathbf{A} &= (U^2 - c_0^2) n_x^2 + (V^2 - C_0^2) n_y^2 + 2UV n_x n_y \\
\mathbf{B} &= (U^2 - c_0^2) n_y^2 + (V^2 - C_0^2) n_x^2 - 2UV n_x n_y \\
\mathbf{C} &= 2(-U^2 + V^2) n_x n_y + 2UV (n_x^2 - n_y^2) \\
\mathbf{D} &= U n_x + V n_y \\
\mathbf{E} &= -U n_y + V n_x
\end{aligned}$$

We now see that this formulation is expressed in terms of the normal and tangential coordinate system and further has the same form as (III.17). We can proceed in the same manner as outlined in Chapter III to eliminate the normal derivatives to yield the new formulation

of the J^{th} -order NRBC on Γ summarized as follows:

$$\beta_0 \dot{\eta} + \frac{\partial \eta}{\partial n} = \phi_1, \quad (\text{I.12})$$

$$\alpha_j \ddot{\phi}_{j-1} + \gamma_j \dot{\phi}'_{j-1} - \mathbf{B} \phi''_{j-1} + \beta_j \dot{\phi}_j - \mathbf{C} \phi'_j - f^2 \phi_{j-1} = \mathbf{A} \phi_{j+1} \quad (\text{I.13})$$

$$\begin{aligned} \beta_0 &= \frac{1}{C_1}, & \alpha_j &= \frac{2 \mathbf{D}}{C_j} - 1 - \frac{\mathbf{A}}{C_j^2}, \\ \gamma_j &= \frac{\mathbf{C}}{C_j} - 2 \mathbf{E}, & \beta_j &= \mathbf{A} \left(\frac{1}{C_j} + \frac{1}{C_{j+1}} \right) - 2 \mathbf{D} \\ \phi_0 &\equiv \eta & \phi_J &\equiv 0. \end{aligned} \quad (\text{I.14})$$

Here, prime indicates tangential differentiation along Γ . As desired, the new boundary condition does not involve any normal derivatives and there are no high tangential or time derivatives beyond second order.

There are a few remaining concerns. First, we must be able to compute the normal and tangential components of the vectors mandated by the mapping (VII.2). Additionally, we have several terms which require the integration of tangential derivatives along a general boundary. The question arises, how do we evaluate these terms along a particular boundary? Finally, we must still relate this boundary formulation back into the interior formulation and consider the appropriate values for the C_j terms.

A. COMPUTING THE NORMAL AND TANGENTIAL VECTOR COMPONENTS

Consider (VII.2), which gives us a way to write the normal and tangential derivatives in terms of the standard $x - y$ coordinates. We can extend this via the chain rule to map each of these components in terms of our canonical $\xi - \eta$ coordinates. Before we do any of this, however, we must first be able to compute the normal vectors at each point on the boundary. To see this, consider the normal and tangential vectors of a canonical element as shown in Figure 36.

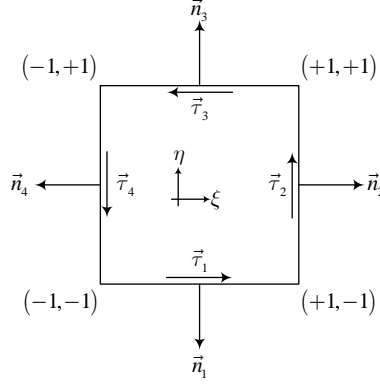


Figure 36: Normal and tangential vectors along a canonical element boundary.

After introducing the nonsingular mapping $\xi = \xi(x, y)$ and $\eta = \eta(x, y)$, these normal vectors [47] are given by:

$$\vec{n} = \eta \frac{\nabla \eta}{|\nabla \eta|} \Big|_{\eta=\pm 1}, \quad \vec{n} = \xi \frac{\nabla \xi}{|\nabla \xi|} \Big|_{\xi=\pm 1}.$$

Each of these normal vectors can then be used to compute the tangential vectors by taking the cross product of the normal vectors with the unit vector $(0, 0, -1)^T$. In the case of Figure 36, the normalized tangential vectors are:

$$\begin{aligned} \vec{\tau}_1 &= \frac{1}{\sqrt{\frac{\partial \eta^2}{\partial y^2} + \frac{\partial \eta^2}{\partial x^2}}} \begin{pmatrix} +\frac{\partial \eta}{\partial y} \\ -\frac{\partial \eta}{\partial x} \end{pmatrix}, & \vec{\tau}_2 &= \frac{1}{\sqrt{\frac{\partial \xi^2}{\partial y^2} + \frac{\partial \xi^2}{\partial x^2}}} \begin{pmatrix} -\frac{\partial \xi}{\partial y} \\ +\frac{\partial \xi}{\partial x} \end{pmatrix}, \\ \vec{\tau}_3 &= \frac{1}{\sqrt{\frac{\partial \eta^2}{\partial y^2} + \frac{\partial \eta^2}{\partial x^2}}} \begin{pmatrix} -\frac{\partial \eta}{\partial y} \\ +\frac{\partial \eta}{\partial x} \end{pmatrix}, & \vec{\tau}_4 &= \frac{1}{\sqrt{\frac{\partial \xi^2}{\partial y^2} + \frac{\partial \xi^2}{\partial x^2}}} \begin{pmatrix} +\frac{\partial \xi}{\partial y} \\ -\frac{\partial \xi}{\partial x} \end{pmatrix}. \end{aligned}$$

When put in terms of (IV.8), the unit tangential vectors are:

$$\begin{aligned} \vec{\tau}_1 &= \frac{1}{|J^s|} \begin{pmatrix} +\frac{\partial x}{\partial \xi} \\ +\frac{\partial y}{\partial \xi} \end{pmatrix}, & \vec{\tau}_2 &= \frac{1}{|J^s|} \begin{pmatrix} +\frac{\partial x}{\partial \eta} \\ +\frac{\partial y}{\partial \eta} \end{pmatrix}, \\ \vec{\tau}_3 &= \frac{1}{|J^s|} \begin{pmatrix} -\frac{\partial x}{\partial \xi} \\ -\frac{\partial y}{\partial \xi} \end{pmatrix}, & \vec{\tau}_4 &= \frac{1}{|J^s|} \begin{pmatrix} -\frac{\partial x}{\partial \eta} \\ -\frac{\partial y}{\partial \eta} \end{pmatrix}. \end{aligned} \tag{I.15}$$

where:

$$|J^s| = \begin{cases} \sqrt{\left(\frac{\partial x}{\partial \xi}\right)^2 + \left(\frac{\partial y}{\partial \xi}\right)^2} & \eta = \pm 1 \\ \sqrt{\left(\frac{\partial x}{\partial \eta}\right)^2 + \left(\frac{\partial y}{\partial \eta}\right)^2} & \xi = \pm 1. \end{cases}$$

We now have a way to compute the normal and tangential components required for this formulation.

B. INTEGRATION OF TANGENTIAL DERIVATIVES

In (I.13), we have several terms that will require the integration of first and second order tangential derivatives along a general boundary (after weak integral formulation). The question arises, how do we evaluate these terms along a particular boundary?

1. Integration of First Order Tangential Derivatives

To examine this arbitrary domain formulation in greater detail, consider a single element where we evaluate an integral that contains a first order tangential derivative along a single canonical side.

$$\begin{aligned} & \int_{\Gamma_s} \psi_i \frac{\partial \phi(x, y)}{\partial \tau} d\Gamma_s, & \partial_\tau &= \vec{\tau} \cdot \nabla \\ &= \int_{\Gamma_s} \psi_i \vec{\tau} \cdot \nabla \phi(x, y) d\Gamma_s \\ &= \int_{\Gamma_s} \psi_i \left(\tau_x \frac{\partial \phi}{\partial x} + \tau_y \frac{\partial \phi}{\partial y} \right) d\Gamma_s \\ &= \sum_{q=1}^Q w_q |J_q^s| \psi_i^q \left(\tau_x^q \frac{\partial \phi^q}{\partial x} + \tau_y^q \frac{\partial \phi^q}{\partial y} \right) & Q &= \text{number of quadrature points on a side} \end{aligned}$$

Here, $|J_q^s|$ is the Jacobian of the transformation along the side (side length) and w_q is the quadrature weight for Lobatto integration. If we use collocated quadrature, the cardinality property of the basis functions ensures that only the i^{th} basis function is nonzero (in fact unity) at quadrature point i . This rids us of the summation over all quadrature points for

basis function i yielding:

$$\int_{\Gamma_s} \psi_i \frac{\partial \phi(x, y)}{\partial \tau} d\Gamma_s = w_i |J_i^s| \left(\tau_x^i \frac{\partial \phi^i}{\partial x} + \tau_y^i \frac{\partial \phi^i}{\partial y} \right)$$

Now, expand our variable ϕ in terms of our canonical coordinates (ξ, η) and perform basis function expansions using our 2-D basis functions ($M_N = (N + 1)^2$).

$$\begin{aligned} &= w_i |J_i^s| \left(\tau_x^i \sum_{j=1}^{M_N} \frac{\partial \psi_j^i}{\partial x} \phi_j + \tau_y^i \sum_{j=1}^{M_N} \frac{\partial \psi_j^i}{\partial y} \phi_j \right) \\ &= w_i |J_i^s| \left(\tau_x^i \sum_{j=1}^{M_N} \left(\frac{\partial \psi_j^i}{\partial \xi} \frac{\partial \xi^i}{\partial x} + \frac{\partial \psi_j^i}{\partial \eta} \frac{\partial \eta^i}{\partial x} \right) \phi_j + \tau_y^i \sum_{j=1}^{M_N} \left(\frac{\partial \psi_j^i}{\partial \xi} \frac{\partial \xi^i}{\partial y} + \frac{\partial \psi_j^i}{\partial \eta} \frac{\partial \eta^i}{\partial y} \right) \phi_j \right) \end{aligned}$$

Of course our boundary integral implies that we are integrating strictly on a side. For definiteness in the example, consider side 2 where $\xi = +1, \eta \in [-1, +1]$. Now, we expand using (IV.8) and (I.15):

$$\begin{aligned} &= w_i |J_i^s| \left(\frac{1}{|J_i^s|} \frac{\partial x^i}{\partial \eta} \sum_{j=1}^{M_N} \left(\frac{\partial \psi_j^i}{\partial \xi} \left(\frac{1}{|J_i^e|} \frac{\partial y^i}{\partial \eta} \right) + \frac{\partial \psi_j^i}{\partial \eta} \left(-\frac{1}{|J_i^e|} \frac{\partial y^i}{\partial \xi} \right) \right) \right) \phi_j \\ &+ w_i |J_i^s| \left(\frac{1}{|J_i^s|} \frac{\partial y^i}{\partial \eta} \sum_{j=1}^{M_N} \left(\frac{\partial \psi_j^i}{\partial \xi} \left(-\frac{1}{|J_i^e|} \frac{\partial x^i}{\partial \eta} \right) + \frac{\partial \psi_j^i}{\partial \eta} \left(\frac{1}{|J_i^e|} \frac{\partial x^i}{\partial \xi} \right) \right) \right) \phi_j \end{aligned}$$

Simplifying and using the definition of the element Jacobian (IV.7), our task now requires evaluating:

$$= w_i \left(\frac{1}{|J_i^e|} \left(-\frac{\partial x^i}{\partial \eta} \frac{\partial y^i}{\partial \xi} + \frac{\partial y^i}{\partial \eta} \frac{\partial x^i}{\partial \xi} \right) \sum_{j=1}^{M_N} \frac{\partial \psi_j^i}{\partial \eta} \phi_j \right) = w_i \sum_{j=1}^{M_N} \frac{\partial \psi_j^i}{\partial \eta} \phi_j$$

Now, consider the term $\frac{\partial \psi_j^i}{\partial \eta}$, which means “the partial derivative with respect to η of the j^{th} basis function evaluated at the i^{th} quadrature point”. We note that the 2-D basis functions ψ_j are formed using tensor products of 1-D basis functions $\nu_k(\xi)$ and $\nu_l(\eta)$ such that $j = 1, \dots, M_N$ where the mapping from 1-D to 2-D is $j = \{(k - 1)(N + 1) + l : \}$

$k, l = 1, \dots, N + 1\}$. Therefore:

$$\frac{\partial \psi_j}{\partial \eta} (+1, \eta_i) = \nu_k (+1) \frac{d\nu_l}{d\eta} (\eta_i)$$

Using this and the cardinality property of the basis functions, we can evaluate the integral of the first order tangential derivative as:

$$\int_{\Gamma_s} \psi_i \frac{\partial \phi(x, y)}{\partial \tau} d\Gamma_s = w_i \sum_{j=1}^{N+1} \frac{d\nu_j^i}{d\eta} \phi_j$$

A similar argument holds for other canonical sides being evaluated on the boundaries.

2. Integration of Second Order Tangential Derivatives

Recall, the second order term from the auxiliary formulation of the form:

$$\begin{aligned} \int_{\Gamma_s} \psi_i \frac{\partial^2 \phi}{\partial \tau^2} d\Gamma_s &= \int_{\Gamma_s} \frac{\partial}{\partial \tau} \left(\psi_i \frac{\partial \phi}{\partial \tau} \right) d\Gamma_s - \int_{\Gamma_s} \frac{\partial \psi_i}{\partial \tau} \frac{\partial \phi}{\partial \tau} d\Gamma_s \\ &= \underbrace{\psi_i \frac{\partial \phi}{\partial \tau} \Big|_{\text{start}}^{\text{end}}}_{=0 \text{ if closed boundary}} - \int_{\Gamma_s} \frac{\partial \psi_i}{\partial \tau} \frac{\partial \phi}{\partial \tau} d\Gamma_s. \end{aligned}$$

Now, suppose that we expand each term, as in the previous section.

$$\begin{aligned} \int_{\Gamma_s} \frac{\partial \psi_i}{\partial \tau} \frac{\partial \phi}{\partial \tau} d\Gamma_s &= \int_{\Gamma_s} \left(\tau_x \frac{\partial \psi_i}{\partial x} + \tau_y \frac{\partial \psi_i}{\partial y} \right) \left(\tau_x \frac{\partial \phi}{\partial x} + \tau_y \frac{\partial \phi}{\partial y} \right) d\Gamma_s \\ &= \sum_{q=1}^Q w_q |J_q^s| \underbrace{\left(\tau_x^q \frac{\partial \psi_i^q}{\partial x} + \tau_y^q \frac{\partial \psi_i^q}{\partial y} \right)}_{\textcircled{1}} \underbrace{\left(\tau_x^q \frac{\partial \phi^q}{\partial x} + \tau_y^q \frac{\partial \phi^q}{\partial y} \right)}_{\textcircled{2}} \end{aligned}$$

Consider ① evaluated on side 2.

$$\begin{aligned}
\tau_x^q \frac{\partial \psi_i^q}{\partial x} + \tau_y^q \frac{\partial \psi_i^q}{\partial y} &= \tau_x^q \left(\frac{\partial \psi_i^q}{\partial \xi} \frac{\partial \xi^q}{\partial x} + \frac{\partial \psi_i^q}{\partial \eta} \frac{\partial \eta^q}{\partial x} \right) + \tau_y^q \left(\frac{\partial \psi_i^q}{\partial \xi} \frac{\partial \xi^q}{\partial y} + \frac{\partial \psi_i^q}{\partial \eta} \frac{\partial \eta^q}{\partial y} \right) \\
&= \frac{1}{|J_q^s|} \frac{\partial x}{\partial \eta} \left(\frac{\partial \psi_i^q}{\partial \xi} \left(\frac{1}{|J_q^e|} \frac{\partial y}{\partial \eta} \right) + \frac{\partial \psi_i^q}{\partial \eta} \left(-\frac{1}{|J_q^e|} \frac{\partial y}{\partial \xi} \right) \right) \\
&\quad + \frac{1}{|J_q^s|} \frac{\partial y}{\partial \eta} \left(\frac{\partial \psi_i^q}{\partial \xi} \left(-\frac{1}{|J_q^e|} \frac{\partial x}{\partial \eta} \right) + \frac{\partial \psi_i^q}{\partial \eta} \left(\frac{1}{|J_q^e|} \frac{\partial x}{\partial \xi} \right) \right) \\
&= \frac{1}{|J_q^s| |J_q^e|} \left(-\frac{\partial x}{\partial \eta} \frac{\partial y}{\partial \xi} + \frac{\partial y}{\partial \eta} \frac{\partial x}{\partial \xi} \right) \frac{\partial \psi_i^q}{\partial \eta} \\
&= \frac{1}{|J_q^s|} \frac{\partial \psi_i^q}{\partial \eta}
\end{aligned}$$

Now, combining this result with the expansion of ② as found in Appendix I.B, we find:

$$\begin{aligned}
\int_{\Gamma_s} \frac{\partial \psi_i}{\partial \tau} \frac{\partial \phi}{\partial \tau} d\Gamma_s &= \sum_{q=1}^Q w_q \frac{1}{|J_q^s|} \frac{\partial \psi_i^q}{\partial \eta} \sum_{j=1}^{M_N} \frac{\partial \psi_j^q}{\partial \eta} \phi_j \\
&= \sum_{q=1}^Q w_q \frac{1}{|J_q^s|} \frac{d\nu_i^q}{d\eta} \sum_{j=1}^{N+1} \frac{d\nu_j^q}{d\eta} \phi_j
\end{aligned}$$

As in Appendix I.B, similar results can be obtained for each of the other canonical sides.

C. RELATING THE BOUNDARY AND INTERIOR FORMULATIONS

The final four terms of (IV.3) are all boundary integrals where the NRBC must be applied. To simplify our discussion, we note that these integrals only apply to h on Γ , thus we will denote these terms as \hat{h} . Much like the auxiliary variable formulation, we note that the NRBC is defined in terms of normal derivatives (∂_n) while the boundary terms of (IV.3) are defined in terms of standard Cartesian derivatives (∂_x and ∂_y). Again, we consider a linear transformation of the final four terms as defined in (VII.2). This yields, for the first boundary term:

$$\lambda_x \int_{\Gamma} \Psi_i \frac{\partial h}{\partial x} n_x d\Gamma = \lambda_x \int_{\Gamma} \Psi_i \frac{\partial \hat{h}}{\partial x} n_x d\Gamma = \lambda_x \int_{\Gamma} \Psi_i \left(n_x \frac{\partial \hat{h}}{\partial n} - n_y \frac{\partial \hat{h}}{\partial \tau} \right) n_x d\Gamma \quad (\text{I.16})$$

Now, we can directly use (I.3) to join the two formulations:

$$\lambda_x \int_{\Gamma} \Psi_i \left(n_x \frac{\partial \hat{h}}{\partial n} - n_y \frac{\partial \hat{\eta}}{\partial \tau} \right) n_x d\Gamma = \lambda_x \int_{\Gamma} \Psi_i \left(n_x \left(\phi_1 - \beta_0 \dot{\hat{h}} \right) - n_y \frac{\partial \hat{h}}{\partial \tau} \right) n_x d\Gamma \quad (\text{I.17})$$

Now, we note that the boundary integral can be discretized on the boundary alone – in terms of tangential derivatives, time derivatives, and the auxiliary variable ϕ_1 . Performing these substitutions in each boundary term of (IV.3), we get the revised weak form of the problem:

$$\begin{aligned} & \int_{\Omega} \Psi_i \ddot{h} d\Omega - \lambda_x \int_{\Omega} \frac{\partial \Psi_i}{\partial x} \frac{\partial h}{\partial x} d\Omega - \lambda_y \int_{\Omega} \frac{\partial \Psi_i}{\partial y} \frac{\partial h}{\partial y} d\Omega \\ & - UV \int_{\Omega} \frac{\partial \Psi_i}{\partial y} \frac{\partial h}{\partial x} d\Omega - UV \int_{\Omega} \frac{\partial \Psi_i}{\partial x} \frac{\partial h}{\partial y} d\Omega \\ & + 2U \int_{\Omega} \Psi_i \frac{\partial \dot{h}}{\partial x} d\Omega + 2V \int_{\Omega} \Psi_i \frac{\partial \dot{h}}{\partial y} d\Omega + f^2 \int_{\Omega} \Psi_i h d\Omega \\ & + \lambda_x \int_{\Gamma} \Psi_i \phi_1 n_x^2 d\Gamma - \lambda_x \int_{\Gamma} \Psi_i \dot{\hat{h}} \beta_0 n_x^2 d\Gamma - \lambda_x \int_{\Gamma} \Psi_i \frac{\partial \hat{h}}{\partial \tau} n_y n_x d\Gamma \\ & + \lambda_y \int_{\Gamma} \Psi_i \phi_1 n_y^2 d\Gamma - \lambda_y \int_{\Gamma} \Psi_i \dot{\hat{h}} \beta_0 n_y^2 d\Gamma + \lambda_y \int_{\Gamma} \Psi_i \frac{\partial \hat{h}}{\partial \tau} n_x n_y d\Gamma \\ & + UV \int_{\Gamma} \Psi_i \phi_1 n_x n_y d\Gamma - UV \int_{\Gamma} \Psi_i \dot{\hat{h}} \beta_0 n_x n_y d\Gamma - UV \int_{\Gamma} \Psi_i \frac{\partial \hat{h}}{\partial \tau} n_y^2 d\Gamma \\ & + UV \int_{\Gamma} \Psi_i \phi_1 n_x n_y d\Gamma - UV \int_{\Gamma} \Psi_i \dot{\hat{h}} \beta_0 n_x n_y d\Gamma + UV \int_{\Gamma} \Psi_i \frac{\partial \hat{\eta}}{\partial \tau} n_x^2 d\Gamma = 0, \end{aligned} \quad (\text{I.18})$$

which, as desired, evaluates boundary integrals with data derived from *only* the boundary.

D. SELECTION OF C_J TERMS

If we examine the auxiliary variable formulation (I.13), we see that the selection of appropriate C_j values has yet to be addressed. As has been previously shown, *any* choice of C_j is guaranteed to reduce spurious reflection as the order of the NRBC (J) increases. Armed with this, we choose convenient values for our C_j 's that cause the second order in

time (α_j) terms to vanish for all j . In this case:

$$\begin{aligned}
\alpha_j = 0 &= \frac{2\mathbf{D}}{C_j} - 1 - \frac{\mathbf{A}}{C_j^2} \\
\Rightarrow C_j &= \mathbf{D} \pm \sqrt{\mathbf{D}^2 - \mathbf{A}} \\
&= Un_x + Vn_y \pm \sqrt{c_0^2 (n_x^2 + n_y^2)} \\
&= Un_x + Vn_y \pm c_0
\end{aligned}$$

This implies a special value of C_j for each boundary point, independent of NRBC order, i.e., $C_j = C(x, y)$ for all j . Further, this implies that the other coefficients in the auxiliary formulation are independent of NRBC order:

$$\gamma_j = \gamma = \frac{\mathbf{C}}{C(x, y)} - 2\mathbf{E}, \quad \beta_j = \beta = \frac{2\mathbf{A}}{C(x, y)} - 2\mathbf{D}.$$

The Higdon boundary condition, while general in nature, implicitly assumes that by the time a wave pulse gets to the artificial boundary, it is traveling primarily as a *plane* wave normal to the boundary. This choice for C_j can be thought of as a choice that accounts for any advection ***and*** “corrects” for the geometry of the problem – i.e., non-normal impingement on the boundary.

LIST OF REFERENCES

- [1] A. Bayliss and E. Turkel, “Radiation boundary conditions for wave-like equations,” *Communications on Pure and Applied Mathematics*, vol. 33, no. 6, pp. 707–725, 1980.
- [2] F. Collino, “High order absorbing boundary conditions for wave propagation models. Straight line boundary and corner cases,” in *Proceedings of the 2nd International Conference on Mathematical & Numerical Aspects of Wave Propagation* (R. Kleinman *et al.*, eds.), (Delaware), pp. 161–171, SIAM, 1993.
- [3] M. Grote and J. Keller, “Nonreflecting boundary conditions for time dependent scattering,” *Journal of Computational Physics*, vol. 127, no. 1, pp. 52–65, 1996.
- [4] I. Sofronov, “Conditions for complete transparency on the sphere for the three-dimensional wave equation,” *Russian Acad. Sci. Dokl. Math.*, vol. 46, pp. 397–401, 1993.
- [5] I. Sofronov, “Artificial boundary conditions of absolute transparency for two- and three- dimensional external time-dependent scattering problems,” *European Journal of Applied Mathematics*, vol. 9, no. 6, pp. 561–588, 1998.
- [6] T. Hagstrom and S. I. Hariharan, “A formulation of asymptotic and exact boundary conditions using local operators,” *Applied Numerical Mathematics*, vol. 27, no. 4, pp. 403–416, 1998.
- [7] M. Guddati and J. Tassoulas, “Continued-fraction absorbing boundary conditions for the wave equation,” *Journal of Computational Acoustics*, vol. 8, no. 1, pp. 139–156, 2000.
- [8] D. Givoli, “High-order non-reflecting boundary conditions without high-order derivatives,” *Journal of Computational Physics*, vol. 170, no. 2, pp. 849–870, 2001.
- [9] D. Givoli and I. Patlashenko, “An optimal high-order non-reflecting finite element scheme for wave scattering problems,” *International Journal for Numerical Methods in Engineering*, vol. 53, no. 10, pp. 2389–2411, 2002.
- [10] D. Givoli, “Recent advances in the dtn finite element method for unbounded domains,”
- [11] D. Alevras, “Simulating tsunamis in the indian ocean with real bathymetry by using a high-order triangular discontinuous galerkin oceanic shallow water model,” Master’s thesis, Naval Postgraduate School, Monterey, California, March 2009.

- [12] B. Cushman-Roisin, *Introduction to Geophysical Fluid Dynamics*. New Jersey: Prentice-Hall, 1994.
- [13] J. Pedlosky, *Geophysical Fluid Dynamics*. New York: Springer-Verlag, 2nd, ed., 1986.
- [14] F. Batchelor, *An Introduction to Fluid Dynamics*. Cambridge: Cambridge University Press, 1967.
- [15] P. Barnes-Svarney, ed., *The New York Public Library Science Desk Reference*. New York: MacMillan, 1995.
- [16] V. J. van Joolen, *Application of Higdon Non-Reflecting Boundary Conditions to Shallow Water Models*. PhD dissertation, Naval Postgraduate School, Monterey, California, 2003.
- [17] J. R. Dea, *High-Order Non-Reflecting Boundary Conditions for the Linearized Euler Equations*. PhD dissertation, Naval Postgraduate School, Monterey, California, 2008.
- [18] D. Givoli, “Non-reflecting boundary conditions,” *Journal of Computational Physics*, vol. 94, no. 1, pp. 1–29, 1991.
- [19] B. Engquist and A. Majda, “Radiation boundary conditions for acoustic and elastic calculations,” *Communications on Pure and Applied Mathematics*, vol. 32, no. 3, pp. 313–357, 1979.
- [20] S. V. Tsynkov, “Numerical solution of problems on unbounded domains. A review,” *Applied Numerical Mathematics*, vol. 27, no. 4, pp. 465–532, 1998.
- [21] D. Givoli, “High-order local non-reflecting boundary conditions: a review,” *Wave Motion*, vol. 39, no. 4, pp. 319–326, 2004.
- [22] R. L. Higdon, “Absorbing boundary conditions for difference approximations to the multi-dimensional wave equation,” *Mathematics of Computation*, vol. 47, no. 176, pp. 437–459, 1986.
- [23] R. L. Higdon, “Numerical absorbing boundary conditions for the wave equation,” *Mathematics of Computation*, vol. 49, no. 179, pp. 65–90, 1987.
- [24] R. L. Higdon, “Radiation boundary conditions for elastic wave propagation,” *SIAM Journal on Numerical Analysis*, vol. 27, no. 4, pp. 831–869, 1990.
- [25] R. L. Higdon, “Absorbing boundary conditions for elastic waves,” *Geophysics*, vol. 56, no. 2, pp. 231–241, 1991.
- [26] R. L. Higdon, “Absorbing boundary conditions for acoustic and elastic waves in stratified media,” *Journal of Computational Physics*, vol. 101, no. 2, pp. 386–418, 1992.

- [27] R. L. Higdon, “Radiation boundary conditions for dispersive waves,” *SIAM Journal on Numerical Analysis*, vol. 31, no. 1, pp. 64–100, 1994.
- [28] R. Haberman, *Applied Partial Differential Equations with Fourier Series and Boundary Value Problems*. New Jersey: Prentice Hall, 4th, ed., 2004.
- [29] D. Givoli and B. Neta, “High-order non-reflecting boundary conditions for dispersive waves,” *Wave Motion*, vol. 37, no. 3, pp. 257–271, 2003.
- [30] V. J. van Joolen, B. Neta, and D. Givoli, “High-order higdon-like boundary conditions for exterior transient wave problems,” *International Journal for Numerical Methods in Engineering*, vol. 63, no. 7, pp. 1041–1068, 2005.
- [31] V. J. van Joolen, B. Neta, and D. Givoli, “High-order boundary conditions for linearized shallow water equations with stratification, dispersion and advection,” *International Journal for Numerical Methods in Fluids*, vol. 46, no. 4, pp. 361–381, 2004.
- [32] W. Mulder, “Experiments with higdon’s absorbing boundary conditions for a number of wave equations,” *Computational Geosciences*, vol. 1, no. 1, pp. 85–108, 1997.
- [33] D. Givoli and B. Neta, “High-order non-reflecting boundary scheme for time-dependent waves,” *Journal of Computational Physics*, vol. 186, no. 1, pp. 24–46, 2003.
- [34] J. R. Dea, F. X. Giraldo, and B. Neta, “High-order non-reflecting boundary conditions for the linearized 2-d Euler equations: no mean flow case,” *Wave Motion*, vol. 46, no. 3, pp. 210–220, 2009.
- [35] D. Givoli, B. Neta, and I. Patlashenko, “Finite element analysis of time-dependent semi-infinite wave-guides with high-order boundary treatment,” *International Journal for Numerical Methods in Engineering*, vol. 58, no. 13, pp. 1955–1983, 2003.
- [36] T. Hagstrom and T. Warburton, “A new auxiliary variable formulation of high-order local radiation boundary conditions: corner compatibility conditions and extensions to first-order systems,” *Wave Motion*, vol. 39, no. 4, pp. 327–338, 2004.
- [37] D. Givoli, T. Hagstrom, and I. Patlashenko, “Finite element formulation with high-order absorbing boundary conditions for time-dependent waves,” *Computer Methods in Applied Mechanics and Engineering*, vol. 195, no. 29-32, pp. 3666–3690, 2006.
- [38] T. Hagstrom, A. Mar-Or, and D. Givoli, “High-order local absorbing conditions for the wave equation: Extensions and improvements,” *Journal of Computational Physics*, vol. 227, no. 6, pp. 3322–3357, 2008.
- [39] A. T. Patera, “A spectral element method for fluid dynamics: Laminar flow in a channel expansion,” *Journal of Computational Physics*, vol. 54, no. 3, pp. 468–488, 1984.

- [40] L. Kuchеров and D. Givoli, “High-order absorbing boundary conditions incorporated in a spectral element formulation,” *International Journal for Numerical Methods in Biomedical Engineering*, 2008. doi: 10.1002/cnm.1188.
- [41] J. M. Lindquist, B. Neta, and F. X. Giraldo, “A spectral element solution of the Klein-Gordon equation with high-order treatment of time and non-reflecting boundary,” *Wave Motion*, vol. 47, no. 5, pp. 289–298, 2010.
- [42] F. Giraldo, “Element-based galerkin methods.” Course Notes for MA4245 Mathematical Foundations of Galerkin Methods.
- [43] F. X. Giraldo and M. Restelli, “A study of spectral element and discontinuous galerkin methods for the Navier-Stokes equations in nonhydrostatic mesoscale atmospheric modeling: Equation sets and test cases,” *Journal of Computational Physics*, vol. 227, no. 8, pp. 3849–3877, 2008.
- [44] C. Pozrikidis, *Introduction to Finite and Spectral Element Methods using MATLAB*®. Florida: Chapman & Hall/CRC, 2005.
- [45] K. H. Huebner, D. L. Dewhurst, D. E. Smith, and T. G. Byrom, *The Finite Element Method for Engineers*. New York: Wiley Interscience, 4th, ed., 2001.
- [46] G. Zhao and M. Xinwa, “Automesh 2-d: A fully automatic adaptive quadrilateral mesh generator.” <http://www.automesh2d.com/default.htm> [Accessed: February 12, 2010].
- [47] F. X. Giraldo, J. S. Hesthaven, and T. Warburton, “Nodal high-order discontinuous galerkin methods for the spherical shallow water equations,” *Journal of Computational Physics*, vol. 181, no. 2, pp. 499–525, 2002.
- [48] F. X. Giraldo, M. Restelli, and M. Läuter, “Semi-implicit formulations of the navier-stokes equations: Application to nonhydrostatic atmospheric modeling,” *SIAM Journal on Scientific Computing*. In Review.
- [49] P. Stone, “Maple worksheets on the derivation of Runge-Kutta schemes.” <http://www.peterstone.name/Maplepgs/RKcoeff.html> [Accessed: October 7, 2009].
- [50] F. X. Giraldo and T. Warburton, “A high-order triangular discontinuous galerkin oceanic shallow water model,” *International Journal for Numerical Methods in Fluids*, vol. 56, no. 7, pp. 899–925, 2008.
- [51] A. Majda, *Introduction to PDEs and Waves for the Atmosphere and Ocean*. New York: Courant Institute of Mathematical Sciences, 2003.
- [52] A. R. Curtis, “High-order explicit Runge-Kutta formulae, their uses, and limitations,” *IMA Journal of Applied Mathematics*, vol. 16, pp. 35–53, 1975.

- [53] J. M. Lindquist, F. X. Giraldo, and B. Neta, "Klein-gordon equation with advection on unbounded domains using spectral elements and high-order non-reflecting boundary conditions," *Applied Mathematics and Computation*. In Review.
- [54] R. Huan and T. L. L., "Accurate radiation boundary conditions for the time-dependent wave equation on unbounded domains," *International Journal for Numerical Methods in Engineering*, vol. 47, no. 9, pp. 1569–1603, 2000.
- [55] L. L. Thompson and R. Huan, "Implementation of exact non-reflecting boundary conditions in the finite element method for the time-dependent wave equation," *Computer Methods in Applied Mechanics and Engineering*, vol. 187, no. 1–2, pp. 137–159, 2000.
- [56] L. L. Thompson and R. Huan, "Computation of far-field solutions based on exact nonreflecting boundary conditions for the time-dependent wave equation," *Computer Methods in Applied Mechanics and Engineering*, vol. 190, no. 11–12, pp. 1551–1577, 2000.
- [57] L. L. Thompson and R. Huan, "Finite element formulation of exact non-reflecting boundary conditions for the time-dependent wave equation," *International Journal for Numerical Methods in Engineering*, vol. 45, no. 11, pp. 1607–1630, 1999.
- [58] L. L. Thompson and R. Huan, "Computation of transient radiation in semi-infinite regions based on exact nonreflecting boundary conditions and mixed time integration," *Journal of the Acoustical Society of America*, vol. 106, no. 6, pp. 3095–3108, 1999.
- [59] L. L. Thompson and R. Huan, "Accurate radiation boundary conditions for the two-dimensional wave equation on unbounded domains," *Computer Methods in Applied Mechanics and Engineering*, vol. 191, no. 1, pp. 311–351, 2001.
- [60] V. van Joolen, D. Givoli, and B. Neta, "High-order non-reflecting boundary conditions for dispersive waves in cartesian, cylindrical and spherical coordinate systems," *International Journal of Computational Fluid Dynamics*, vol. 17, no. 4, pp. 263–274, 2003.
- [61] J. Zhu, O. Zienkiewicz, H. E., and J. Wu, "A new approach to the development of automatic quadrilateral mesh generation," *International Journal for Numerical Methods in Engineering*, vol. 32, no. 4, pp. 849–866, 1991.
- [62] T. S. Lau, S. H. Lo, and C. K. Lee, "Generation of quadrilateral mesh over analytical curved surfaces," *Finite Elements in Analysis and Design*, vol. 27, no. 3, pp. 251–272, 1997.
- [63] M. Bern, D. Eppstein, and S. Teng, "Quadrilateral meshing by circle packing," *International Journal of Computational Geometry & Applications*, vol. 10, no. 4, pp. 347–361.

- [64] S. Hine, F. B. Atalay, D. Xu, and S. Ramaswami, “Quadrilateral meshes with bounded minimum angle,” in *SCG '09: Proceedings of the 25th annual symposium on Computational geometry*, (New York), pp. 90–91, ACM, 2009.
- [65] X. Liang, E. M. S., and Z. Yongjie, “Guaranteed-quality all-quadrilateral mesh generation with feature preservation,” in *Proceedings of the 18th International Meshing Roundtable*, pp. 45–63, 2009.
- [66] P. Jamet, “Estimation of the interpolation error for quadrilateral finite elements which can degenerate into triangles,” *SIAM Journal on Numerical Analysis*, vol. 14, no. 5, pp. 925–930, 1977.
- [67] L. Li, X. Han, and S. Xu, “Study on the degeneration of quadrilateral element to triangular element,” *Communications in Numerical Methods in Engineering*, vol. 20, no. 9, pp. 671–679, 2004.
- [68] G. Smith, *Numerical Solution of Partial Differential Equations: Finite Difference Methods*. Oxford University Press, New York: Clarendon Press, Oxford, third ed., 1985.

INITIAL DISTRIBUTION LIST

1. Defense Technical Information Center
Ft. Belvoir, Virginia
2. Dudley Knox Library
Naval Postgraduate School
Monterey, California
3. Dr. Beny Neta
Naval Postgraduate School
Monterey, California
4. Dr. Francis X. Giraldo
Naval Postgraduate School
Monterey, California
5. Dr. Clyde Scandrett
Naval Postgraduate School
Monterey, California
6. Dr. Young Kwon
Naval Postgraduate School
Monterey, California
7. Dr. Hong Zhou
Naval Postgraduate School
Monterey, California
8. Dr. Saša Gaberšek
Naval Research Laboratory
Monterey, California
9. Dr. Carlos Borges
Naval Postgraduate School
Monterey, California
10. Lt Col John Dea
Air Force Institute of Technology
Wright-Patterson Air Force Base, Ohio
11. CDR Vince van Joolen
United States Naval Academy
Annapolis, Maryland

12. COL Michael Phillips
United States Military Academy
West Point, New York
13. MAJ Joseph Lindquist
Center for Army Analysis
Fort Belvoir, Virginia